2020

Monogenic Defects of the Type I Interferons Signaling Pathway in Humans: Molecular and Clinical Implications

Nicholas Hernandez

MONOGENIC DEFECTS OF THE TYPE I INTERFERON SIGNALING PATHWAY IN HUMANS: MOLECULAR AND CLINICAL IMPLICATIONS

A Thesis Presented to the Faculty of

The Rockefeller University

in Partial Fulfillment of the Requirements for

the degree of Doctor of Philosophy

by

Nicholas Hernandez

June 2020

MONOGENIC DEFECTS OF THE TYPE I INTERFERON SIGNALING PATHWAY IN HUMANS: MOLECULAR AND CLINICAL IMPLICATIONS

Nicholas Hernandez, Ph.D.

The Rockefeller University 2020

The germ theory of disease, which dictates that microorganisms colloquially referred to as "germs" can invade humans or other hosts and cause disease, has remained the dominant conceptualization of infectious disease since the late nineteenth century. Since that time, growing appreciation for the extent of subclinical infections, that is, infections where the germ is detectable in its host without causing overt disease, and the Mendelian inheritance patterns of some infectious diseases have reinvigorated the study of the human genetic basis of infectious disease. This theory, so far demonstrated for a number of bacterial, fungal, and viral infections, holds that germs are a necessary but not sufficient condition for infectious disease with susceptibility determined by the genetics of individual members of the host species.

In the first part of this thesis, I describe a child with inherited, complete interferon regulatory factor-9 (IRF9) deficiency who suffered from a life-threatening pulmonary influenza infection. This discovery adds to the growing body of evidence which indicates that susceptibility to severe primary infections, even from common pathogens such as influenza virus, is genetically determined. IRF9 is a critical regulator of innate anti-viral immunity in the type I and III interferon (IFN) signaling pathways, which share many signaling proteins. Consistent with this role, I show that the patient's cells had drastically

reduced responses to type I IFN which led to increased influenza virus replication. Profiling the transcriptome of the patient's cells following stimulation with type I IFN revealed that the transcriptional response to IFN is not completely abolished in the patient's cells. Indeed, the patient's cells induced a small but partially overlapping set of antiviral mediators when compared to transcriptional responses from healthy control cells. Unfortunately, type III IFN signaling could not be directly assessed as fibroblasts, the cell line used throughout for viral and biochemical analyses, do not express the type III IFN receptor. These data demonstrate that IRF9 deficiency disturbs type I, and likely type III, IFN signaling, and that this deficiency underlies the patient's severe influenza infection.

In the second part of this thesis, I describe the first cases of inherited IFN IFNα/β receptor-1 (IFNAR1) deficiency in children who suffered severe complications following vaccination with attenuated viral vaccines but who were otherwise healthy. IFNAR1 is one of the two subunits that form the receptor for type I IFNs, and I show that type I IFN signaling is abolished in the patients' cells. Consistent with a defect in type I IFN signaling, the patients' cells exhibit a profound susceptibility to all viruses tested *in vitro*, in contrast with the patients' specific and, compared to other primary immunodeficiencies, relatively mild phenotype. This susceptibility was dependent on the absence of a functional IFNAR1 receptor, which we established through complementation experiments. Taken together, these two studies interrogate the functions of the type I and III IFN pathways that are critical for human immunity to viral diseases and provide evidence for an underappreciated non-redundancy within these pathways.

ACKNOWLEDGEMENTS

I would like to thank my thesis committee, Dr. Luciano Marraffini, Dr. Charles Rice, and Dr. Lionel Ivashkiv, for critically assessing my thesis research at regular points and offering constructive input and essential direction. I am also grateful for Dr. David Levy's participation as external examiner on my committee. I wish to thank Olaf Andersen, Catharine Boothroyd, Ruthie Gotian, Renee Horton, Elaine Velez, Ken Javier, and Hanna Silvast for making the MD/PhD program run as smoothly as it does. Likewise, I would like to thank Cris Rosario, Stephanie Fernandez, Marta Delgado, Kristen Cullen, Emily Harms, and Sid Strickland at the Dean's office at Rockefeller University for their tireless assistance.

Within the lab, I am thankful, especially, to Michael Ciancanelli, Scott Drutman, and Serkan Belkaya without whose good humor and knowledge I could not have completed this project. I am also thankful to Noé Ramírez-Alejo, Rubén Martínez-Barricarte, Hye Kyung Lim, Yoon Seung Lee, Mary Hasek, Eduardo Javier García Reino for these same reasons. I would like to thank my supervisors within the lab, including Qian Zhang, Stéphanie Boisson-Dupuis, Emmanuelle Jouanguy, and Shen-Ying Zhang. Additionally, great thanks are due to Dominic Papandrea, Yelena Nemirovskaya, and Tatiana Kochetkov, all of whom keep the lab running. Lastly, I thank Jean-Laurent Casanova and Laurent Abel, the two heads of the St. Giles Laboratory of Human Genetics of Infectious Diseases, who have both profoundly influenced my scientific thinking and guided me along my current path.

I would like to thank the many collaborators with whom I worked on this project, especially Isabelle Melki, Giorgia Bucciol, Leen Moens, Jérémie Le Pen, and Huie Jing.

Chapters 2 and 3 of this thesis have previously been published in edited forms. For chapter 2, I produced figures 2.1, 2.2B-G, 2.3, and 2.5A-D. I produced figure 2.4 jointly with Susie Huang and Nico Marr, while figures 2.5E-H and 2.6 were produced by Huie Jing and Jeffrey Danielson. I also produced figure 2.S2 and 2.S3, as well as table 2.S1. Tables 2.S2 and 2.S3, and figure 2.1A were produced by Isabelle Melki. Figure 2.S1 was produced by Tomasz Kula. For chapter 3, I produced figures 3.1, 3.2, 3.S1, and 3.S2. I also generated figures 3.3A, 3.3C, and 3.3E; 3.3B and 3.3D were produced by Jérémie Le Pen, Andrea Jurado, and Dick Zijlmans, in addition to figures 3.S3G & 3.S4G-J. I generated figures 3.S4A-F and 3.S3A-E. Figure 3.S3F & H were produced by Leen Moens and Giorgia Bucciol. I wrote both manuscripts in collaboration with my mentor, Jean-Laurent Casanova, and all coauthors helped prepare them for publication. The experimental program for these papers was decided jointly with Dr. Casanova and other senior authors of these manuscripts, notably Qian Zhang, Emmanuelle Jouanguy, Charles Rice, Margaret MacDonald, Xavier Bossuyt, Isabelle Meyts, and Helen Su.

I am especially thankful to the patients and families who consented to participate in these studies, and whose all-too-real suffering enables our lab to search for treatments for their disease and for knowledge to prevent them. I am grateful as well to the many physicians who treat these patients, and without whom our work would also not be possible.

I am grateful to all of my family and friends outside of the lab for their, at times quite substantial, support. I look forward to rejoining you in the real world.

TABLE OF CONTENTS

LIST OF FIGURES

LIST OF TABLES

Chapter 1: Introduction

The ability of each organism to differentiate self from non-self is fundamental to the organism's continued survival and necessary for the development of even the most rudimentary immune system. This differentiation may occur at a cellular or multicellular level, or at increasingly subtle subcellular levels, including the proteome, the transcriptome, or the genome of a given cell[1]. Following identification of a non-self element, be it a pathogen or simply a mis-translated protein, an organism must modify its behavior to neutralize the presumed threat, redirecting its energy and resources, at least momentarily, to this end. Yet it is not advantageous for an organism to remain in this state while it could be more aggressively pursuing its other biological imperatives. The diminution of the immune response is therefore equally important to a well-functioning immune system and, together with the stochastic nature of infection, gives rise to the periodic immunological crescendo-decrescendo of transient infection with which we are all familiar.

Similarly, this contrapuntal dance of a pathogen with its host's immune response defined scientists' early understanding of infectious disease in the modern era, forming the basis of the germ theory of disease. Beginning in the mid-nineteenth century, the germ theory, which held that microorganisms called "germs" or pathogens invaded a host and caused disease in doing so, began to supplant the miasma theory of disease, which held that many diseases were caused by noxious "bad air". This shift was inaugurated in 1865 with Louis Pasteur's work on silk worms and culminated in Robert Koch's isolation of the causative agent of tuberculosis in 1882[2]. Studying two diseases which killed silk worms and disturbed the cloth industry in France, Pasteur connected his earlier work on bacterial fermentation with these diseases and hypothesized that microorganisms were responsible

for the worms' illnesses. Furthermore, based on microscopic examination of the worms' eggs, Pasteur developed an effective mechanism of prophylaxis[4]. These victories were inconclusive, however, as they had not offered true proof that the pathogens were responsible for the observed diseases; a more rigorous demonstration was later accomplished by Koch.

Following his work on the anthrax bacillus, Koch travelled to London and began research on tuberculosis, the most feared and deadly disease of the time[5]. Once he had pioneered new methods of tissue staining, Koch was quickly able to isolate a bacterium from symptomatic patients, yet he needed more evidence to prove that the bacterium caused the disease[5]. This goal led him to develop four postulates that must be met to establish causality in bacterial infections[6]. These postulates required that the bacteria and disease coincide in symptomatic patients, that the bacteria be isolated in pure culture, and that inoculation of healthy subjects with the isolated bacteria would lead to the development of disease[5]. Following these criteria, Koch discovered that the bacteria isolated from tuberculosis patients would form tubercles upon inoculation into animals that were proportional to the size of the bacterial inoculum, thereby establishing that the bacillus was the generative agent of tuberculosis[6]. He presented these findings in 1882 to great acclaim and international fame. With this, the germ theory of disease had effectively supplanted the miasma theory as the dominant explanation of disease.

Yet it was not a perfect explanation; violations of Koch's postulates were known even to Koch at the time, and more significant objections would be raised in the coming years[7]. In particular, Charles Nicolle's work documenting inapparent (subclinical) infections and Clemens Von Pirquet's development of the tuberculin skin test,

demonstrated that known pathogens could be present in humans without any evidence of disease[2,8,9]. These issues may be considered collectively as problems of interindividual variability in response to infection. Human geneticists including Archibold Garrod and Karl Pearson, among others, proposed a germline theory of infectious disease to explain this variability and provided strong evidence in this direction[2]. Epidemiological studies, for example, showed that appendicitis segregated as an autosomal dominant trait in a number of multiplex kindreds[10]. More convincingly, elegant twin studies on tuberculosis were carried out, which demonstrated concordance rates of 80% in monozygotic twins, but only 20% in dizygotic twins[11,12]. Even more broadly, early death from infection has been shown to correlate highly with the death of the individual's biological, but not adoptive parents, from infection[13]. The contemporaneous description of Bruton's agammaglobulinemia, the first primary immunodeficiency (PID), established the existence of Mendelian inborn errors of immunity[14]. However, the gap between the broad infectious phenotypes of the first immunodeficiencies and the pathogen-specificity of interindividual variability was sizable.

The advent of modern molecular biological and genetic techniques has enabled the dissection of additional Mendelian infectious diseases such as Mendelian susceptibility to mycobacterial disease (MSMD)[15,16]. MSMD is characterized by susceptibility to poorly virulent mycobacterial species (most commonly the live Bacillus Calmette-Guérin [BCG] vaccine) and, more rarely, intramacrophagic pathogens such *Salmonella*[17]. Following the identification of autosomal recessive (AR) complete interferon-γ receptor-1 (IFN-γR1) deficiency as the first genetic etiology for MSMD, the search for genetic bases to infectious diseases was broadened to include additional defects in IFN-γ signaling in MSMD, as well

as defects in non-mycobacterial infections[18–21]. In 2002, the work of Gerard Orth on epidermodysplasia verruciformis (EV), a dermatologic disease caused by infection with nonpathogenic human β-papillomaviruses (β-HPV), demonstrated that viral diseases could also be explained by single gene errors of immunity[22]. Although a number genes underlying EV have been described, the molecular mechanism of disease remain elusive for its three primary etiologies, biallelic null mutations of *EVER1*, *EVER2*, and *CIB1* (calcium and integrin binding protein-1), limiting the extent to which the insights provided by these studies can be generalized to other viral diseases[22,23]. More broadly applicable lessons would be learned from the study of herpes simplex encephalitis (HSE).

HSE is a rare complication of infection with herpes simplex virus-1 or -2 (HSV-1 or -2, respectively), with HSV-1 being the more common cause of disease[24]. HSV-1 is a nearly ubiquitous pathogen and most humans experience infection without adverse consequences during their life[25]. Despite the sparsity of multiplex kindreds suffering from HSE, a retrospective survey revealed that 12% of French children with the disease were born to consanguineous parents[26]. Together, these data suggested that HSE could be caused by monogenic inborn errors of immunity, with incomplete clinical penetrance producing the observed non-Mendelian pattern of inheritance. Working off earlier hints that defects in type I or III IFN signaling may underlie HSE, Casrouge et al. and Zhang et al. each identified two HSE patients with defects in either UNC93-B or Toll-like receptor-3 (TLR3), both of which are critical for the production of type I and III IFNs following recognition of double-stranded RNA (dsRNA)[27–31]. Both type I and type III IFNs are secreted signaling proteins critical for defense against viral pathogens[32,33]. Furthermore, their mechanisms of induction and downstream signaling components (outside of the IFN

molecules themselves and the specific receptors to which they bind) are largely overlapping (FIGURE 1.1)[33]. Further studies on children suffering from HSE revealed a number of associated deficiencies that underlie the disease, including deficiencies in TANK binding kinase-1 (TBK1), TNF receptor associated factor-3 (TRAF3), TIR-domain-containing adapter-inducing IFN-β (TRIF), or IRF3[34–37]. Heartened by the success of these efforts, geneticists have recently worked to expand the list of viral diseases known to result from single-gene inborn errors in immunity.

Although the prevailing wisdom suggests that susceptibility to most severe viral infections is a polygenic trait mediated by the combined effect of numerous loci, an increasing number of viral diseases have been shown to have monogenic etiologies[38]. First, Byun et al. published two papers providing genetic explanations of Kaposi sarcoma, a human herpesvirus-8 (HHV-8)-induced tumor which develops in a small subset of infected individuals[39,40]. Significantly, the defects described in these papers, stromal interaction molecule-1 (STIM1) deficiency and OX40 deficiency, resulted in impoverished T cell compartments; the clinical distinctiveness of KS and HSE patients appropriately reflected in the mechanistic independence of the pathways uncovered in the genetic analysis of each condition. Next, in 2015, Ciancanelli et al. described autosomal recessive IRF7 deficiency in a child suffering from a life-threatening episode of acute respiratory distress syndrome (ARDS) following primary infection with influenza virus[41]. IRF7 is a transcription factor critical for induction of type I and III IFNs and is constitutively expressed in plasmacytoid dendritic cells (pDCs), the major type I and III IFN-producing cells[42,43]. The production of type I and III IFNs was severely diminished in the patient's leukocytes, and the patient's cells also replicated much higher levels of influenza virus *in vitro*[41,44]. Both phenotypes

could be rescued by complementation with wild-type (WT) IRF7, or by treatment with exogenous IFN in the case of the viral replication defect specifically[41]. This work demonstrated that common, isolated, viral diseases of childhood that were not previously thought to be genetic could be caused by monogenic errors of immunity.

Following this, Lamborn et al. characterized MDA5 deficiency in a child with recurrent human rhinovirus (HRV) infections[45]. Similar to TLR3, MDA5 senses dsRNA produced as viral byproducts or intermediates, although TLR3 monitors the endosomal compartment while MDA5 surveils the cytoplasm[46,47]. Interestingly, although this patient also suffered from influenza A virus (IAV) and respiratory syncytial virus (RSV) infections, reintroduction of WT MDA5 could not restrict IAV or RSV replication *in vitro*, although it did restrict HRV replication in this setting[45]. Together, these data provide evidence that MDA5 deficiency underlies susceptibility to HRV, a pervasive viral pathogen. More recently, Belkaya et al. described a patient with fulminant viral hepatitis and inherited IL-18 binding protein (IL-18BP) deficiency[48]. The authors showed that in the absence of IL-18BP, excessive natural killer (NK) cell activation led to unchecked killing of hepatocytes *in vitro*, again implicating a distinct cell type and signaling pathway in a discrete viral disease[48]. Additional work has focused on defects in the type I and/or type III IFN signaling pathways themselves, in particular on defects in signal transducer and activator of transcript-2 (STAT2), which is common to both type I and III IFN signaling pathways, and defects in IFNα/β receptor-2 (IFNAR2), which is utilized only by type I IFNs[49–52]. These studies, largely carried out by Sophie Hambleton's group in the UK, outline a clinical phenotype characterized by severe, adverse reaction to measles, mumps, and rubella (MMR) vaccination and, for patients deficient in STAT2, frequent infection

with common environmental pathogens, such as HRV and RSV[49–52]. This work, while also expanding the catalog of viral diseases shown to have a genetic etiology, further draws into question how defects in these two pathways could result in multiple, seemingly discrete, clinical phenotypes.

Despite the mounting evidence that isolated, severe viral infections can result from single gene inborn errors of immunity in a manner contingent on the pathway disrupted, the centrality of type I and III IFN signaling to HSE, IAV, HRV, RSV, and MMR immunity suggests that there may be an underappreciated sensitivity within this pathway to explain these divergent clinical presentations. If so, we might further hypothesize that undescribed defects within the type I and/or III IFN signaling pathways may serve as genetic etiologies for viral diseases that are not currently considered to be genetic. In this thesis, two additional studies involving patients with genetically determined susceptibility to viral infections are presented as first-steps to addressing these hypotheses.

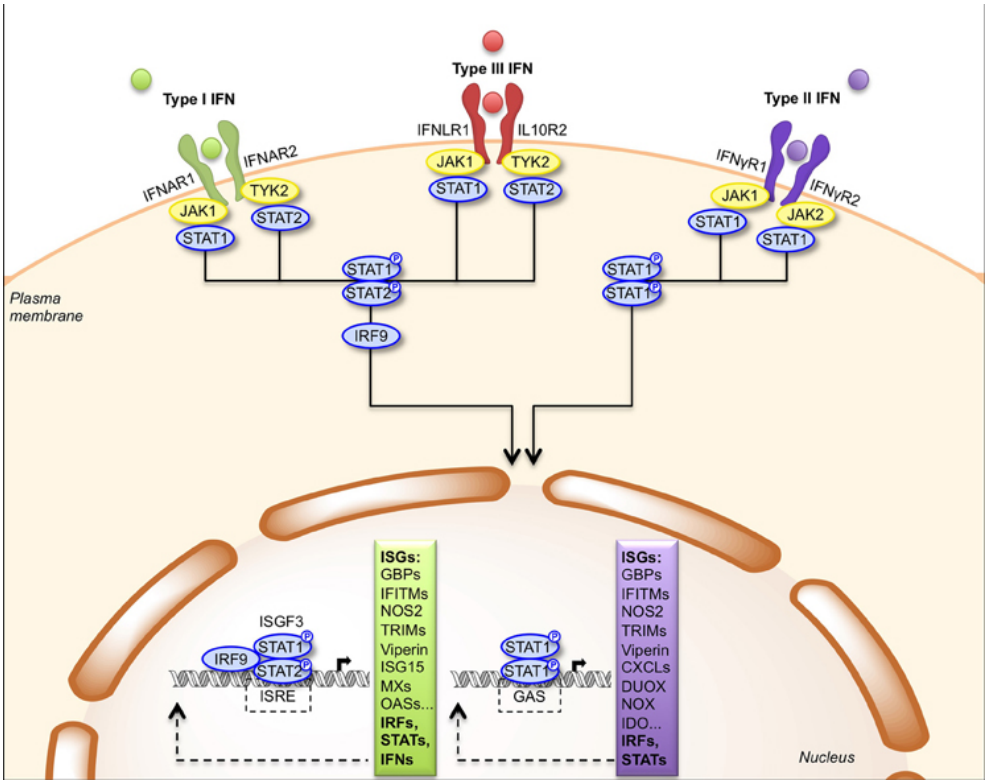

Figure 1.1 Signal transduction in the type I, II, and III IFN signaling pathways. Binding of IFN with the appropriate receptor results in activation of a JAK-STAT signaling cascade, leading to the phosphorylation of various STAT proteins and the formation of transcription factors such as ISGF3 (a heterotrimer of pSTAT1, pSTAT2, and IRF9) and GAF (a pSTAT1 homodimer). These bind to their corresponding ISRE or GAS DNA sequences and initiate transcription of various interferon stimulated genes (ISGs). Image taken from Dussurget et al.[53]

Chapter 2:

Inherited IRF9 deficiency as a genetic etiology of life-threatening influenza infections[1]

[1] Chapter 2, and portions of the materials and methods, are edited from: Hernandez, N. *et al.* Life-threatening influenza pneumonitis in a child with inherited IRF9 deficiency. *J. Exp. Med.* (2018). doi:10.1084/jem.20180628
This manuscript can be found at http://jem.rupress.org/content/215/10/2567. Author contributions are available in the acknowledgements section of this thesis, in addition to being more fully explicated in the manuscript itself.

Introduction

Influenza virus is a common human pathogen that typically causes self-limiting respiratory disease in children, but can also lead to severe fulminating illness with pneumonia and an acute respiratory distress syndrome[54]. Seasonal epidemics and pandemics demonstrate that virus strain differences can influence the frequency and severity of infections, yet these differences cannot explain the inter-individual variability in a population infected by an identical virus[55–57]. Furthermore, almost no risk factors for severe influenza infections in children have been identified. The few risk factors that have been identified generally include acquired comorbidities, such as chronic pulmonary or cardiovascular disease, and old age[58–60]. Consequently, the pathogenesis of life-threatening pulmonary influenza in children remains largely unexplained[61]. In contrast to focusing on the genetics of the influenza virus itself, the recent work of Ciancanelli et al. established AR, complete IRF7 deficiency in humans as the first genetic etiology for life-threatening influenza ARDS in an otherwise healthy patient[41]. This work demonstrated that IRF7 is critical for the amplification of type I and type III IFNs in human pDCs, peripheral blood mononuclear cells (PBMCs), and induced pluripotent stem cell (iPSC)-derived pulmonary epithelial cells. The inability of the patient's cells to induce type I and III IFNs likely underlies their susceptibility to influenza. GATA2 haploinsufficiency has also been described to result in severe influenza infections, although these patients typically have multiple infections and abnormal development of various myeloid and lymphoid subsets, including pDCs[62–64]. Three GATA2 deficient patients experienced severe influenza episodes at ages 18, 31, and 54, but influenza was the first infection requiring hospitalization for only one patient[62–64]. Although the mechanism by which GATA2-deficiency results in susceptibility to severe influenza infections is unknown, the lack of

pDCs in these patients is suggestive, due to their high basal expression of IRF7 and their efficacy in inducing IFNs[65,66]. Lastly, IAV-ARDS has recently been described in three kindreds with TLR3-deficiency, further supporting the centrality of type I and III IFNs to this disease[45,67,68]. Perplexingly, however, inborn errors of MDA5-dependent production of IFNs are not known to underlie severe influenza. Only one such patient has been comprehensively studied, although nine other putative patients have been identified[45,69,70]. It is therefore possible that future studies will uncover MDA5 deficiency in patients with IAV-ARDS. Similarly, patients with IL-10RB deficiency, who are therefore unresponsive to type III IFN, have not been shown to suffer from severe influenza infections, suggesting that type I IFN may be more relevant than type III IFNs in immunity to influenza virus[71,72]. Counter to this hypothesis, STAT1-, STAT2-, Janus kinase 1- (JAK1-), Tyrosine kinase 2- (TYK2-), and IFNAR2-mutated patients, with defective type I IFN responses, were also not reported to suffer from severe influenza infections[49–52,73–75]. In addition, severe influenza has not been reported in any of the patients suffering from any of the >350 other known inborn errors of immunity, including patients lacking T cells, or B cells, or both[76,77]. Taken together, these data suggest that the human TLR3-, GATA2-, and IRF7-dependent production of type I and/or type III IFNs is essential for protective immunity against influenza virus.

Mice either homozygous for an *Irf7* null allele or heterozygous for a *Gata2* null allele have also been characterized, as well as numerous strains deficient in TLR3. *Gata2* +/- mice have not been studied for infectious diseases, although they possess dramatically reduced pDC counts, as research has instead focused on hematopoietic and vascular integrity[78–80]. Viral susceptibility has been studied in *Irf7* -/- mice, which display reduced

induction of IFN-α/β following either viral infection or stimulation with synthetic TLR agonists, as well as increased vulnerability to infection with HSV-1 or encephalomyocarditis virus (EMCV)[81,82]. Furthermore, *Irf7* was identified as one of 25 differentially expressed genes (DEGs) between C57BL/6J and DBA/2J mice infected with IAV that overlapped with DEGs previously identified to be important for IAV replication in siRNA screens[83]. Continuing this work, the authors compared *Irf7 -/-* mice with *Irf3 -/-* mice and double knockouts and found that, while deletion of IRF3 had a moderate impact on IFN expression, absence of IRF7 abolished IFN-α production[84]. Consistent with Ciancanelli et al., IFN-β induction was modestly preserved in some cell types in the absence of IRF7, although this induction was dependent on the presence of IRF3[84]. Furthermore, *Irf7 -/-* mice infected with IAV experienced greater morbidity and mortality than healthy control mice[83]. Unfortunately, the C57BL/6 parental strain used to generate the mice in these studies does not contain a functional *Mx1* allele[85,86]. Due to the critical role of *Mx1* in immunity to influenza virus in mice, however, these data, and those from many other mouse studies of IAV, merit cautious reexamination[85–87]. Buttressing the hypothesis that type I IFN is essential for control of IAV in mice, however, *Ifnb1* -/- mice in an Mx1-positive background were significantly more sensitive to IAV than mice with WT *Ifnb1* alleles were[88]. Additional studies, also performed in an Mx1-replete background, have found IFNAR1, TLR7, and MyD88 signaling to be critical for defense against influenza virus[88,89]. Mice with impaired type III IFN immunity have been shown to display marginally elevated influenza virus replication relative to WT mice, and to be hypersusceptible to influenza virus when type I IFN signaling was also ablated[90]. A more recent study has shown that mice lacking a functional type III IFN receptor (*Ifnlr -/-*) shed

significantly more viral particles and transmitted the infection more easily to naive mice than did WT mice or mice defective in type I IFN signaling, suggesting some non-redundancy in these two pathways during IAV infection[91]. These data thus suggest that type I and type III IFNs may have non-overlapping roles and may therefore both be critical for immunity against influenza virus in humans and mice. We hypothesized that defects of type I and/or type III IFN production or signaling, other than GATA2 and IRF7 deficiencies, may underlie severe influenza infections in otherwise healthy individuals. To test this hypothesis, we analyzed the whole-exome sequencing data of 20 children who suffered severe influenza infections, focusing especially on genes related to type I and/or III IFN.

Results

Homozygosity for a splice site mutation in *IRF9*

We studied a seven-year old girl (patient, P) who was born to first-cousin Algerian parents and who was hospitalized for a severe infection with IAV requiring mechanical ventilation and Tamiflu treatment at age two (Fig. 2.1A). In addition, she had a history of recurrent benign bronchiolitis, biliary perforation following MMR vaccination at 1 year of age, and recurrent fevers without a causative pathogen identified. P also was infected with RSV within her first year of life, leading to hospitalization but not admission to the intensive care unit (ICU). To confirm her clinical course, we first performed VirScan analysis on P's plasma, taken at age two, seven weeks prior to intravenous immunoglobulin (IVIg) administration yet after disappearance of maternal antibodies, to determine her history of viral infections[92]. As well as confirming P's IAV and RSV infections, we

detected specific antibodies against viruses including HSV-1, human cytomegalovirus (HCMV), HRV, and enterovirus in her plasma (Fig.2.S1). Following her recovery from IAV infection, P also experienced adenovirus and parainfluenza virus (PIV) infections for which she was admitted to the hospital, although neither required admission to the ICU. Both infections were confirmed by VirScan. We performed whole exome sequencing (WES) on this kindred (trio design) and identified a c.991G>A mutation in *IRF9*, which encodes a critical element of the type I and III IFN signaling pathways, IRF9[93–95]. Sanger sequencing confirmed that the patient was homozygous for this mutation while both her parents and her healthy sister were heterozygous (Fig. 2.1B). Additionally, the patient's exome showed 6.8% homozygosity, consistent with her parents being first cousins[96]. This segregation is therefore consistent with an AR pattern of inheritance with complete penetrance[97].

P's variant, which occurs in the final nucleotide of exon 7, is predicted to disrupt the essential splice donor site at this location, while also mutating an aspartic acid to asparagine at amino acid (aa) 331 (p.D331N). Because of the uncertainty in the ultimate consequences of this mutation on IRF9 structure, we will presently refer to this allele by its effect on the cDNA, c.991G>A. Computational prediction of the deleteriousness of this mutation by calculation of its combined annotation dependent depletion (CADD) score indicated that it was likely to be deleterious, since its CADD score was well above the mutation significance cutoff (MSC) (Fig. 2.1C)[98,99]. Significantly, this variation was absent from public databases, including 1,000 genomes, Bravo, and GnomAD (Genome Aggregation Database) – a database that encompasses the ExAC (exome aggregation consortium) database. We also searched P's exome for other homozygous or compound

heterozygous non-synonymous rare variations (MAF <0.01), and identified such mutations in 19 other genes. None of these other genes are known to be disease causing. Two missense mutations were identified in genes encoding topoisomerase 2A (TOP2A) and 5'-3' exoribonuclease 2 (XRN2), the only two genes connected to known PID genes in a connectome analysis[100]. The only three genes that carried homozygous variations predicted to be loss-of-function were unrelated to PIDs: disheveled binding antagonist of beta catenin 2 (DACT2), ENTH domain containing 1 (ENTHD1), and Forssman glycolipid synthase-like protein (GBGT1). Overall, these data suggested that P had AR IRF9 deficiency and consequently, that homozygosity for c.991G>A was the most plausible genotype responsible for her severe influenza infection.

Population genetics of human *IRF9*

IRF9 encompasses 9 exons, 8 of which are protein-coding (exons 2 through 9) (Fig. 2.1D). To assess how commonly *IRF9* is mutated and its function altered among healthy people, we next calculated the gene damage index (GDI) of *IRF9*, and its McDonald-Kreitman neutrality index[101]. Although *IRF9's* GDI is moderate (1.16), its McDonald-Kreitman neutrality index of 0.088 indicates that the gene is under negative selection[101]. Examining GnomAD for the presence of comparable variants, only one non-synonymous exonic variant and two intronic variants were found in homozygosity: c.381G>C:p.Q127H, c.991+119T>G, and c.991+189C>A, with minor allele frequencies (MAFs) of 0.001, 0.01, and 0.001, respectively. Individuals were identified carrying all three variants from our in-house WES cohort of 4,892 patients with severe infectious diseases. The two intronic variants found in the heterozygous state in multiple individuals and the Q127H variant found in the homozygous state in one individual. Only one of the three variants was

predicted to alter protein sequence and may therefore impact IRF9 function, while the latter two mutations occur in an intron, are not predicted to create a splice site, and actually do not utilize or create an alternative splice site (Fig. 2.S2). The individual homozygous for the Q127H allele in our cohort suffered from a fungal infection of the central nervous system and had no history of viral disease. In addition to the variants found in gnomAD, our own WES cohort contained a third homozygous non-synonymous variation in *IRF9*, c.874C>T:p.R292C (Fig. 2.1C). Unfortunately, the individual harboring this variant also bore a homozygous mutation in *HOIL1* that resulted in chronic autoinflammation, invasive bacterial infections and muscular amylopectinosis[102]. In addition to these conditions, however, he also experienced profound HCMV viremia[102]. Combined, homozygosity for any of these three variants (Q127H, R292C, and c.991G>A) is predicted to affect fewer than 1 in 10,000 individuals. Thus, even if all variants produced life-threatening influenza infections, the incidence of such infections would not be higher than is currently observed. Consistent with these variants potentially altering IRF9 structure and function, their CADD scores were all above the MSC (Fig. 2.1C)[99]. Consequently, we aimed to assess the impact of P's variant on IRF9 function, as well as the function of the two other *IRF9* missense alleles found in homozygosity in rare individuals from the general population (Q127H) or our in-house cohort (R292C).

Expression of a truncated mRNA and protein by the mutant *IRF9* allele

We hypothesized that the c.991G>A mutation would produce an aberrantly spliced *IRF9* transcript, as it occurs in an essential splice site at the terminal nucleotide of exon 7. To test this, we transiently transfected a segment of P's *IRF9* allele encompassing introns

5 through 8, as well as a segment from an identical region of a WT allele, into IRF9 deficient U2A fibrosarcoma cells, a gift from Sandra Pellegrini (Fig. 2.S3)[103]. We then sequenced the resulting cDNAs, detecting two transcripts produced from P's *IRF9* allele (Fig. 2.1E). The dominant transcript exhibited absence of exon 7 with normal exons 6 and 8. The second, minor transcript also lacked exon 7 but utilized an alternative splice acceptor site in exon 8. The WT allele, however, produced 4 different transcripts two of which were rare, with the other two being roughly equally common. One of the more common transcripts demonstrated correct splicing at exons 6/7 and 7/8 junctions while the other common product lacked exon 7 but correctly utilized the splice sites in exons 6 and 8. Of the two rare transcripts, one was a product of an alternative splice acceptor site in exon 7, whereas another resulted from use of an alternative splice acceptor site in intron 5 (Fig. 2.1E). Sequencing cDNAs generated from *IRF9* transcripts present in healthy control B-LCLs (EBV-transformed B lymphoblastoid cell lines) and SV40 large T antigen immortalized fibroblasts (SV40-F cells) revealed only correctly spliced transcripts, suggesting that the other transcripts observed in the overexpression setting are not present endogenously. Additionally, sequencing cDNAs from P's B-LCLs and SV40-F cells revealed only transcripts lacking exon 7, and none that would result in a D331N mutation in the protein (Fig. 2.1F). The deletion of exon 7 is in-frame and does not introduce a premature stop codon. This mutant protein (and the corresponding allele) will thus now be referred to as IRF9-Δex7. Next, we evaluated *IRF9* mRNA levels in P's PBMCs and SV40-F cells. Consistent with the cDNA sequencing results, only *IRF9* transcripts lacking exon 7 were detected in P's PBMCs by quantitative reverse transcription polymerase chain reaction (qRT-PCR), while a reduced number of full-length *IRF9* transcripts were detected

in both individuals harboring the c.991G>A variant in proportion to the dosage of this allele (Fig. 2.2A). Western blot (WB) analysis of P's cells and those of her mother with a polyclonal antibody (pAb) revealed a truncated IRF9 species in both individuals' cells (Fig. 2.2B). Significantly, full-length IRF9 was not detected in P's cells (Fig. 2.2B). The molecular weight (MW) of the truncated protein we detected is roughly 12 kDa below the MW of WT IRF9, consistent with a lack of exon 7 (142 amino acids). This region forms a substantial portion of the IRF-association domain (IAD) which is critical for the interaction of STAT proteins with IRF9 (Fig. 2.1D)[104]. Overall, these findings established that the patient suffered from AR IRF9 deficiency.

Normal activation of STAT1 and STAT2 in cells expressing mutant IRF9

We then set out to define the consequences of IRF9 deficiency, first by examining the function of the mutated IRF9 protein, focusing initially on the proximal signaling events immediately downstream of the type I IFN receptor. To this end, plasmids encoding IRF9-Δex7, the other two missense mRNAs found in homozygosity in public databases or our cohort (Q127H, R292C), or WT IRF9 were stably transfected into U2A cells and IRF9 expression was verified by WB (Fig. 2.2C). K81R and R292Q *IRF9* alleles were included throughout the study since they have been reported to be loss-of-function in *in vitro* studies[105]. All *IRF9* alleles were expressed at comparable levels, indicating that these variants can be normally transcribed and translated, and that the encoded mRNAs and proteins are stable in these conditions (Fig. 2.2C). Consistent with this, stable transfection of WT *IRF9* in P's SV40-F cells restored normal expression of IRF9, suggesting that the poor expression of IRF9 in her cells was due to the homozygous Δex7 mutation in *IRF9*

itself, rather than other mutations also present within her cells (Fig. 2.2D). Following stimulation with IFN-α2b, a type I IFN, P's cells normally phosphorylated STAT1 and STAT2, suggesting that IRF9 is dispensable for this process (Fig. 2.2B). These data are consistent with previous reports that STAT1 and STAT2 phosphorylation occurs immediately following type I IFN-stimulation of U2A cells[106,107]. We therefore conclude that the truncated IRF9 protein produced by the *IRF9-Δex7* allele does not affect IFNAR-proximal signaling, at least in SV40-F cells and U2A fibrosarcoma cells.

Abolished activation of ISGF3 in cells expressing mutant IRF9

STAT1, STAT2, and IRF9 jointly form the ISGF3 transcription factor in an interaction mediated by IRF9's IAD[104]. IRF9 is also predicted to participate in the binding of the heterotrimeric complex to DNA[94,108–110]. We therefore hypothesized that IRF9-Δex7 may be unable to engage with STAT1 and STAT2 to form a functional ISGF3 due to the absence of a complete IAD[104]. To address this hypothesis, we fractionated nuclear and cytoplasmic compartments of P's SV40-F cells to determine the localization of P's IRF9 protein under basal conditions (Fig. 2.2E). Consistent with the presence of an NLS in the N-terminus of IRF9, IRF9 was visible in the nucleus even under basal conditions. Although expressed at substantially lower levels than the full-length protein, IRF9-Δex7 was also detectable in the nucleus. To test for the presence of any functional ISGF3 complexes, we examined the ability of U2A cells transfected with the various *IRF9* alleles to drive luciferase transcription from an IFN-stimulated response element (ISRE) promoter. Significantly, no ISRE-driven luciferase was detectable in cells transfected with IRF9-Δex7 but normal luciferase levels were observed when transcription was driven by a

promoter containing a gamma activation sequence (GAS), when compared with the responses of healthy controls (Fig. 2.2F). In contrast, the Q127H and WT variants were able to induce transcription of luciferase from both ISRE and GAS promoters while both R292Q and R292C variants displayed an intermediate phenotype, with roughly 50% activity compared with the WT allele. Taken together, these data strongly suggest that P's *IRF9* variant, Δex7, is unable to encode an IRF9 protein that forms a functional ISGF3 transcription factor, while R292C and R292Q are hypomorphic and Q127H is neutral. To confirm these data, we also performed electrophoretic mobility shift assays (EMSAs) on P's cells following IFN-α2b stimulation and were not able to visualize ISRE-binding of the ISGF3 complex, although her cells were able to form GAF complexes and bind GAS elements under the same conditions (Fig. 2.2G). Although we cannot exclude the possibility that the splicing defect is leaky in untested cells where IRF9 D331N is expressed, resulting in a severe but incomplete IRF9 deficiency, the most parsimonious conclusion is that the patient is homozygous for a null *IRF9* allele.

IRF9 deficiency impairs induction of ISGs

Because P's cells were unable to form a functional ISGF3 complex, we further hypothesized that her cells would display a severe impairment in ISG upregulation following IFN stimulation. Unlike cells from healthy controls, stimulation of P's SV40-F and B-LCL cells with type I IFN of did not substantially induce *MX1*, *IFIT1*, or *OAS1* gene products as assessed by qRT-PCR at the transcriptional level and WB at the protein level (Figs. 2.3A-D). Importantly, stable transfection of P's SV40-F cells with a plasmid encoding WT IRF9 was able to rescue the impaired induction of ISGs (Fig. 2.3E).

Consistent with this, U2A cells stably transfected with WT *IRF9* induced transcription of classic ISGs normally, while cells transfected with *IRF9-Δex7* were not able to do so (Fig. 2.3F). To verify the health of these cells and confirm that their defective response to type I IFN was specific to that pathway, rather than a global defect in cytokine signaling, *CXCL9* expression following stimulation with type II IFN was used throughout these qRT-PCR experiments as a positive control. Type I IFN signaling induces a substantially broader transcriptional response than upregulating the few genes tested above; in many cell types, potentially hundreds of genes display altered expression levels[111]. We therefore performed mRNA-sequencing (mRNA-seq) analysis of P's B-LCL cells and primary fibroblasts following *in vitro* stimulation with IFN-α2b in order to more fully characterize the transcriptional responses of P's cells to type I IFN. P's B-LCL cells (Figs. 2.4B, D-G) and primary fibroblasts (Figs. 2.4A, C, E-G) demonstrated an inability to regulate a broad array of genes there were not limited to ISGs, but also included negatively regulated transcripts. Importantly, the transcriptional response type I IFN in P's cells was not completely abolished. Indeed, from all transcripts detected in P's cells, 118 transcripts from her B-LCLs and 267 transcripts from her primary fibroblasts passed our filter criteria for being IFN-α2b-regulated and were also found to be regulated by IFN in the Interferome database v2.01 (Figs 2.4C & D). Interestingly, the extent of ISG induction differed between P's cells and those of healthy controls, even when considering only those ISGs induced in P's cells. For instance, many of the up-regulated ISGs were significantly less induced in P's cells than those same ISGs were in healthy control cells, although a small subset of ISGs was actually induced at higher levels in IRF9 deficient cells (Figs. 2.4E & F). To further dissect the ISG network and its dysregulation in P's B-LCL cells, we next identified a subset of 84

transcripts that were consistently strongly induced (> 5-fold linear scale) following IFN-α2b stimulation of cells from healthy controls. Of these transcripts, only 37 were found to be induced at any level (>1.5 fold) in her B-LCLs, while 47 were not induced. These transcripts were then queried for ISGs in the Interferome v2.01 database, again using a 1.5-fold cut-off to differentiate between IFN-responsive and non-responsive genes. Of these 37 responsive and 47 non-responsive transcripts in P's cells, 24 and 39 transcripts, respectively, were identified as ISGs in the Interferome v2.01 database. These transcripts were then used in an ISG response network analysis using GeneMANIA (https://genemania.org) to predict which cellular functions may be disrupted by the lack of ISG induction in P's cells (Fig. 2.4G). Notably, genes encoding IFIT family proteins, ISG15, and components of the ISGylation system such as USP18 and HERC5, were among those ISGs not induced in P's cells. Conversely, a number of ISGs, such as DDX58, those for Guanylate-Binding Proteins (GBP1, GBP4, and GBP5), ISG20 and STAT2 were induced by IFN-α2b in P's cells. Although most of these ISGs were not induced to a comparable level in P's cells as in healthy controls, these data are consistent with the presence of ISGF3-independent transcription factors such as phosphorylated STAT1 homodimers downstream of the IFN receptor. Collectively, our studies indicate that P's cells are able to form functional GAF complexes and induce a small subset of ISGs, but lack functional ISGF3 complexes due to expression a loss-of-function *IRF9* allele that severely narrows the transcriptional responses to type I IFN in multiple cell types.

The patient's fibroblast-intrinsic type I IFN immunity to viruses is impaired

Next, we assessed the impact of IRF9 deficiency on cell-intrinsic, non-hematopoietic immunity by infecting P's SV40-F cells with either IAV or vesicular stomatitis virus (VSV). At 48 hours post-infection (hpi), we observed an approximately 10-fold difference in IAV titer between P's cells and those from healthy controls or P's heterozygous mother (Fig. 2.5A). We then considered whether the residual type I IFN signaling enabled by the ISGF3-independent mechanisms could inhibit viral replication following pretreatment with exogenous IFN. Pre-treatment with IFN-α2b substantially reduced viral replication in healthy control cells but did not diminish replication in P's cells, which produced roughly 100-fold higher IAV titers than cells with intact type I and III IFN signaling pathways (Fig. 2.5A). Consistent with these data, we also found that P's SV40-F cells were substantially more susceptible to VSV at 12 hpi in the absence of pre-treatment with type I IFN. Pre-treatment with IFN-α2b was also unable to rescue this phenotype, as P's cells demonstrated a roughly 1,000-fold elevation in viral titer compared with healthy controls at all time points beyond 8 hours (Fig. 2.5B). To determine whether or not these defects in IAV and VSV immunity were IRF9-dependent, we then stably transfected P's SV40-F cells with various *IRF9* alleles, or an empty vector (EV), and analyzed the ability of the transfected cells to control VSV and IAV infection (Figs 2.5C & D). Importantly, expression of WT IRF9 was able to rescue the inability of P's cells to control of infection with either pathogen, as did expression of the Q127H variant, suggesting that this allele may not be deleterious in the context of type I IFN signaling and anti-viral immunity, consistent with the lack of severe viral infections experienced by the individual carrying this mutation in homozygosity. Conversely, expression of K81R or

IRF9-Δex7 was unable to rescue the elevated viral replication phenotypes of P's SV40-F cells. Introduction of the R292Q or R292C alleles resulted in an intermediate phenotype, as these cells were somewhat able to control infection with VSV or IAV, though not at the level of the WT IRF9 allele. This, then, suggests that a partial form of IRF9 deficiency may have contributed to the viral infections of the HOIL1 deficient patient[102]. To test whether IRF9 deficiency resulted in impaired cell-intrinsic anti-viral immunity to other human pathogens, we next infected patient and controls SV40-F cells with GFP-expressing PIV and RSV (Figs. 2.5E-H). Consistent with our results in IAV and VSV infections, we observed a larger proportion of infected cells, and greater replication of viruses in P's cells, as assessed by GFP intensity, than in healthy controls at 48 hpi (Figs. 2.5E-H). Lastly, to further demonstrate that IRF9 mediates susceptibility to viral infection *in vitro*, we transfected primary dermal fibroblasts from healthy individuals with siRNAs targeting IRF9, mitochondrial-antiviral signaling protein (MAVS), or a non-targeting siRNA (siNeg) (Fig. 2.6A). Knockdown of either IRF9 or MAVS resulted in increased HRV viral transcripts compared to cells transfected with siNeg (Fig. 2.6A). Similarly, knockdown of IRF9 or MAVS increased the number of infected cells and relative number of viral transcripts following infection with either RSV or PIV (Figs. 6C-E). These data therefore suggest that IRF9 is nonredundant for immunity to positive-sense RNA viruses in addition to the negative-sense viruses already tested. Collectively, these studies indicate that IRF9 deficiency leads to a broad defect in cell-intrinsic immunity to viruses *in vitro*, and that inherited IRF9 deficiency underlies P's impaired immunity to influenza infection and her subsequent hospitalization for ARDS *in natura*.

Discussion

This study describes autosomal recessive, complete IRF9 deficiency in a child who suffered a life-threatening influenza infection. Our data establish a causal relationship between IRF9 deficiency and this patient's severe pulmonary influenza[97]. Thus, IRF9 deficiency constitutes the fourth genetic etiology for life-threatening influenza pneumonitis, after AR IRF7 deficiency, GATA2 haploinsufficiency, and AD TLR3 deficiency[2,17,68]. Whereas IRF7 deficiency disrupts the amplification of antiviral IFNs, IRF9 deficiency results in an inability of all cell types to respond effectively to type I, and likely type III, IFNs[41]. The obvious mechanistic connection between IRF7 and IRF9 deficiency suggests that the type I IFN responses driven by IRF7 amplification and mediated by IRF9 signaling are essential for defense against influenza virus in humans. Counter to this hypothesis, however, patients with other defects in type I IFN signaling pathway, including deficiencies in STAT1, STAT2, JAK1, TYK2, or IFNAR2 are not known to have experienced severe influenza infections[49–52,73–75]. A number of alternative hypotheses could explain this discrepancy: (i) patients with these defects may have died from other severe infections prior to exposure to influenza virus, (ii) influenza virus can be controlled independently of these signaling proteins, or, similarly, (iii) at least some type I IFNs can signal without these proteins, or, (iv) some of the defects previously described are partial, as opposed to complete, due to the hypomorphic nature of some mutant alleles [49,51,112,113]. Our data suggest that IRF9 and IRF7 regulate transcription of a key subset of ISGs that specifically mediate immunity to influenza virus. A clearer picture of the contributions of type I and III IFN signaling to human protective immunity against

influenza virus will emerge as more inborn errors of immunity are discovered and as more patients with previously described defects are diagnosed.

Subsequent to the completion of this study, a second patient with inherited IRF9 deficiency was identified with a broader clinical phenotype, including ICU admission following vaccination against varicella zoster virus (VZV), as well as enterovirus, Zika virus, and dengue virus infections, and an IAV-induced pneumonia which required hospitalization but not admission to the ICU[114]. In contrast with MDA5 deficient patient who was prone to severe, recurrent HRV and RSV infections, as well as other viral infections of the respiratory tract not including influenza, P was not admitted to the ICU following infection with RSV or HRV, both of which were confirmed by serology and VirScan[45,69,70]. Similarly, the second IRF9 deficient patient was also not admitted to the ICU following RSV or HRV infections[114]. Together, these data suggest that IRF9 deficiency and MDA5-deficiency may result in largely non-overlapping viral susceptibilities, with MDA5 deficiency leading to severe respiratory tract infections excluding influenza, while IRF9 deficiency results in especially profound susceptibility to influenza virus, and possibly to non-respiratory viruses such as enterovirus and some flaviviruses. MDA5 and IRF9 may therefore be necessary for control of different sets of respiratory viruses. Intriguingly, IRF7 deficiency results in a narrow infectious phenotype, as the only reported case in humans was uniquely susceptible to influenza infection at last follow-up, aged 9 years, and has not received prophylaxis against further viral infections other than an annual influenza vaccination[41]. In comparison with IRF7 deficiency, then, IRF9 deficiency may result in a broader infectious phenotype not limited to infection with influenza virus, but also including other viruses unrelated to the respiratory tract.

Significantly, P's clinical phenotype might have been even broader if the patient had not been started on IVIgs at 2 years of age. Despite this, IRF9 deficiency is still clinically more similar to IRF7 deficiency than it is to GATA2 deficiency. Indeed, all known patients with GATA2 deficiency suffered from many other severe infections, including mycobacterial infections, papilloma virus infections, blastomycosis, and repeated viral infections of the respiratory tract[62]. Severe influenza was the presenting feature in only a single GATA2 deficient patient who thereafter displayed other phenotypes, infectious and otherwise[64]. The broad infectious phenotypes seen in these patients are consistent with the immunological phenotype of GATA2 deficiency, which is not restricted to a lack of IFN-producing pDCs but can include monoMAC syndrome-like monocytopenia with B and NK cell lymphopenia, in addition to myelodysplastic syndromes[78,115]. Significantly, only a single case of IRF7 deficiency has been reported thus far, and only two cases of IRF9 deficiency. Further studies are needed to more comprehensively define the viral susceptibilities resulting from these deficiencies, to determine the extent to which IRF7- and IRF9-dependent type I and III IFN immunity is redundant for protective immunity against viral infections, and to suggest what other factors may compensate for deficiencies in this pathway.

Considering other patients with defects in the type I or III IFN signaling pathways, complications from MMR vaccination have been reported in patients with IFNAR2, STAT1, or STAT2 bi-allelic mutations[49–52,116]. Although comparatively rare in STAT1 deficient individuals, a severe though incompletely characterized adverse was reported in the only individual with AR complete STAT1-deficiency who was vaccinated against MMR[116]. Furthermore, it is unclear whether the patients with STAT2 and IFNAR2

deficiency have a complete or partial deficiency[49–52]. Interestingly, MMR vaccine complications have not observed in patients with AR partial STAT1 deficiency, nor have they been reported in patients with partial JAK1 or complete TYK2 deficiency who were vaccinated[73–75]. These data suggest a possible divergence from mice, where STAT1 is dispensable for protection against measles virus while STAT2 is not[117,118]. One possible explanation for the discrepancy between mice and humans is that STAT2 and IRF9 mediate a physiologically relevant branch(es) of the IFN signaling pathway(s) in mice independently of STAT1, while some subset of these branches is relevant for measles virus immunity in humans in a STAT1-dependent manner. Previous studies have described STAT2-IRF9 complexes in both mice and humans, although it is unclear if they are transcriptionally active enough to drive the cellular changes required for defense against viral infection[119,120]. This hypothesis would be consistent with previous experiments in mice demonstrating that the different components of the ISGF3 complex regulate distinct, non-redundant subsets of ISGs in addition to a jointly-regulated core of genes[121]. Alternatively, the different MMR phenotypes in patients with various inborn errors of type I and/or III IFN immunity may simply reflect the impact of modifier genes in these individuals, or of the environment itself, including the MMR inoculum. Ultimately, the experiment of nature deciphered in this report reveals the non-redundant roles of human IRF9 in the type I and/or III IFN signaling pathways for cell-intrinsic immunity against influenza virus and likely also the MMR vaccine.

Figure 2.1. A private IRF9 variant alters mRNA splicing in a child with severe influenza pneumonitis. (A) Pedigrees of the IRF9 deficient family. The double lines connecting the parents indicate consanguinity. The proband is indicated by an arrow. Filled shapes indicate affected individuals while open shapes identify unaffected individuals. (B) Chromatograms demonstrating c.991G>A mutation in patient PBMC-derived DNA (red arrow). (C) Population genetics of homozygous coding missense and predicted loss of function *IRF9* mutations taken from GnomAD and in-house cohorts. The patient's variant is private and shown in red, while two other variants, shown in blue, were also identified in our cohort. (CADD: Combined Annotation Dependent Depletion; MAF: Minor allele frequency; MSC: Mutation Significance Cutoff) (D) Schematic illustration of the *IRF9* gene. The exons are numbered 1-9 and regions corresponding to functionally significant domains are colored brown (for the DNA-binding domain, DBD), grey (nuclear localization sequence, NLS), or purple (IRF-association domain, IAD). Patient mutation indicated in red, other mutations indicated in blue. (E) *IRF9* transcripts (left panel) and relative frequencies (right panel) produced during exon trapping in U2A cells. The results are representative of two independent experiments. (F) cDNA sequencing to detect the splicing of *IRF9* mRNA from F-SV40 cells. Numbers of total and abnormal clones sequenced are indicated. Results representative of two experiments.

Figure 2.1

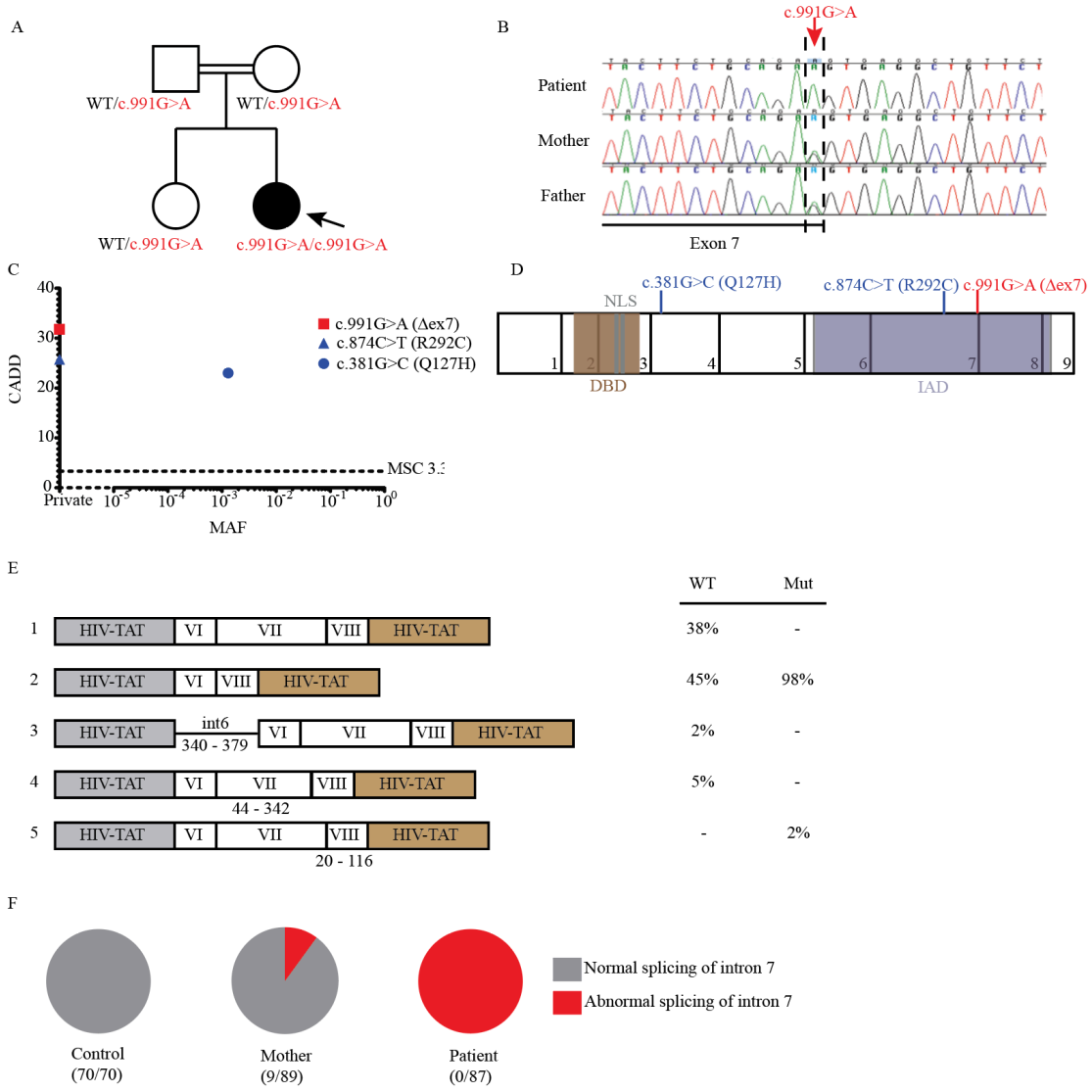
A
WT/c.991G>A
WT/c.991G>A
WT/c.991G>A
c.991G>A/c.991G>A
B
c.991G>A
Patient
Mother
Father
Exon 7
C
CADD
c.991G>A (Δex7)
c.874C>T (R292C)
c.381G>C (Q127H)
MSC 3.3
Private
MAF
D
c.381G>C (Q127H)
c.874C>T (R292C)
c.991G>A (Δex7)
NLS
DBD
IAD
E
WT
Mut
HIV-TAT
VI
VII
VIII
int6
340 - 379
44 - 342
20 - 116
38%
-
45%
98%
2%
-
5%
-
-
2%
F
Normal splicing of intron 7
Abnormal splicing of intron 7
Control
(70/70)
Mother
(9/89)
Patient
(0/87)

Figure 2.2. Impact of IRF9 Δex7 on IFN receptor-proximal signaling. (A) qRT-PCR measuring of *IRF9* mRNA levels in PBMCs from the patient, her mother, and a healthy control with two probes; one probe spanning intron 7, and a second probe spanning intron 1. (B) Upper panel: Western blot of endogenous IRF9 in patient F-SV40 cells; GAPDH was used as a loading control. Lower panel: STAT and phospho-STAT (pSTAT) levels were also assessed following stimulation with 1000 U/ml of either IFN–α2b or –γ for 0.5 hours on F-SV40 cells from two healthy controls (C1 and C2), the IRF9-deficient patient (IRF9 -/-), her mother (IRF9 +/-), a STAT1-deficient patient (STAT1 -/-), a STAT2-deficient patient (STAT2 -/-), an IFNGR2-deficient patient (IFNGR2 -/-), and an IRF7-deficient patient (IRF7 -/-). Representative results of three independent experiments are shown. (C) Western Blot of IRF9 in IRF9-deficient U2A cells stably transfected with indicated variants (green: variants reported to be loss of function in *in vitro* assays, blue: variants found in-house, red: patient). GAPDH was used as loading control. (D) Western Blot of IRF9 in patient F-SV40 cells stably transfected with indicated variants. GAPDH was used as loading control. (E) Western blot analysis of IRF9 localization in F-SV40 cells from two healthy controls (C1 and C2), the IRF9-deficient patient (IRF9 -/-), her mother (IRF9 +/-), a STAT1-deficient patient (STAT1 -/-), a STAT2-deficient patient (STAT2 -/-), an IFNGR2-deficient patient (IFNGR2 -/-), and an IRF7-deficient patient (IRF7 -/-). GAPDH and LaminA/C were used as loading controls. Representative results of three independent experiments are shown. (F) Reporter assays of ISRE or GAS-dependent firefly luciferase tested in U2A cells stimulated with 1000 U/ml of either IFN -α2b or -γ for 16 hours after being stably transfected with indicated variants (green: variants reported to be loss of function in *in vitro* assays, blue: variants found in-house, red: patient). The specific

response to IFN stimulation was calculated by the ratio of firefly luciferase reporter gene activity to constitutively expressed renilla luciferase activity (RLU, relative luciferase ratio). Representative results of three independent experiments are shown. (G) EMSA analysis of ISRE and GAS binding by IFN stimulated B-LCLs from three healthy controls (C1, C2, and C3), the IRF9-deficient patient (IRF9 -/-), her mother (IRF9 +/-), a STAT1-deficient patient (STAT1 -/-), a STAT2-deficient patient (STAT2 -/-), and an IRF7-deficient patient (IRF7 -/-). Representative results of two independent experiments are shown.

Figure 2.2

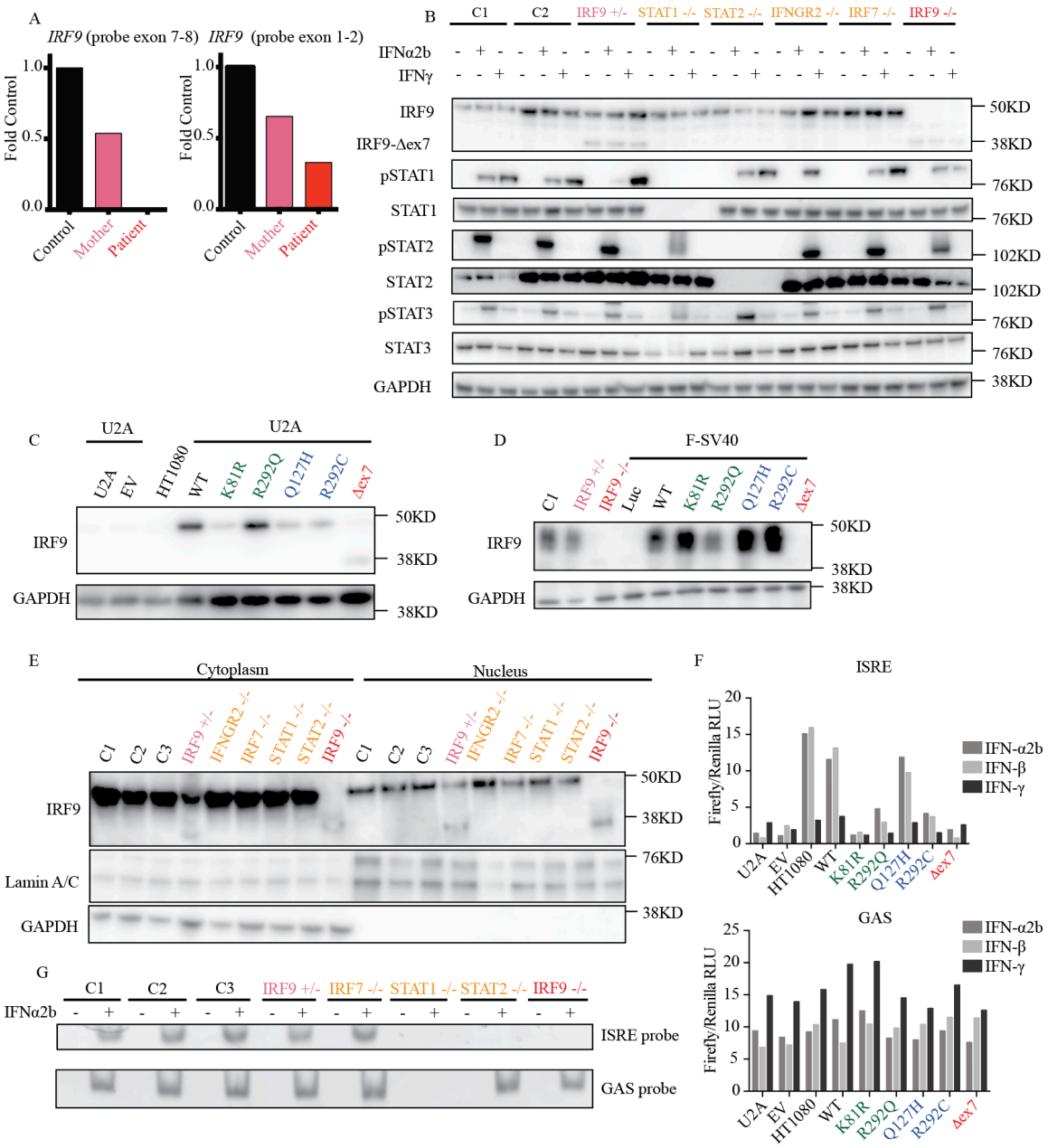
A
IRF9 (probe exon 7-8)
IRF9 (probe exon 1-2)
Fold Control
1.0
0.5
0.0
Control
Mother
Patient
B
C1
C2
IRF9 +/-
STAT1 -/-
STAT2 -/-
IFNGR2 -/-
IRF7 -/-
IRF9 -/-
IFNα2b
IFNγ
IRF9
IRF9-Δex7
pSTAT1
STAT1
pSTAT2
STAT2
pSTAT3
STAT3
GAPDH
50KD
38KD
76KD
102KD
C
U2A
HT1080
WT
K81R
R292Q
Q127H
R292C
Δex7
D
F-SV40
C1
Luc
E
Cytoplasm
Nucleus
Lamin A/C
F
ISRE
GAS
Firefly/Renilla RLU
IFN-α2b
IFN-β
IFN-γ
G
ISRE probe
GAS probe

Figure 2.3. Impaired ISG induction in IRF9-deficient cells. (A) Transcription levels of *MX1*, *IFIT1*, *IFIT3*, and *CXCL9* assessed by qRT-PCR on F-SV40 cells treated with 1000U/ml of either IFN –α2b, -β, or –γ for 2 hours. Cells were from three healthy controls (C1, C2, and C3), an IRF9-deficient patient (IRF9 -/-), her mother (IRF9 +/-), STAT1-deficient (STAT1 -/-), STAT2-deficient (STAT2 -/-), IRF7-deficient (IRF7 -/-), and IFNGR1-deficient (IFNGR1 -/-) patients. Representative results of three independent experiments are shown. (B and C) Western blot of MX1 and IFIT3 on F-SV40 (B) or B-LCL (C) cells treated with 1000U/ml of IFN–α2b for various time points. GAPDH was used as a loading control. (D) Transcription levels of *MX1*, *IFIT1*, *IFIT3*, and *CXCL9* assessed by qRT-PCR of B-LCL (D) cells treated with 1000U/ml of either IFN –α2b, -β, or –γ for 2 hours. Cells were from three healthy controls (T1, T2, and T3), an IRF9-deficient patient (IRF9 -/-), her mother (IRF9 +/-), STAT1-deficient (STAT1 -/-), STAT2-deficient (STAT2 -/-), IRF7-deficient (IRF7 -/-), and IFNGR2-deficient (IFNGR2 -/-) patients. Representative results three independent experiments are shown. (E) Transcription levels of of *MX1*, *IFIT1*, and *CXCL9* assessed by qRT-PCR in F-SV40 cells from healthy control (C1), P's mother (IRF9 +/-), and P (IRF9-/-) stably transfected with luciferase as a control (luc) or indicated IRF9 variants (WT: wild type IRF9, green: reported loss of function variants, blue: variants found in-house, red: patient variant). Cells were stimulated with 1000 U/ml of either IFN -α2b, -β, -γ for 2 or 8 hours. Representative results of two independent experiments are shown. (F) Similar to (E), qRT-PCR analysis of *MX1*, *IFIT1*, and *CXCL9* expression in parental HT1080 cells and U2A cells. Cells were stimulated with 1000 U/ml of either IFN -α2b, -β, or -γ for 2 or 8 hours. Representative results of three independent experiments are shown.

Figure 2.3

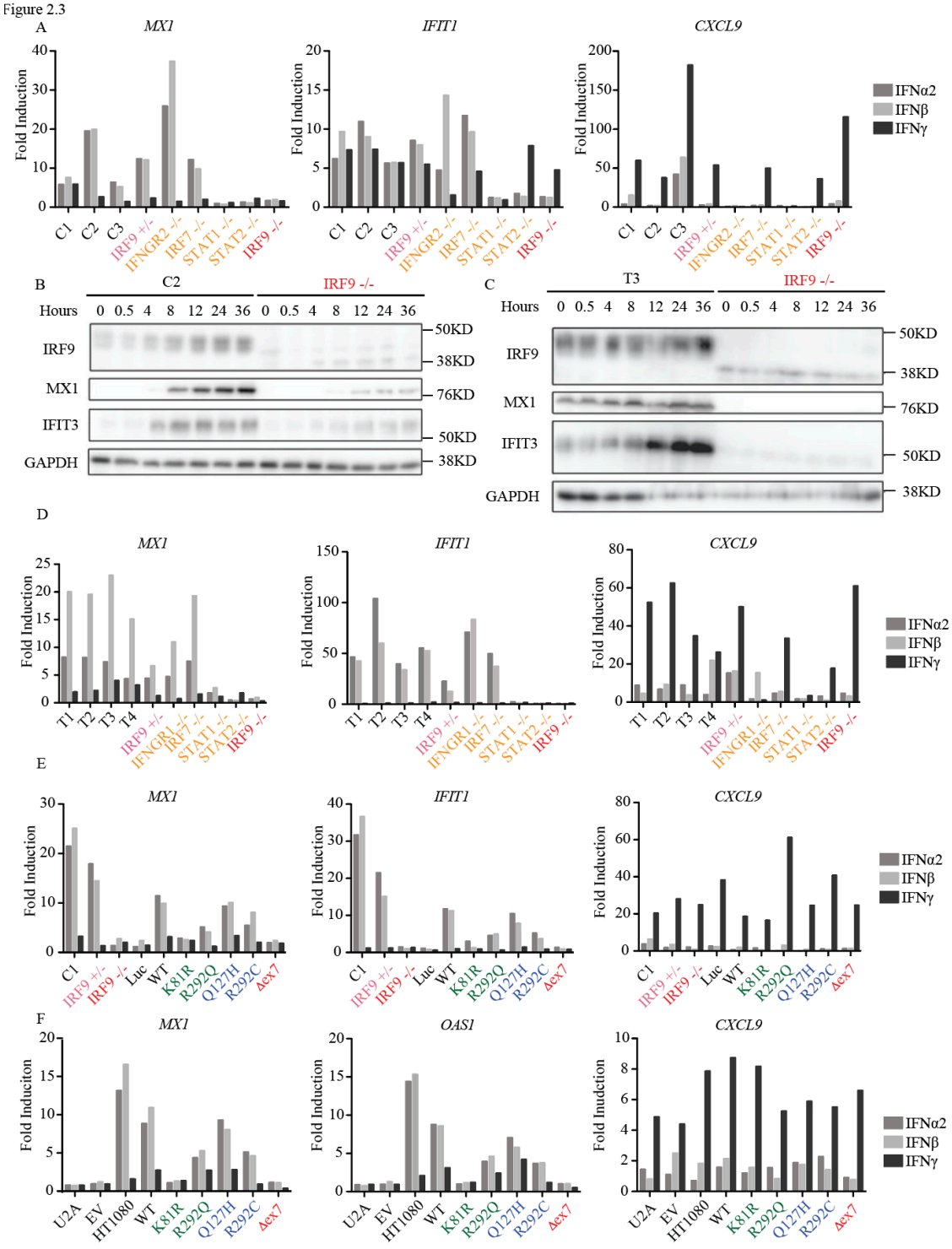
A
MX1
IFIT1
CXCL9
Fold Induction
IFNα2
IFNβ
IFNγ
C1
C2
C3
IRF9 +/-
IFNGR2 -/-
IRF7 -/-
STAT1 -/-
STAT2 -/-
IRF9 -/-
B
C2
IRF9 -/-
Hours
0 0.5 4 8 12 24 36 0 0.5 4 8 12 24 36
IRF9
MX1
IFIT3
GAPDH
50KD
38KD
76KD
C
T3
D
T1
T2
T3
T4
E
Luc
WT
K81R
R292Q
Q127H
R292C
Δex7
F
U2A
EV
HT1080
OAS1
Fold Induciton
Fold Inudction

Figure 2.4. Transcriptomic analysis of ISGs in IRF9-deficient cells. mRNA-seq analysis of primary fibroblasts (A & C) and B-LCLs (B & D) from three healthy controls (C1, C2, and C3), the IRF9-deficient patient (IRF9 -/-). Cells were treated with 1000U/ml IFN –α2b for 2 hours. Heatmaps (A & B) show log2 FC values of all ISGs that were found to be differentially regulated (>= 1.5 fold) in all three control subjects relative to unstimulated cells. Bar graphs (C & D) quantify the number of ISGs that were differentially regulated (>= 1.5 fold) compared to unstimulated cells in healthy controls or the IRF9 deficient patient. (E) Shown are Δ log2 fold change values of a subset of interferon stimulated genes (ISGs) that were found to be induced ≥ 1.5 fold (linear scale) in B-LCL cells (upper panels) or primary fibroblasts (lower panels) of the IRF9-deficient patient upon *in vitro* stimulation with IFN-α. To select this subset of ISGs, the IFN-α2b-induced genes in the healthy controls identified in the mRNA-Seq analysis were used. In the IRF9-deficient patient, these genes were first passed through a filter by querying the gene identifiers against the interferome database and by retaining genes that were responsive to *in vitro* interferon stimulation. ISGs that failed to be induced at least 1.5 fold (linear scale) in patient cells were excluded. The retained ISGs were stratified in three groups of less ($\Delta < -0.585$), similar ($-0.585 < \Delta < 0.585$) and higher ($\Delta > 0.585$) induced genes relative to the average responses in the healthy control subjects. The number of genes in each group are shown in brackets. *** denotes significant differences at $p<0.0001$ by the Kruskal-Wallis test. (F) Log2 FC of induced ISGs in IRF9-deficient B-LCLs (upper panels) or primary fibroblasts (lower panels) and their corresponding values in healthy donors. (G) Network analysis of a subset of highly inducible (> 5 fold linear scale) ISGs among control subjects' B-LCLs and their responsiveness in the IRF9-deficient patient. Biological

pathway and physical interactions are depicted as blue and red lines, respectively. 1.5 FC was used as cut-off to distinguish responsive (red circle) and non-responsive (blue circle) ISGs. The highly inducible ISGs that were used for query are shaded in yellow.

Figure 2.4

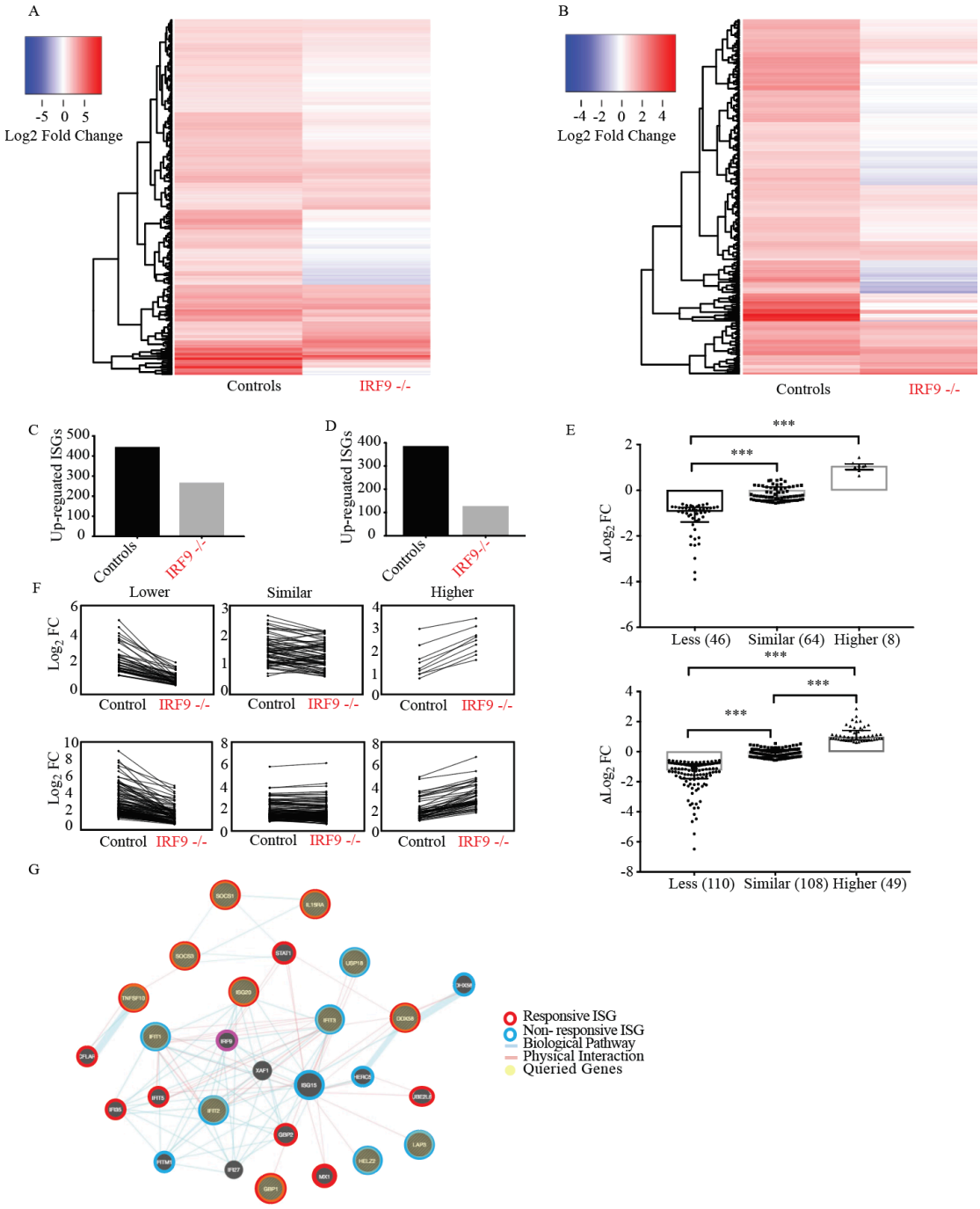
A
-5 0 5
Log2 Fold Change
Controls
IRF9 -/-
B
-4 -2 0 2 4
Log2 Fold Change
Controls
IRF9 -/-
C
Up-reguated ISGs
Controls
IRF9 -/-
D
Up-reguated ISGs
Controls
IRF9-/-
E
ΔLog2 FC
Less (46) Similar (64) Higher (8)
Less (110) Similar (108) Higher (49)
F
Lower
Similar
Higher
Log2 FC
Control IRF9 -/-
G
Responsive ISG
Non- responsive ISG
Biological Pathway
Physical Interaction
Queried Genes

Figure 2.5. Crippled control of IAV and other viral infections in IRF9-deficient cells. (A) IAV titers in F-SV40 unstimulated (left) or pre-treated (right) with 1000U/ml IFN-α2b for 16 hours, followed by infection with (A/H1N1/CA/2009) IAV at MOI = 1. Means ± SD (n = 3) are shown. Cells from three healthy controls were included (C1, C2, and C3), as well as those from the IRF9-deficient patient (IRF9 -/-), her mother (IRF9 +/-), and STAT1-deficient (STAT1 -/-), STAT2-deficient (STAT2 -/-), and IRF7-deficient (IRF7 -/-) patients. (B) VSV titers in F-SV40 cells unstimulated (left) or pre-treated (right) with 1000U/ml IFN-α2b for 16 hours, followed by infection with VSV at MOI = 3. Three independent experiments (means ± SD) are shown. (C) IAV titers in stably transfected F-SV40 cells unstimulated (left) or pre-treated (right) with 1000U/ml IFN-α2b for 16 hours, followed by infection with IAV at MOI = 1. Cells were from a healthy control (C1), a STAT1-deficient patient (STAT1-/-), P (IRF9-/-), and P's cells stably transfected with luciferase or wild type IRF9 (grey), variants reported to be loss-of-function in *in vitro* assays (green), variants found in-house (blue), or the patient's variant (red). Three independent experiments (means ± SD) are shown. (D) VSV titers in stably transfected F-SV40 cells unstimulated (left) or pre-treated (right) with 1000U/ml IFN-α2b for 16 hours, followed by infection with VSV at MOI = 3. Three independent experiments (means ± SD) are shown. (E) Percentage of RSV-infected (GFP+) F-SV40 cells at 24 and 48 hours post-infection. Cells from three healthy controls were included (C1, C4, and C5, black), as well as those from the IRF9-deficient patient (IRF9 -/-, red), and cells from STAT1-deficient (STAT1 -/-), STAT2-deficient (STAT2 -/-), and IRF7-deficient (IRF7 -/-) patients. Three independent experiments (means ± SD) are shown. (F) Mean fluorescence intensity (MFI) of RSV-infected (GFP+) F-SV40 cells at 24 and 48 hours post-infection. Three

independent experiments (means ± SD) are shown. (G) Percentage of PIV-infected (GFP+) F-SV40 cells at 24 and 48 hours post-infection. Three independent experiments (means ± SD) are shown. (H) MFI of PIV-infected (GFP+) F-SV40 cells at 24 and 48 hours post-infection. Three independent experiments (means ± SD) are shown. MFI of GFP positive cells in individual samples were normalized to the averaged MFI of the three healthy controls at 24 hours post-infection in (F) and (H).

Figure 2.5

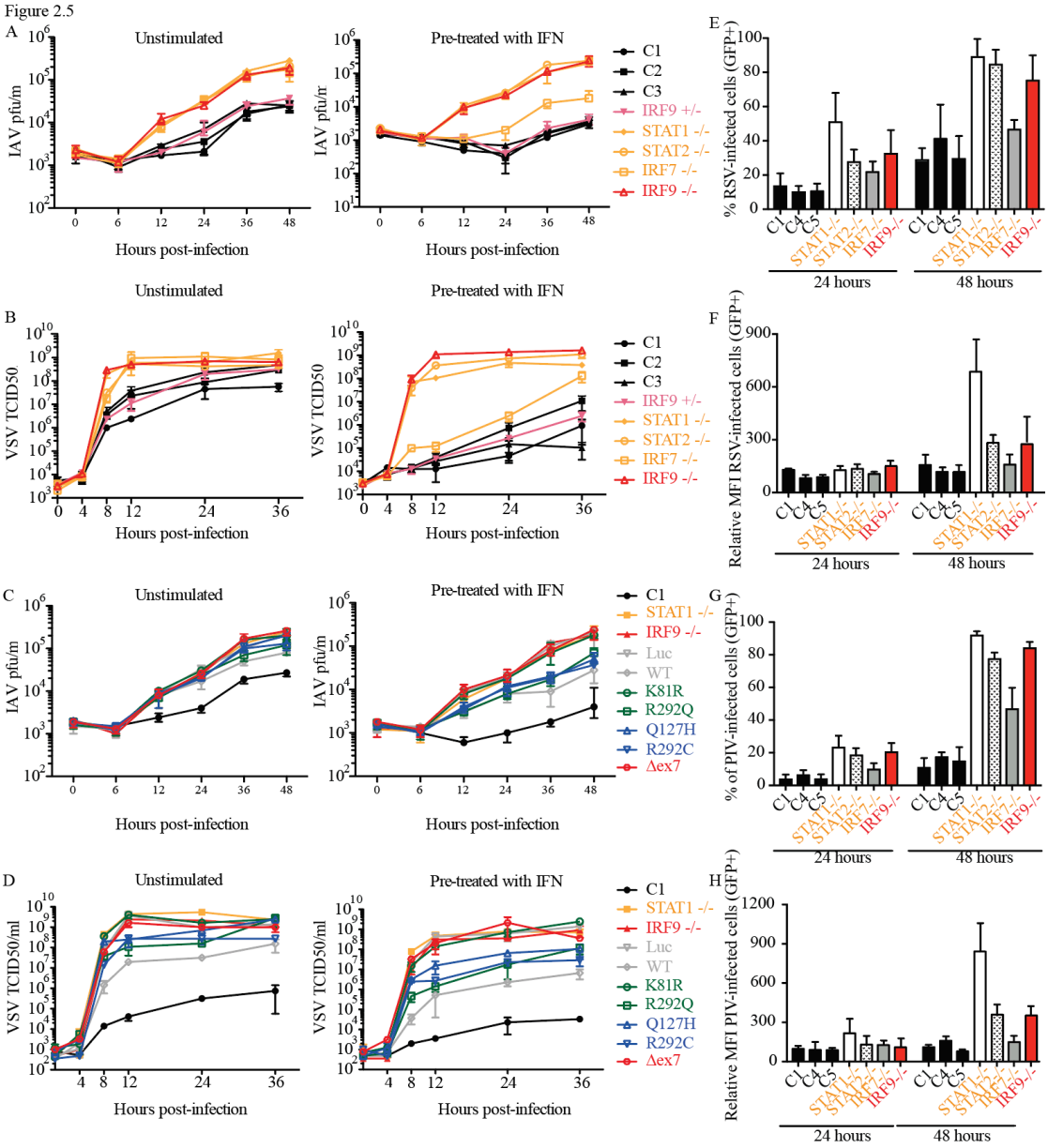
A
Unstimulated
Pre-treated with IFN
IAV pfu/m
IAV pfu/m
Hours post-infection
Hours post-infection
C1
C2
C3
IRF9 +/-
STAT1 -/-
STAT2 -/-
IRF7 -/-
IRF9 -/-
E
% RSV-infected cells (GFP+)
C1
C2
C3
STAT1-/-
STAT2-/-
IRF7-/-
IRF9-/-
24 hours
48 hours
B
Unstimulated
Pre-treated with IFN
VSV TCID50
VSV TCID50
Hours post-infection
Hours post-infection
F
Relative MFI RSV-infected cells (GFP+)
C
Unstimulated
Pre-treated with IFN
IAV pfu/m
IAV pfu/m
Hours post-infection
Hours post-infection
C1
STAT1 -/-
IRF9 -/-
Luc
WT
K81R
R292Q
Q127H
R292C
Δex7
G
% of PIV-infected cells (GFP+)
D
Unstimulated
Pre-treated with IFN
VSV TCID50/ml
VSV TCID50/ml
Hours post-infection
Hours post-infection
H
Relative MFI PIV-infected cells (GFP+)

Figure 2.6. IRF9 is required for optimal control of viral infections. (A) WB confirms the efficiency of RNAi of IRF9 or MAVS in primary dermal fibroblasts. (B-F) Primary human dermal fibroblasts previously transfected with the indicated siRNA (negative control, IRF9, MAVS) were tested for control of HRV, RSV, and PIV. Cells were infected with HRV-A16 at MOI of 10 (B), RSV at MOI of 0.5 (C & D), or PIV3 at MOI of 0.1 (E & F). Relative HRV transcripts (B) were measured by qRT-PCR and values were normalized to the siNeg control. % infected cells (C & E) and relative virus per infected cell (D & F) were measured by flow cytometric analysis of GFP positive cells. MFI of GFP positive cells in individual samples were normalized to negative control at 24 hours (D, F). Shown are the mean ± SD of six (B-F) experiments. *, $p < 0.05$; **, $p < 0.01$, by Kruskal-Wallis test.

Figure 2.6

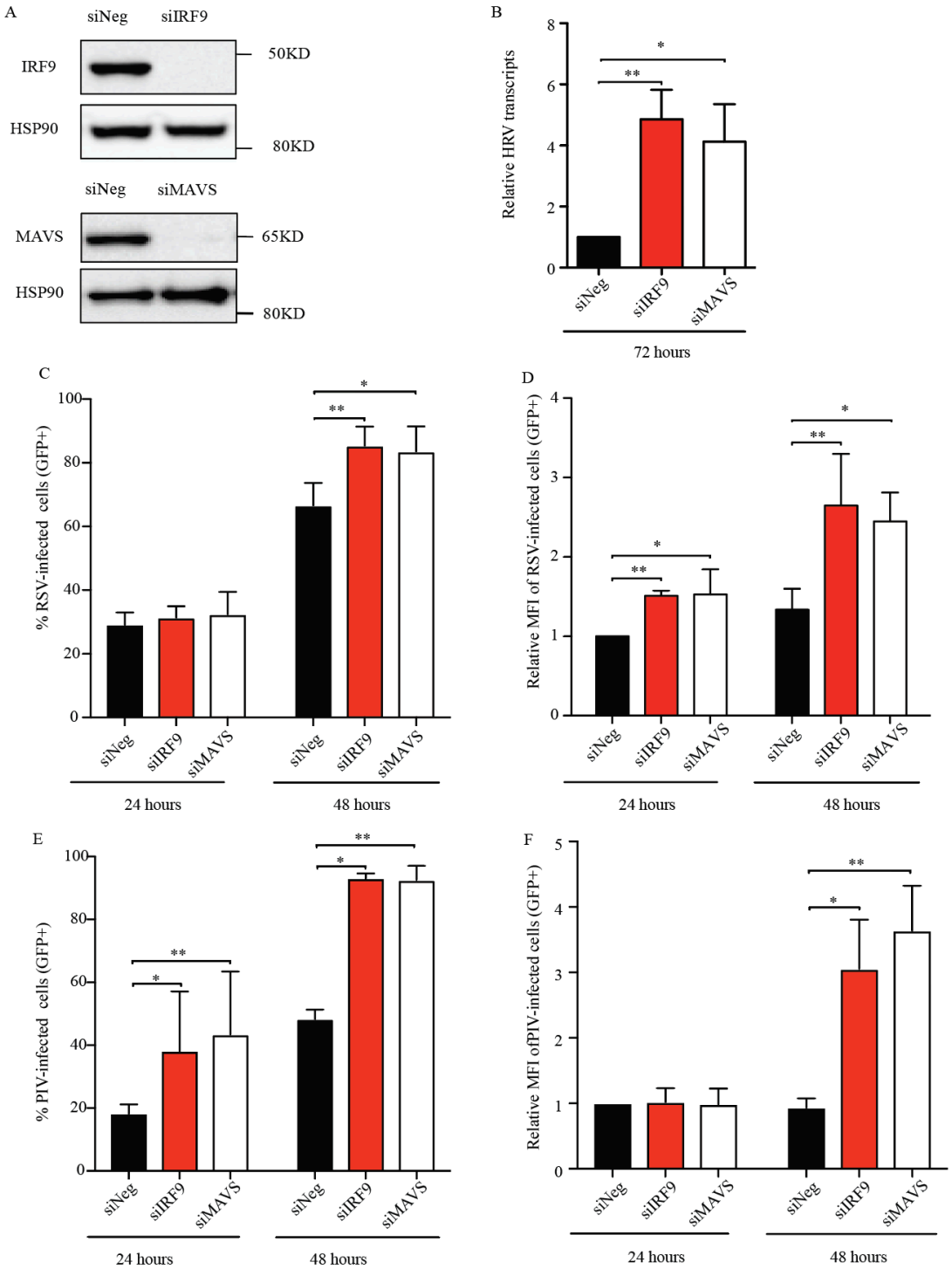
A
siNeg
siIRF9
IRF9
50KD
HSP90
80KD
siNeg
siMAVS
MAVS
65KD
HSP90
80KD
B
Relative HRV transcripts
siNeg
siIRF9
siMAVS
72 hours
C
% RSV-infected cells (GFP+)
24 hours
48 hours
D
Relative MFI of RSV-infected cells (GFP+)
24 hours
48 hours
E
% PIV-infected cells (GFP+)
24 hours
48 hours
F
Relative MFI ofPIV-infected cells (GFP+)
24 hours
48 hours

Figure 2.S1

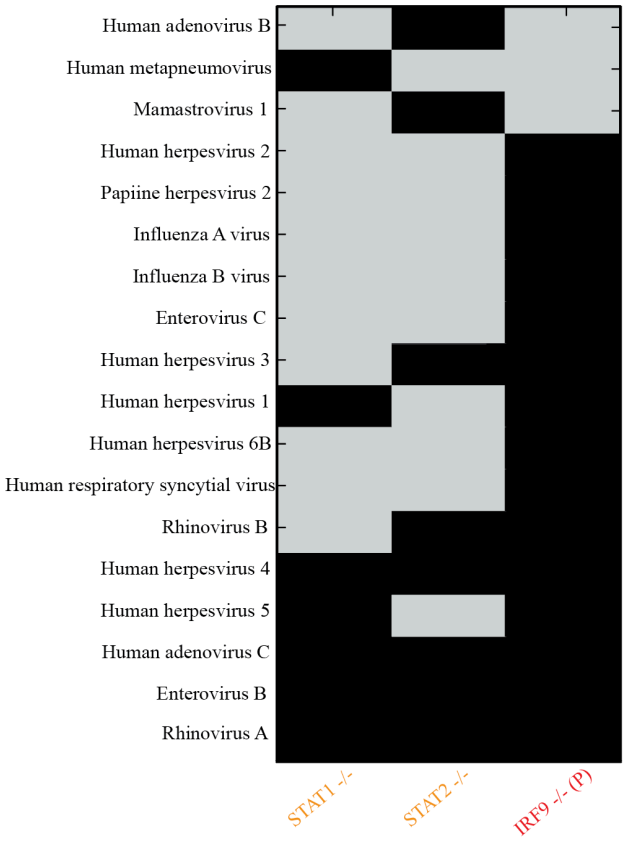

Figure 2.S1. VirScan analysis of specific anti-viral antibodies detected in patient sera. Positive identification requires antibodies recognizing at least three epitopes specific to a given virus. Positive cells are colored black, whereas negative cells are colored light grey.

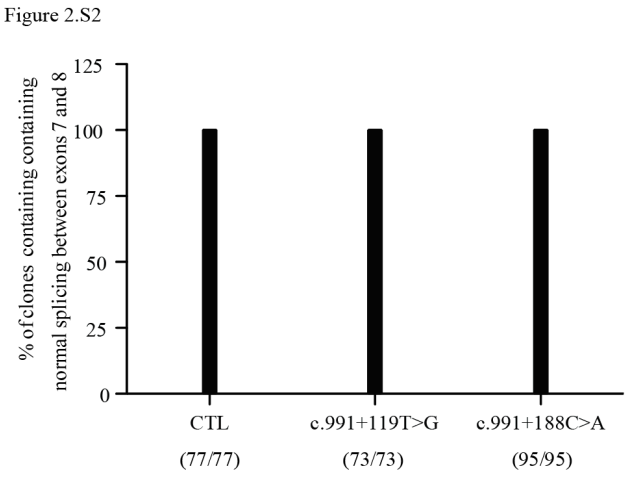

Figure 2.S2. *IRF9* splicing in patients with c.991+119T>G and c.991+188C>A mutations. cDNA sequencing was performed to detect the splicing of *IRF9* mRNA in patients heterozygous for mutations in a possible alternatively spliced transcript which retains an additional exon between exons 7 and 8 of the canonical transcript. cDNAs were generated from patient and control (CTL) F-SV40 cells. Numbers of total and abnormal clones sequenced are indicated. Results are representative of two experiments.

Figure 2.S3

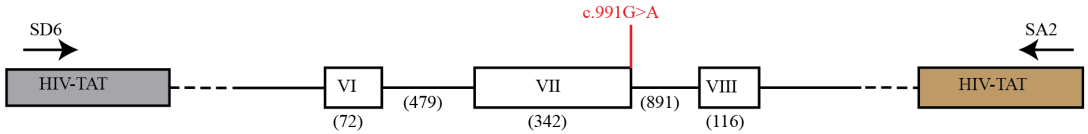

Figure 2.S3. Exon trapping scheme. Diagram of *IRF9* mRNA in the region containing exon 7 inserted into the pSPL3 exon trapping system with or without the c.991G>A mutation indicated with a vertical red line. Exons are depicted as boxes while noncoding sequences are lines. Primers used in cDNA sequencing are demonstrated, and the nucleotide lengths of the features are shown in parenthesis. HIV-TAT sequences present in the pSPL3 vector are colored grey and brown.

Table 2.S1. Rare homozygous or possible compound heterozygous variants found by exome sequencing of P. Genes listed in red are homozygous while those in black may be compound heterozygous or may occur on the same allele. † indicates a gene containing a stop-gain mutation, while ‡ indicates a gene that is predicted to be related to PIDs via a connectome analysis[100].

BCAR3	TMEM1	TGM6	APEX2‡	FAM189B	CATSPERD	IRF9‡
TOP2A‡	CHAMP2	CDH26	CBFA2T3‡	GCFC2	XRN2‡	BRDT
NBAS	DACT2†	NINL	BMP6‡	MAP3K15‡	ENTHD1†	
NUMA1	UBTPF	SLC12A	GBGT1†	CXCL11	CCSER1	
ABHD4	RP11	COG1	TPCN1	PLCB4	MAPT	

Table 2.S2. Immunophenotyping of P's lymphocytes. Clinical immunophenotyping was performed on fresh PBMCs isolated from the patient at age 2. Standard values for a child in this age range are given on the right, and atypical values are bolded.

Parameter	Patient values	Normal range for 2-5 years old
Total lymphocytes (cells/µL)	4100	
T lymphocytes		
CD3+ %	57	56 - 75
CD3+	2337	1400 - 3700
CD4+ %	32	28 - 47
CD4+	1312	700 - 2200
CD8+ %	18	16 - 30
CD8+	738	490 - 1300
CD45RO+/CD4+ %	36.5	
CD45RA+/CD4+ %	63.5	73 - 86
CD31+/CD4+%	58	
CD31+/CD45RA/CD4+ %	**48**	57 - 65
B lymphocytes		
CD21++CD24+/CD19+ %	87	
CD27+ IgD+/CD19+ %	**4**	4.6 - 16.3
CD27- IgD+/CD19+ %	86	69.2 - 90.5
CD24++CD38++/CD19+ %	4	
CD24++D38++CD27-IgD+/CD19+ %	5	
CD24-CD38++/CD19+ %	0.2	
CD21-CD38-/100 lymphocytes	3	
CD19+ %	**32**	7.6 - 28.2
CD19+	**1312**	319 - 1244
CD27+/CD19+ %	10	7 - 24.3
CD27+ IgD-/CD19+ %	6	2.7 - 12.5
NK lymphocytes		
CD16+CD56+ %	9	4 - 17
CD16+CD56+	369	130 - 720
Diverse T lymphocyte markers		
CCR7-CD45RA+/CD8+ %	**13**	16 - 28
CCR7+CD45RA+/CD8+ %	52	52 - 68
CCR7-CD45RA-/CD8+ %	**29**	11 - 20
CCR7+CD45RA-/CD8+	**6**	3 - 4

Table 2.S3. Proliferation of P's lymphocytes. Lymphocytes were isolated from P's blood and stimulated with the given antigens. Cell numbers were assessed on day 3 (PHA) or day 6 (all other stimuli).

Condition	**Cell number** (cpm/10^3)
Non stimulated (day 3)	1.6
PHA	67
Non stimulated (day 6)	1.1
Tuberculin	71
Candidin	59
Tetanus	2.5
Cytomegalovirus	2.5
Herpes simplex virus	5.5

Chapter 3:

Inherited IFNAR1 deficiency as a genetic etiology for adverse reactions to MMR and yellow fever virus live vaccines[2]

[2] Chapter 3, and portions of the materials and methods, are edited from: Hernandez, N. *et al.* Inherited IFNAR1 deficiency in otherwise healthy patients with adverse reaction to measles and yellow fever live vaccines. *The Journal of Experimental Medicine* jem.20182295 (2019). doi:10.1084/jem.20182295
This manuscript can currently be found at http://jem.rupress.org/content/early/2019/07/02/jem.20182295.
Author contributions are available in the acknowledgements section of this thesis, in addition to being more fully elaborated in the manuscript itself.

Introduction

There are currently eleven live attenuated viral (LAV) vaccines in use worldwide, all of which have been shown or suspected to cause life-threatening disease in rare individuals. To date, inborn errors of immunity have been shown to underlie severe disease due to three LAV vaccines, in at least some patients. Patients with agammaglobulinemia due to an inborn errors of T or B cells can develop vaccine-associated paralytic poliomyelitis following administration of the live (oral) poliovirus vaccine[120]. Similarly, patients with severe combined immunodeficiencies can develop life-threatening dehydration following administration of the oral rotavirus vaccine[123]. Lastly, a life-threatening vaccine-strain mumps infections has been reported in a single patient with RAG1 deficiency and a lack of T and B cell adaptive immunity[124]. More recently, a number of defects within genes that control cellular responses to type I and/or III IFNs, including STAT1 and STAT2 (both of which mediate type I and III IFN signaling), and IFNAR2 (which mediates type I IFN signaling alone), have been described in patients with disseminated measles infections following MMR vaccination[49–51,116]. Additional defects in the type I IFN signaling pathway have also been associated with adverse reaction to the MMR vaccine. One patient with a complete deficiency in IRF7, which controls the amplification of type I and III IFNs, developed a self-limiting rash post vaccination. The IRF9 deficient child described in Chapter 2, meanwhile, experienced a biliary perforation of unknown etiology one week after MMR vaccination[41,125]. These defects are unable to account for the majority of adverse reactions to the MMR vaccine. Genetic causes have not been established for severe adverse reactions to live vaccines for rubella virus, yellow fever virus (YFV), influenza virus, VZV, vaccinia virus, or hepatitis A virus. We studied two

otherwise healthy patients who developed disseminated, life-threatening disease following LAV vaccination: a 9-year-old Iranian boy who developed disease following MMR vaccination at 1 year and whose younger sister died at 1 year following MMR vaccination, and a 14-year-old Brazilian girl who developed disease following YF vaccination at age 12.

Results

Two unrelated patients with adverse reactions to LAV vaccines

We studied two unrelated patients whose pedigrees are shown in Figure 3.1A, and for whom full case reports are available in the materials and methods section. Patient 1 (P1) was born to consanguineous parents in Iran and had no notable past medical history. He presented at one year of age with disseminated vaccine-strain measles (Fig. 3.1A), roughly ten days after inoculation with the MMR vaccine. The patient developed a generalized exanthem, fever and neurological symptoms consistent with encephalitis. Analysis of P1's cerebrospinal fluid (CSF) demonstrated leukocytosis (350 lymphocytes/uL, 2 neutrophils/uL), and PCR for measles was positive both in blood and CSF. A computed tomography (CT) of P1's brain evidenced mild cerebral edema. P1 recovered and is now 9 years old. He remains in good health, without experiencing subsequent life-threatening infections. Additionally, P1 had a younger sibling who died four weeks after routine MMR vaccination at age 1 year, although no material from this child was available for genetic analysis. Finally, P1's mother electively terminated a third pregnancy following prenatal genetic identification of the same homozygous variant in *IFNAR1* that was present in P1. Patient 2 (P2) is a 14 year-old Brazilian girl born to non-

consanguineous parents (Fig. 3.1A). P2 had no significant medical history until age 12, when she presented with fever, hypotension, vomiting, and lethargy seven days following YF vaccination. She became obtunded, developed severe renal and hepatic dysfunction, and ultimately required intubation and mechanical ventilation. YFV RNA was detected in the patient's blood by PCR at this time, and a CT scan of her chest demonstrated pleural effusions and atelectasis (Fig. 3.1B). Sequencing of the YFV recovered from the patient confirmed that the vaccine-strain YFV, rather than an environmental strain, was the cause of her illness (Fig. 3.S1)[126]. On this basis, a diagnosis of yellow fever vaccine-associated viscerotropic disease (YEL-AVD) was made. She does not belong to any known risk groups for YEL-AVD, which include the elderly, individuals with autoimmune diseases such as lupus, and those who have undergone thymectomy for thymoma treatment[127]. Two years after recovery, P2 remains healthy. Especially notable in this context, P2 received two MMR vaccinations at 12 and 16 months of age, as well as the oral poliovirus and BCG vaccines, without incident. Serological analysis detected neutralizing antibodies against YFV in levels associated with seroprotection, and seropositivity to measles, rubella, diphtheria, and tetanus antigens, indicating that her adaptive immune responses were intact.

Bi-allelic private nonsense or splicing *IFNAR1* variations in the patients

We hypothesized that inborn errors of immunity may underlie these patients' vaccine-related diseases. To test this, we first performed WES analysis on both patients. Principal component analysis confirmed the ethnicities of the two families, and the percentage of homozygosity in P1 and P2's exomes (2.9% and 0.25%, respectively) was consistent with P1 being born to consanguineous parents[96]. We proceed to analyze each patients' exome for the presence of copy number variations and single nucleotide

variations. We first filtered out common variants (those with a MAF >0.01), as well as noncoding and synonymous single nucleotide variations, excepting those that were predicted to disrupt essential splice sites. We then removed variants that were predicted to be benign (that is, those with a CADD score below the MSC), and variants that occur in frequently damaged genes (those with a GDI >13.84)[98,99,101]. Lastly, we investigated a model of AR inheritance and discarded all variants that were not found either in the homozygous or compound heterozygous states in these individuals. In P1, 48 variants in 39 genes passed our filtering criteria, including a private homozygous mutation in *IFNAR1*, c.674-2A>G (Table 3.S1). In P2, we identified two variants in *IFNAR1*, c.783G>A;p.W261X and c.674-1G>A, in addition to 9 other variants in 5 genes passing our filtering criteria (Table 3.S1) (Fig. 3.1C). The *IFNAR1* gene encodes one subunit of the heterodimeric receptor for the type I IFNs, and is therefore critical for functional type I IFN signaling[128,129]. The three *IFNAR1* mutations are predicted to be deleterious either by disrupting the same essential splice site, (c.674-2A>G and c.674-1G>A, in P1 and P2, respectively), or by creating a premature stop codon (p.W261X in P2). All three *IFNAR1* variants were absent from online databases including 1000 Genomes, Bravo, and gnomAD (Fig. 3.1D). The three variants were confirmed by Sanger sequencing of the patients and their relatives, which also verified that the variants present in P2 occurred on different alleles, consistent with the hypothesis of an AR pattern of inheritance (Figs. 3.1A and 3.S2A). Seven nonsynonymous *IFNAR1* variants were found in homozygosity in gnomAD, none of which were predicted to affect splicing or introduce a premature stop codon (Figure 1D). The lack of known loss-of-function mutations in *IFNAR1*, combined with the rarity of nonsynonymous mutations, indicates that mutations that may affect IFNAR1 function

are selected against. Altogether, these findings suggested that the two patients suffered from AR IFNAR1, a novel and rare inborn error of immunity.

The three mutant *IFNAR1* alleles encode truncated proteins

We then set out to investigate the consequences of the mutations in the patients' *IFNAR1* alleles on transcription and translation of their gene products. In particular, we hypothesized that c.674-1G>A and c.674-2A>G mutations would lead aberrantly spliced transcripts, as they occur at the essential splice acceptor site of exon 6 (Fig. 3.1C). To test this, we amplified *IFNAR1* cDNAs generated from the patients' or a healthy control's SV40-F cells (Figs. 3.2A, 3.S2B & C) and Sanger sequenced individual cDNA clones. Significantly, all *IFNAR1* transcripts present in healthy control cells contained normal splicing at exon 5-6 and 6-7 junctions, whereas three alternative splice products were observed in P1 and P2. In both P1 and P2, approximately 60% of transcripts lacked exon 6, while 30-40% of transcripts lacked the first 24 base pairs of exon 6. Deletion of the entirety of exon 6 introduces a frameshift and a premature stop at aa 228 (p.V225AfsX228), while deletion of the first 24 base pairs in exon 6 results in an in-frame deletion of aa 225 to 232 (p.V225_P232del). Additionally, a trace amount of transcripts utilized an alternative pair of splice donor and acceptor sites within intron 5 to introduce a 56 bp segment into the *IFNAR1* transcript (Fig. 3.S2B). These transcripts were visible by DNA electrophoresis, but were not initially detected by cDNA sequencing. The introduction of this sequence would result in the introduction of a stop codon after three aa (p.T224_V225insESTX). For simplicity, we will refer to these mutations as V225fs, V225_P232del, and T224ins, respectively. In addition to the previously described transcripts, about 10% of transcripts

isolated from P2's cells were found to contain normal splicing at the exon 5-6 and 6-7 junctions. In all such cases, the transcripts also contained the nonsense mutation c.783G>A, p.W261X (subsequently W261X). Western blot analysis of HEK293T cells overexpressing the 4 patient-derived transcripts and WT *IFNAR1* transcripts showed that all 4 proteins can be expressed, albeit with correspondingly lower molecular weights than the WT protein (Fig. 3.2B). These findings suggested that any proteins encoded by the three mutant *IFNAR1* alleles are unlikely to be functional.

The patients' *IFNAR1* alleles abrogate IFNAR1 expression and signaling

We then hypothesized that the patients' *IFNAR1* alleles may impact *IFNAR1* mRNA or protein expression and function. To test this, we first performed qRT-PCR on patients' cells, detecting a significant reduction of *IFNAR1* mRNA when compared with healthy controls, consistent with nonsense-mediated decay of some transcripts (Fig. 3.S2D). To confirm if this decrease in mRNA level would be reflected in the level of IFNAR1 protein in their cells, we then analyzed the patients' cells by both western blotting and flow cytometry, utilizing distinct monoclonal antibodies for each technique (Figs. 3.2C, 3.2D, 3.2F, and 3.S3A). Significantly, IFNAR1 expression was not detectable by either method in patients' SV40-F and B-LCL cells when compared with healthy controls or patients with other defects in the type I IFN signaling pathway, such as IRF7 -/-, STAT1 -/-, STAT2 -/-, and IRF9 -/- patients (Figs. 3.2C, 3.2D, 3.2F, and 3.S3A). Consistent with earlier studies on TYK2 deficient cells, we found IFNAR1 expression to be highly diminished in the absence of TYK2, though not completely abolished[130]. To determine if IFNAR1 was necessary for the stability of its co-receptor, or vice-versa, we also examined

IFNAR2 expression levels in all cell lines (Figs 3.S3B, 3.S3D). Both IFNAR1 and IFNAR2 were normally expressed in the absence of the other, consistent with current models of ligand binding which predict that IFNAR1 binds to an IFN-IFNAR2 complex to initiate signaling[33]. Although IFNAR1 expression was not detectable in either fibroblastic or lymphoid cell lines derived from the patients, we cannot exclude the possibility that IFNAR1 may be properly expressed in other cell types.

To establish the consequences of IFNAR1 deficiency on type I IFN signaling, we next assessed phosphorylation of STAT1 and STAT2 in the patients' SV40-F cells following stimulation with IFN-α2b (Fig. 3.2E). No phosphorylation of STAT1 or STAT2 could be observed in the patients' cells under these conditions, unlike healthy control cells. Importantly, STAT1 was normally phosphorylated following IFN-γ stimulation, in P1 and P2's cells, indicating that the defective phosphorylation observed upon type I IFN stimulation was not due to any global issue impacting JAK-STAT signaling. Consistent with these data, downstream consequences of type I IFN signaling were also affected. Classic ISGs such as *MX1* and *IFIT1* were upregulated in healthy control SV40-F cells in response to IFN-α2b and IFN-β, but no such upregulation was observed in P1 or P2's cells. Interestingly, *CXCL9* induction in patients' cells in response to IFN-γ stimulation was intact, and actually elevated to a level above that of healthy controls (Fig. 3.2G). Previous reports in mice had indicated that the IFNAR1 receptor provides an essential scaffolding function for the type II IFN receptor, and that type II IFN signaling may be reduced in the absence of IFNAR1[131]. Our data do not support the existence of a similar mechanism in humans. The qRT-PCR experiments described here indicated that the patients' cells have significant defects in type I IFN signaling that lead to impairment of *MX1* and *IFIT1*

induction comparable to the impairment observed in other patients with deficiencies in this pathway, including STAT1, STAT2, IRF9, and IFNAR2 deficiencies. We therefore conclude that the absence of responses to IFN-α2b and -β in the patients' fibroblasts is consistent with IFNAR1 deficiency.

Impaired antiviral immunity in the patients' fibroblasts

Next, to assess if the defect in type I IFN signaling in the patients' cells affected their ability to control viral infections *in vitro*, we inoculated patient and healthy control SV40-F cells with VSV following pretreatment of the cells with type I IFN or not (Fig. 3.3A). VSV is exquisitely sensitive to type I IFN and is commonly used to assess the competency of this pathway during infection[132]. Healthy control cells that were pretreated with IFN-α2b were able to control VSV replication by 24 hpi, while replication was not suppressed in the patients' cells, nor in cells from IFNAR2, STAT1, STAT2, and IRF9 deficient patients (Fig. 3.3A). We then tested whether a similar defect in control of viral replication occurred following infection with YFV-17D, a vaccine strain of the yellow fever virus highly similar to the one which caused P2's infection (Fig. 3.3B). Both patients' cells displayed an inability to control YFV-17D replication following pre-treatment with IFN-β, when compared with cells from healthy controls. Interestingly, IRF7 deficient cells were able to control YFV-17D replication to the same degree as healthy controls, in the presence or absence of exogenous IFN-β, while STAT1, STAT2, IRF9, and IFNAR2 deficient cells were unable to control infection in either condition (Fig. 3.3B). This may suggest that IRF7 deficient cells can induce expression of at least some type I IFNs in response to YFV-17D. To test this, we quantified the production of IFN-β, the

predominant type I IFN produced by these fibroblasts, during the course of viral infection (Fig. 3.S3G). Significantly, P1 and P2's SV40-F cells were able to produce elevated amount of IFN-β following infection with YFV-17D when compared with healthy controls, confirming that the defective antiviral immunity was a consequence of abolished IFN responses rather than due to diminished IFN production in the patients' cells (Fig. 3.S3G). Similarly, IFN-β expression in the IRF7 deficient cells was normal, consistent with earlier reports that IFN-β production may not require IFNAR1- or IRF7-dependent amplification[133]. These data strongly suggest that a lack of type I IFN signaling underlies the patients' cell-intrinsic immune defects *in vitro*.

We next hypothesized that the patients' cellular phenotypes may be caused by the lack of full-length IFNAR1, and tested this by transducing the patients' fibroblasts with WT *IFNAR1*, *IFNAR2*, or an empty vector (EV). Significantly, IFNAR1 expression levels were only rescued in cells that had been transduced with WT *IFNAR1* (Figs. 3.S3C and 3.S3E). Consistent with our hypothesis, only transduction of WT *IFNAR1* restored the patients' responses to type I IFN, as assessed by induction of *MX1* and *IFIT1* following stimulation with IFN-α2b or -β (Fig. 3.3C). Similarly, only transduction with WT *IFNAR2* could rescue the type I IFN signaling defect in cells deficient in IFNAR2, confirming the non-redundancy of these proteins. Importantly, patient cells transduced with WT *IFNAR1* were able to better control viral replication than cells transduced with *IFNAR2* or an EV, indicating that the patients' cellular defect in innate immunity is, at least partially, a product of IFNAR1 deficiency (Figs. 3.3D, 3.3E, 3.S3F, and 3.S3H). We hypothesized, as well, that IFNAR1 deficiency in P1 and P2's cells may result in a broader cellular susceptibility than might be expected from their clinical histories, similar to the IRF9 deficient patient

described in Chapter 2. To test this, we infected patients' cells with IAV (A/CA/07/2009/H1N1 strain) and HSV-1, two viruses the patients had been exposed to without developing severe disease (Figs. 3.S4A-F). Consistent with previous viral challenges, both HSV-1 (Figs. 3.S4A-D) and IAV (Figs. 3.S4E & F) replicated to higher titers in the patients' SV40-F cells than in cells from healthy controls. We additionally questioned whether the patients' defects in IFNAR1 signaling might result in susceptibility to other flaviviruses, including non-attenuated viruses which they may not have encountered. To test this, we inoculated the patients' SV40-F cells with either YFV-Asibi, the WT YFV strain from which YFV-17D was developed, or dengue virus and monitored viral titer (Figs. 3.S4G-J). In agreement with all other viruses tested, both patients displayed an inability to control YFV-Asibi or dengue virus replication that could not be rescued by pretreatment with exogenous IFN-β when compared to cells from a healthy control (Figs. 3.S4G-J). It is also likely significant that all defects in the type I IFN signaling pathway result in an extremely similar virological phenotype *in vitro*, though not, apparently, *in natura*. Collectively, these data establish that AR IFNAR1 deficiency results in a broad defect in fibroblast-intrinsic immunity *in vitro* and underlies measles vaccine disease in P1 (and by inference in his deceased sister), as well as YEL-AVD in P2.

Discussion

This work describes AR IFNAR1 deficiency in two unrelated families suffering from severe, vaccine-related diseases. Significantly, AR IFNAR2, STAT1, and STAT2 deficiencies have also been shown to underlie life-threatening complications following MMR vaccination (Table 3.1), while IRF7 and IRF9 deficiency may lead to a poorly

characterized, seemingly less severe susceptibility to measles vaccine disease[41,49–52,114,116,125]. Patients deficient in JAK1 or TYK2 have not been reported to experience disease following MMR vaccination, which may be a consequence of the impaired but not abolished responses to type I IFNs in these cells[73–75,134]. Altogether, these data suggest that control of vaccine-strain measles virus may be mediated by a set of genes jointly regulated by human IFNAR1, IFNAR2, STAT1, and STAT2, and perhaps by IRF7 and IRF9[117,118]. It is notable that IFNAR1 and IFNAR2 deficiencies both result in measles virus vaccine related-disease while deficiency in IL-10RB, a subunit of the type III IFN receptor, has not been reported to produce this phenotype[71,135–137]. Consistent with these studies, the high incidence of measles virus vaccine-related disease in patients with abolished type I IFN signaling suggests that this pathway may be more critical for defense against the vaccine-strain virus than type III IFN signaling. Taken together, these studies therefore identify a nidus of susceptibility to severe MMR disease in the type I IFN signaling pathway, but they do not wholly untangle the mechanism of this susceptibility. Additional consideration of the precise transcriptional consequences of various defects within this pathway may provide insight into this question.

Our data also provide the first genetic explanation for YEL-AVD, demonstrating that AR IFNAR1 deficiency may underlie this rare condition[127]. Although the YF vaccine was among the first dozen vaccines developed, YFV remains a global health threat[138]. Given declining rates in YF vaccination and growing concerns over vaccine safety, validity aside, it is increasingly important to understand the pathogenesis of adverse reactions to LAV vaccines. Furthermore, the study of YFV and its vaccine is of interest to studies of other flaviviruses, and may have implications on the development of vaccines or treatments

for emerging pathogens such as Zika virus. Following this reasoning, the uncertainty regarding the cause(s) of YEL-AVD has accelerated attempts to develop an inactivated alternative vaccine[139–141]. Concurrently, vaccines against dengue virus and Japanese encephalitis virus, constructed from chimeric YF viruses in which specific prM-E sequences are introduced into the YF vaccine virus backbone, are the basis of ongoing clinical trials with controversial results[142–144]. A better understanding of the pathogenesis of YFV infections, both environmental and vaccine-related, is therefore obviously critical to the successful development of safer vaccines related to YFV-17D. Importantly, studies aiming to detect YFV-17D viremia in healthy vaccine recipients typically found virus within 5-7 days following vaccination, and no deficiency of adaptive immunity has been found in individuals with YEL-AVD[145–147]. Furthermore, the YFV-17D virus has been found to promote the induction of critical type I IFN mediators such as STAT1 and IRF7 in humans, and recent work in mice has shown that intact type I IFN signaling is critical for control of YFV-17D[148–151]. Consistent with this report, then, these other studies suggest that YEL-AVD is more likely to be a result of a defect in innate or intrinsic immunity, rather than in adaptive immunity. In this way, our data provide the first genetic etiology of YEL-AVD, while strengthening the suspicion that other defects in type I IFN pathway may underlie additional cases of YEL-AVD.

Most strikingly, these two patients harboring bi-allelic *IFNAR1* variants have survived until the ages of 9 and 14 without any clinically significant viral infections other than the LAV-associated complications. Counter to this extremely narrow clinical phenotype, a patient with combined partial IFNAR1 and complete IFNGR2 deficiencies was recently reported who suffered from an HCMV infection, in addition to BCG

disease[152]. However, due to the digenic defects in this patient's innate immune system, causal attribution of the phenotypes remains problematic. In this regard, we note that both P1 and P2 were IgG^+ and IgM^- for HCMV, and HCMV DNA was not detected in their plasma by PCR. These data confirm that P1 and P2 had been exposed to HCMV without developing overt disease. One possible explanation for this difference would be incomplete penetrance with respect to the HCMV susceptibility phenotype, although, given the previous patient's combined deficiencies in IFNAR1 (partial) and IFNGR2 (complete), a more accurate explanation may be that this patient's defect in type II IFN signaling was significantly involved in the pathogenesis of his disease. This latter hypothesis would also be consistent with the occurrence of HCMV disease in a few patients with complete IFNGR1 or IFNGR2 deficiency[153–156]. We advance three hypotheses which may explain the surprisingly robust anti-viral defense in the two patients with AR complete IFNAR1 deficiency; first, the *IFNAR1* splice allele is hypomorphic in at least some cell types that were not tested, and in which some type I IFN signaling is preserved. Second, IFNAR1 is redundant for some type I IFNs, for at least some ISGs, analogous to signaling through the IFN-β-IFNAR1 complex described in mice[157]. Lastly, a third hypothesis is that IFNAR1 and all type I IFNs are redundant for immunity against most viruses, at least in certain conditions of infection. In this context, it is worth considering patients with IFNAR2, STAT2, or IRF9 deficiency, which impair responses to type I IFNs, and responses to type III IFNs in the cases of STAT2 and IRF9 deficiency. These patients are demonstrate normal resistance to a broad range of viruses, including HCMV, and have frequently survived until 5-11 years of age[49–52,125]. Conversely, all patients with complete STAT1 deficiency, and therefore impaired responses to type I, type II, and type III IFNs, died by 2 years of various

viral or bacterial infections, unless they had received both hematopoietic stem cell transplantation and IgG substitution[29,112,116,158]. Through future studies describing patients with similar defects in innate immunity, we hope to address these hypotheses, to better understand the mechanisms of protective immunity to viruses, and to develop safer vaccines against viral diseases to accommodate patients with inborn errors of type I and/or type III IFNs.

Figure 3.1. Three private *IFNAR1* variants are present in two kindreds associated with life-threatening LAV vaccine disease. (A) Pedigrees of the IFNAR1-deficient families. Double lines connecting two parents indicate consanguinity. The probands are indicated by an arrow. Filled shapes identify affected individuals while open shapes identify unaffected individuals. Asterisks demarcate those individuals who received vaccination against YFV. The pregnancy of a third sibling in pedigree 1 (homozygous for the same mutation as P1) was terminated at 16 weeks of gestational age. (B) CT scan of P2's chest demonstrating pleural effusions and atelectasis following YF vaccination (red arrow). (C) Schematic illustration of the *IFNAR1* gene with 11 coding exons and of the IFNAR1 protein with its 4 fibronectin type-III subdomains (SD1-4). The signal peptide is denoted "SP" and the transmembrane domain "TM". The exons are numbered in roman numerals (I-XI). The previously reported *IFNAR1* variant is indicated in blue, while those of P1 and P2 are indicated in red. (D) Population genetics of homozygous coding missense and predicted loss of function *IFNAR1* mutations taken from GnomAD and in-house cohorts. The patients' variants are private and shown in red and green, while seven variants detected in gnomAD are shown in black. (CADD: Combined Annotation Dependent Depletion; MAF: Minor allele frequency; MSC: Mutation Significance Cutoff).

Figure 3.1

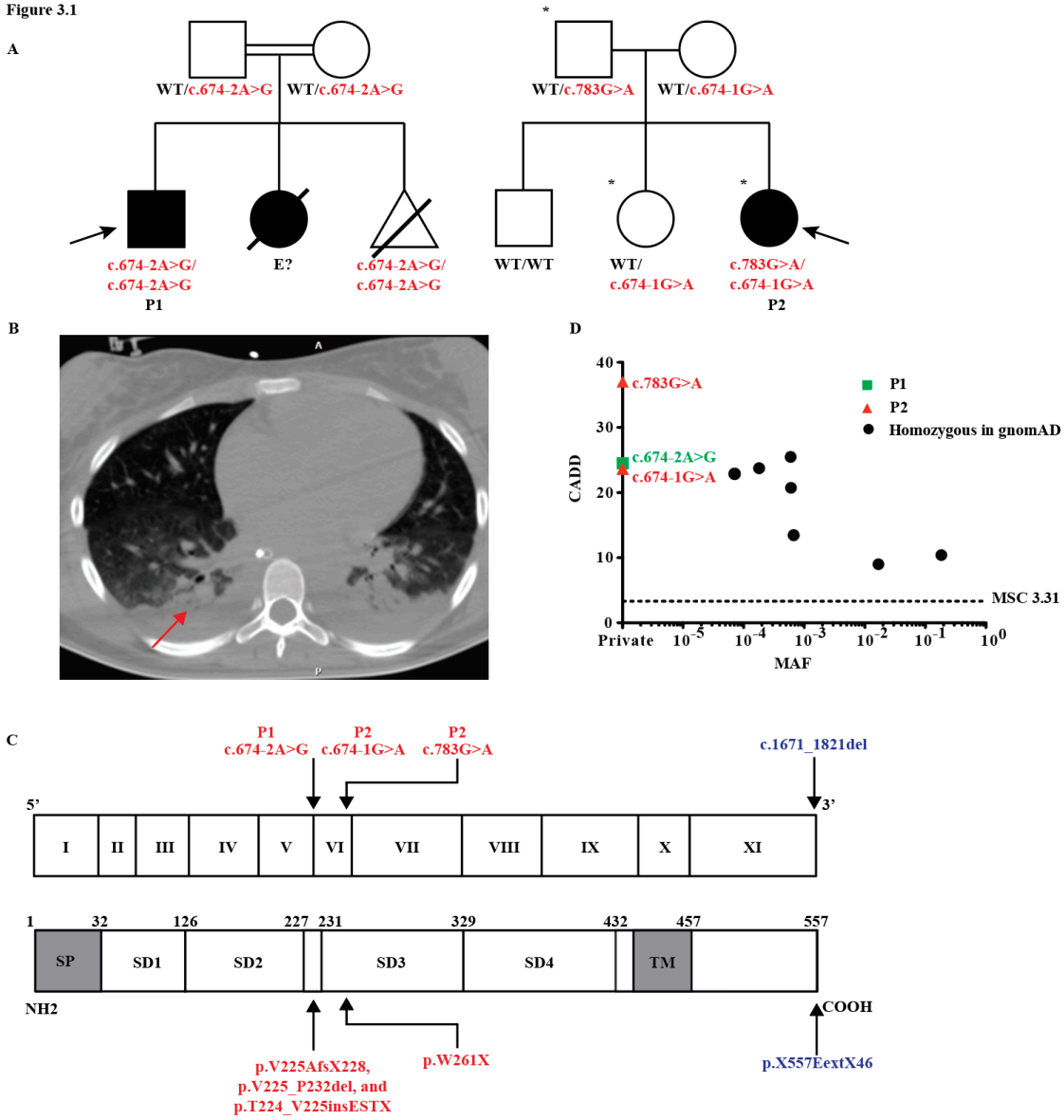
A
WT/c.674-2A>G
WT/c.674-2A>G
WT/c.783G>A
WT/c.674-1G>A
*
*
*
c.674-2A>G/
c.674-2A>G
P1
E?
c.674-2A>G/
c.674-2A>G
WT/WT
WT/
c.674-1G>A
c.783G>A/
c.674-1G>A
P2
B
D
c.783G>A
c.674-2A>G
c.674-1G>A
P1
P2
Homozygous in gnomAD
CADD
MSC 3.31
Private
MAF
C
P1
c.674-2A>G
P2
c.674-1G>A
P2
c.783G>A
c.1671_1821del
5'
3'
I
II
III
IV
V
VI
VII
VIII
IX
X
XI
1
32
126
227
231
329
432
457
557
SP
SD1
SD2
SD3
SD4
TM
NH2
COOH
p.V225AfsX228,
p.V225_P232del, and
p.T224_V225insESTX
p.W261X
p.X557EextX46

Figure 3.2. Impact of *IFNAR1* variants on type I IFN signaling. (A) cDNA sequencing results demonstrate aberrant splicing of *IFNAR1* mRNA from patients' SV40-F cells. The percentage of positively identified transcripts is indicated. At least 150 transcripts were sequenced for each individual. The black numbers under the schematic representations indicate the positions of the included elements relative to their start sites. Results are representative of two experiments. (B) Western blot of IFNAR1 in HEK293T cells transiently transfected with IFNAR1 constructs; GAPDH was used as a loading control. A representative blot from three experiments is shown. (C) Western blot of endogenous IFNAR1 in SV40-F cells from three healthy controls (C1, C2, and C3), P1, P2, IRF7-deficient (IRF7 -/-), IFNGR2-deficient (IFNGR2 -/-), TYK2-deficient (TYK2 -/-), STAT1-deficient (STAT1 -/-), STAT2-deficient (STAT2 -/-), IRF9-deficient (IRF9 -/-), and IFNAR2-deficient (IFNAR2 -/-) patients. A representative blot from three experiments is shown. (D & F) Mean fluorescence intensity (MFI) of IFNAR1 staining on SV40-F (D) and B-LCL (F) cells from three healthy controls (C1, C2, and C3 or T1, T2, and T3), P1, P2, IRF7-deficient (IRF7 -/-), IFNGR2-deficient (IFNGR2 -/-), IFNGR1-deficient (IFNGR1 -/-), TYK2-deficient (TYK2 -/-), STAT1-deficient (STAT1 -/-), STAT2-deficient (STAT2 -/-), and IRF9-deficient (IRF9 -/-) patients as assessed by flow cytometry. Mean (n=3) and SEM are shown. (E) Western blot analysis of phosphorylated STAT1 (pSTAT1) and STAT2 (pSTAT2) levels in SV40-F cells stimulated with 1000 U/ml of IFN-α2b or -γ for 20 minutes. Cells were from two healthy controls (C1, C2), P1, P2, IFNGR2-deficient (IFNGR2 -/-), STAT1-deficient (STAT1 -/-), STAT2-deficient (STAT2 -/-), and IFNAR2-deficient (IFNAR2 -/-) patients. A representative blot from two experiments is shown. (G) Transcription levels of *MX1*, *IFIT1,* and *CXCL9* assessed by

qRT-PCR on SV40-F cells treated with 1000 U/ml of either IFN-α2b, -β, or -γ for 2 hours. Cells were from three healthy controls (C1, C2, and C3), P1, P2, IRF7-deficient (IRF7 -/-), IFNGR2-deficient (IFNGR2 -/-), TYK2-deficient (TYK2 -/-), STAT1-deficient (STAT1 -/-), STAT2-deficient (STAT2 -/-), IRF9-deficient (IRF9 -/-), and IFNAR2-deficient (IFNAR2 -/-) patients. Mean (n=3) and SEM are shown.

Figure 3.2

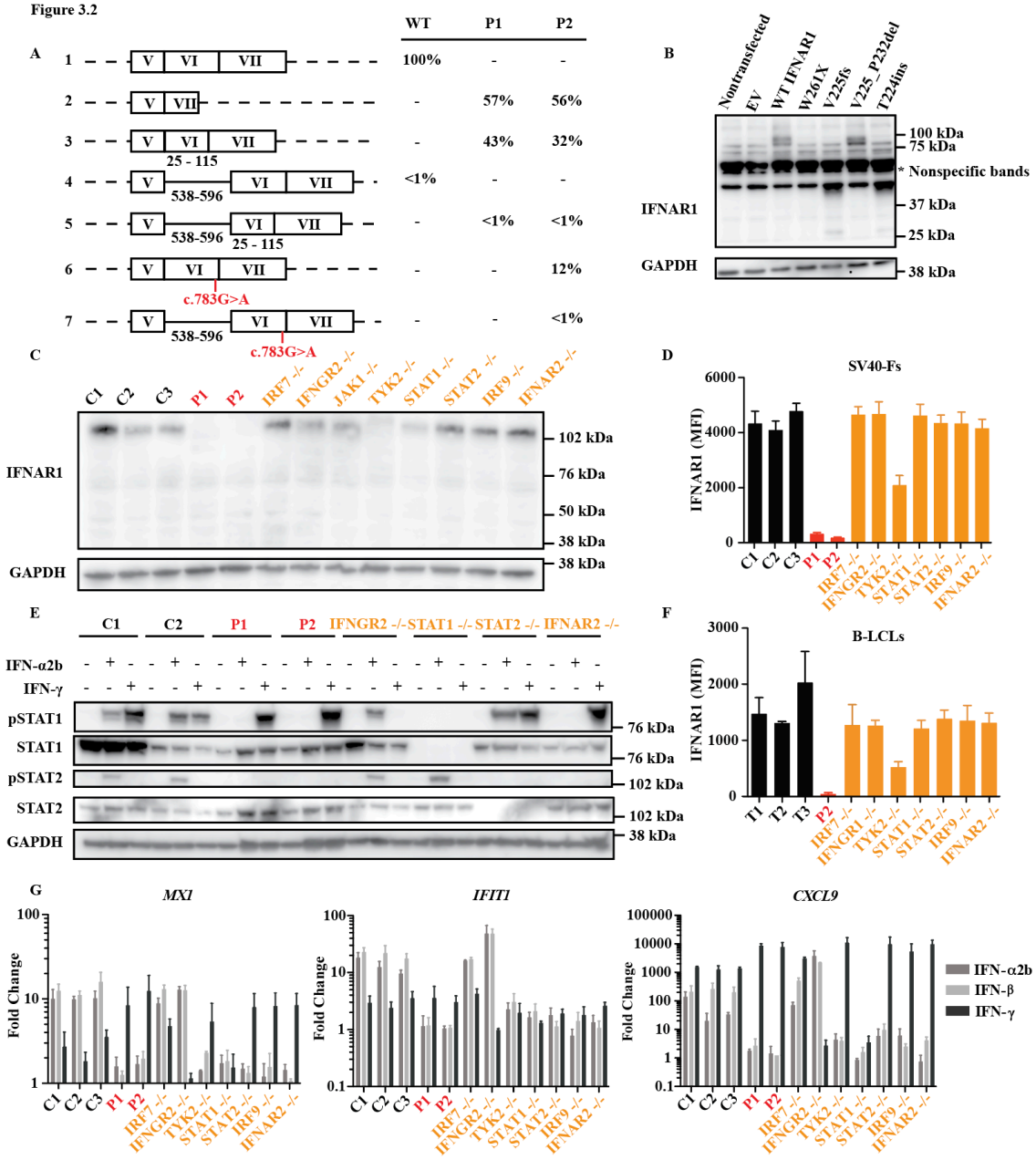
A
WT
P1
P2
100%
57%
56%
43%
32%
<1%
<1%
<1%
12%
<1%
V
VI
VII
25 - 115
538-596
c.783G>A
B
Nontransfected
EV
WT IFNAR1
W261X
V225fs
V225_P232del
T224ins
100 kDa
75 kDa
* Nonspecific bands
37 kDa
25 kDa
38 kDa
IFNAR1
GAPDH
C
C1
C2
C3
P1
P2
IRF7 -/-
IFNGR2 -/-
JAK1 -/-
TYK2 -/-
STAT1 -/-
STAT2 -/-
IRF9 -/-
IFNAR2 -/-
102 kDa
76 kDa
50 kDa
38 kDa
D
SV40-Fs
IFNAR1 (MFI)
E
IFN-α2b
IFN-γ
pSTAT1
STAT1
pSTAT2
STAT2
F
B-LCLs
T1
T2
T3
G
MX1
IFIT1
CXCL9
Fold Change
IFN-α2b
IFN-β
IFN-γ

Figure 3. IFNAR1 is required for type I IFN-mediated cell intrinsic immunity to viral infections. (A) VSV titers in SV40-F cells unstimulated (left) or pre-treated (right) with 1000 U/ml IFN-α2b for 16 hours, followed by VSV infection at an MOI of 3. Cells from three healthy controls were included (C1, C2, and C3), as well as those from P1, P2, IRF7-deficient (IRF7 -/-), STAT1-deficient (STAT1 -/-), STAT2-deficient (STAT2 -/-), IRF9-deficient (IRF9 -/-), and IFNAR2-deficient (IFNAR2 -/-) patients. Mean (n=3) and SEM are shown. (B) YFV titers in SV40-F cells unstimulated (left) or pre-treated (right) with 1000 U/ml IFN-β for 16 hours, followed by infection with YFV-17D at MOI = 0.05. Mean and range (n=2) are shown. Cells from three healthy controls were included (C1, C2, and C3), as well as those from P1, P2, IRF7-deficient (IRF7 -/-), STAT1-deficient (STAT1 -/-), STAT2-deficient (STAT2 -/-), IRF9-deficient (IRF9 -/-), and IFNAR2-deficient (IFNAR2 -/-) patients. (C) Transcription levels of *MX1, IFIT1,* and *CXCL9* assessed by qRT-PCR on SV40-F cells treated with 1000 U/ml of IFN-α2b, -β, or -γ for 2 hours. Cells were from a healthy control, P1, P2, and an IFNAR2-deficient patient that were either transduced with WT *IFNAR1*, WT *IFNAR2*, or an empty vector. Mean (n=3) and SEM are shown. (D) SV40-F cells were infected with YFV-17D at an MOI of 0.05 and the percent of cells positive for YFV viral proteins was assessed by flow cytometry. Cells were from a healthy control, P1, P2, and an IFNAR2-deficient patient (IFNAR2 -/-) and were transduced with either WT *IFNAR1*, WT *IFNAR2*, or an empty vector (EV), and stimulated with 1000 U/ml IFN-β for 16 hours prior to infection. Mean and range (n=2) are shown. (E) SV40-F cells were infected with MeV at an MOI of 0.1 and viral titer was assessed at the given time points. Cells were from a healthy control, P1, P2, and an IFNAR2-deficient patient (IFNAR2 -/-) and were transduced with either WT *IFNAR1*, WT *IFNAR2*, or an empty vector (EV), and stimulated with 1000 U/ml IFN-α2b for 16 hours prior to infection. Mean and SEM (n=3) are shown.

Figure 3.3

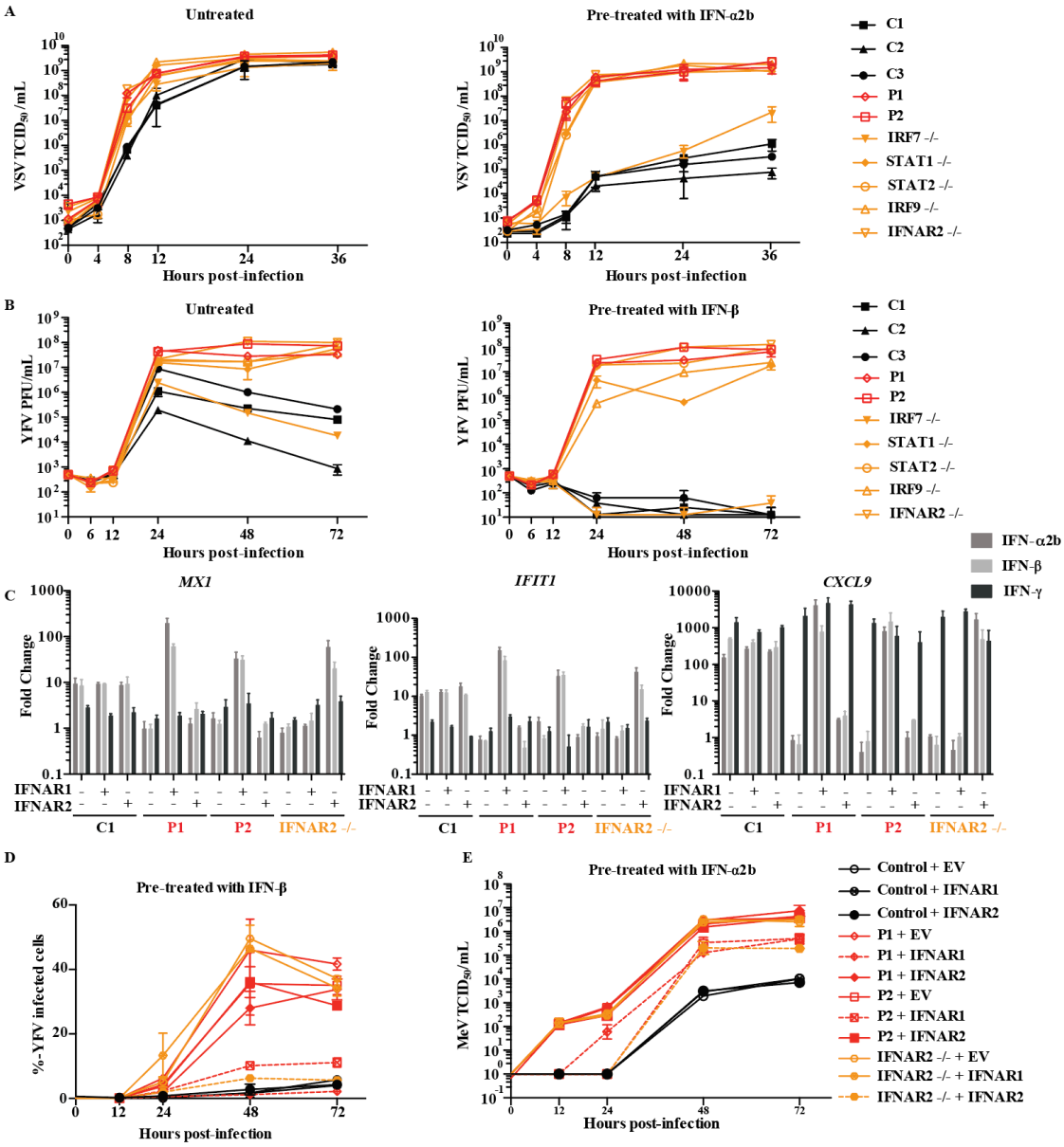
A
Untreated
Pre-treated with IFN-α2b
VSV TCID50/mL
Hours post-infection
C1
C2
C3
P1
P2
IRF7 -/-
STAT1 -/-
STAT2 -/-
IRF9 -/-
IFNAR2 -/-
B
Untreated
Pre-treated with IFN-β
YFV PFU/mL
Hours post-infection
IFN-α2b
IFN-β
IFN-γ
C
MX1
IFIT1
CXCL9
Fold Change
IFNAR1
IFNAR2
C1
P1
P2
IFNAR2 -/-
D
Pre-treated with IFN-β
%-YFV infected cells
Hours post-infection
E
Pre-treated with IFN-α2b
MeV TCID50/mL
Hours post-infection
Control + EV
Control + IFNAR1
Control + IFNAR2
P1 + EV
P1 + IFNAR1
P1 + IFNAR2
P2 + EV
P2 + IFNAR1
P2 + IFNAR2
IFNAR2 -/- + EV
IFNAR2 -/- + IFNAR1
IFNAR2 -/- + IFNAR2

Table 3.1. Patients suffering from MMR vaccine-related disease. Patients with known defects in the type I IFN signaling pathway who are reported to have experienced LAV vaccination are described here. Their age at development of MMR disease, last known follow-up, and clinical course are summarized.

Genetic Defect	Age at first MMR infection (months)	Age (years) at last known followup (deaths indicated by *)	Clinical manifestations
STAT2 P1[51]	18	5	P1: 6 d following MMR vaccination, the patient developed fever, rash, conjunctivitis, and lymphadenopathy, followed by hepatitis and pneumonitis requiring supplemental oxygen. Patient recovered from MMR infection.
STAT2 P2, P3[52]	12, 13	3, 2.5	P2: 1 wk after MMR vaccination, the patient developed a febrile illness. Readmitted 1 mo later with opsoclonus-myoclonus and lymphocytes in the CSF. Readmitted again at 2.5 yrs with impaired renal and liver function, opsoclonus-myoclonus, and seizures. Patient recovered from MMR infection. P3: 1 wk after MMR vaccination, the patient developed a febrile illness, anemia, and lymphopenia. CSF was positive for mumps virus by PCR. Readmitted at 15 mo due to persistent fever and malaise, eventually developed septic shock and metabolic acidosis. Patient recovered from MMR vaccination.
STAT2 P4, P5[50]	24, 18	7*, 11	P4: 1 wk after MMR vaccination, the patient developed a morbilliform rash, tonsillitis, conjunctivitis, lymphadenopathy, hepatosplenomegaly, and arthritis. Patient recovered from MMR infection. Patient experienced frequent severe viral infections during the first 3 yr and died at 7 yr of fulminant viral infection. P5: 1 wk after MMR vaccination, the patient developed disseminated measles, complicated by hepatitis and pneumonitis. Patient recovered from MMR infection.

IFNAR2[49]	13	1.4*	6 d after MMR vaccination, the patient developed a marked injection-site reaction and generalized morbilliform skin rash, recurrent maculopapular rash, fever, and intractable seizures. Patient died on 81 d after vaccination.
IRF7[41]	12	9	1 wk after MMR vaccination, the patient developed a rash suggestive of measles. Patient recovered from MMR infection. Patient also suffered from a life-threatening influenza infection at 3 yr.
IRF9[125]	16	5	2 wk after MMR vaccination, the patient developed an idiopathic biliary perforation. Patient recovered from MMR infection. Patient also suffered a life-threatening influenza infection at 2 yr, parainfluenza virus at age 4, and recurrent fevers without a causative pathogen identified throughout her childhood.
STAT1[116]	13	2	1 week after MMR vaccination, patient developed fever, irritability, rash, and diarrhea, encehpalitis, hemophagocytic lymphohistiocytosis-like syndrome, and was positive for human herpesvirus 6. Patient was readmitted 7 d later with refusal to walk, unsteady gait, and inflammatory cells in the CSF. Patient recovered from MMR infection.
IFNAR1 P1 (this report)	12	9	10 d after MMR vaccination, patient developed a generalized exanthema, fever, and encephalitis. Patient recovered from MMR infection.

Figure 3.S1

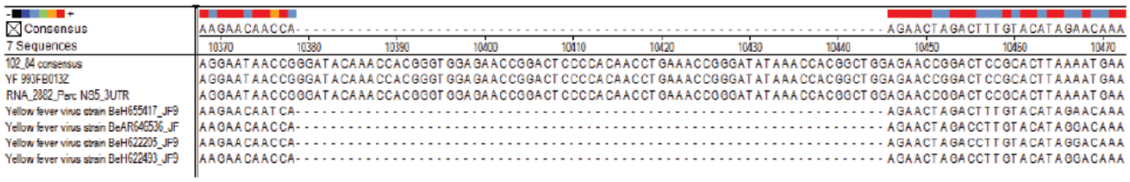

Figure 3.S1. Evidence of YFV virus infection in P2. Sanger sequencing alignments demonstrating an identical insertion in the YFV genome recovered from P2 during her infection. The consensus WT YFV sequence is shown in the top row, while two YFV-17D strains (102_84 and YF993FV013Z) sequenced are directly below that, followed by the sequence from the YFV isolated from the patient (RNA_2882). Environmental YFV isolates are shown in the bottom four rows.

Figure 3.S2. Genetic analysis of IFNAR1 deficient patients. (A) Sanger sequencing chromatograms demonstrating c.674-2A>G, c.674-1G>A, and c.783G>A mutations in patient DNA (black arrows). (B) Agarose gel electrophoresis of *IFNAR1* cDNA products generated from patient mRNA transcripts. The upper image shows subtle changes in the size of the full-length transcript (expected length of 1674 base pairs), while the bottom image demonstrates that additional alternatively spliced mRNAs can be detected at low abundances when only exons IV through VII are amplified, as depicted schematically in C. Numbers in blue correspond to the structure of the transcripts present in a given band, as diagrammed in figure 2A, with nucleotide lengths in parentheses. Representative image from two experiments. (C) Diagram of the *IFNAR1* gene in the region containing exon 6. Exons are depicted with boxes, while introns are depicted with lines. mRNA transcripts from this region were amplified by PCR and inserted into the pGEM-T Easy system. Mutations present in patient cells are indicated with vertical red lines. Primers used in cDNA sequencing are demonstrated (5'-ATAGCTTAGTTATCTGGAAAAACTCTTCAGGTG-3', F; 5'-GGGTAGTTTTGACATTTTCACAGTCAGG-3', R), and the nucleotide lengths of the features are shown in parentheses. (D) qRT-PCR measuring *IFNAR1* mRNA levels in SV40-F cells from P1, P2, three healthy controls (C1, C2, and C3), IRF7-deficient (IRF7 -/-), IFNGR2-deficient (IFNGR2 -/-), TYK2-deficient (TYK2 -/-), STAT1-deficient (STAT1 -/-), STAT2-deficient (STAT2 -/-), IRF9-deficient (IRF9 -/-), and IFNAR2-deficient (IFNAR2 -/-) patients. *IFNAR1*/*GUS* mRNA ratios are shown after normalization to C1. Mean (n=3) and SEM are shown.

Figure 3.S2

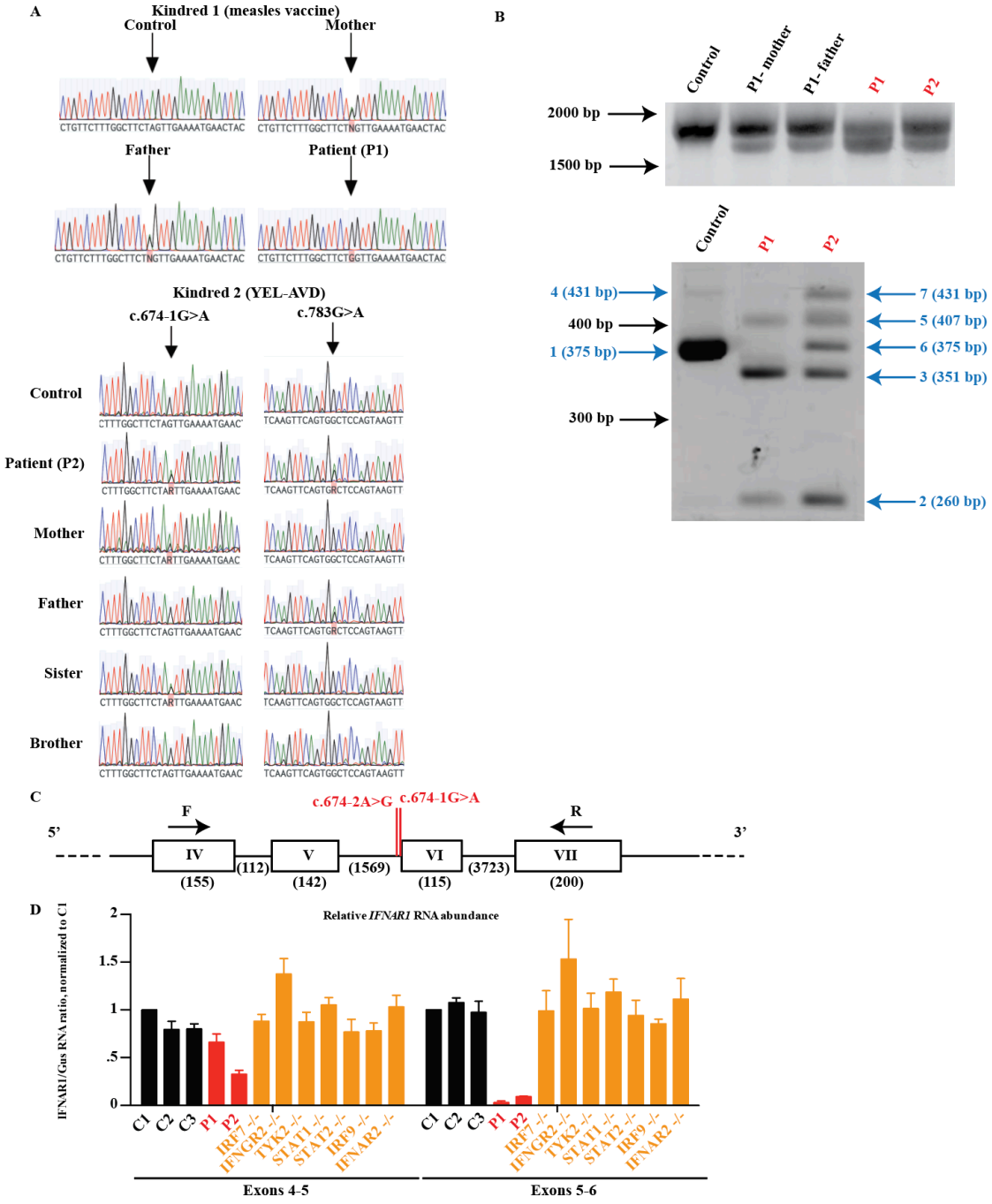
A
Kindred 1 (measles vaccine)
Control
Mother
Father
Patient (P1)
CTGTTCTTTGGCTTCTAGTTGAAAATGAACTAC
CTGTTCTTTGGCTTCTNGTTGAAAATGAACTAC
CTGTTCTTTGGCTTCTNGTTGAAAATGAACTAC
CTGTTCTTTGGCTTCTGGTTGAAAATGAACTAC
Kindred 2 (YEL-AVD)
c.674-1G>A
c.783G>A
Control
Patient (P2)
Mother
Father
Sister
Brother
CTTTGGCTTCTAGTTGAAAATGAAC
TCAAGTTCAGTGGCTCCAGTAAGTT
CTTTGGCTTCTARTTGAAAATGAAC
TCAAGTTCAGTGRCTCCAGTAAGTT
B
Control
P1- mother
P1- father
P1
P2
2000 bp
1500 bp
4 (431 bp)
400 bp
1 (375 bp)
300 bp
7 (431 bp)
5 (407 bp)
6 (375 bp)
3 (351 bp)
2 (260 bp)
C
c.674-2A>G
c.674-1G>A
F
R
5'
3'
IV
V
VI
VII
(155)
(112)
(142)
(1569)
(115)
(3723)
(200)
D
Relative IFNAR1 RNA abundance
IFNAR1/Gus RNA ratio, normalized to C1
C1
C2
C3
P1
P2
IRF7 -/-
IFNGR2 -/-
TYK2 -/-
STAT1 -/-
STAT2 -/-
IRF9 -/-
IFNAR2 -/-
Exons 4-5
Exons 5-6

Figure 3.S3. Disrupted function of the type I IFN signaling pathway in patient cells. (A) Western blot of endogenous IFNAR1 in B-LCL cells from three healthy controls (T1, T2, and T3), P2, IRF7-deficient (IRF7 -/-), IFNGR1-deficient (IFNGR1 -/-), TYK2-deficient (TYK2 -/-), STAT1-deficient (STAT1 -/-), STAT2-deficient (STAT2 -/-), IRF9-deficient (IRF9 -/-), and IFNAR2-deficient (IFNAR2 -/-) patients; GAPDH was used as a loading control. A representative blot from three experiments is shown. (B & D) IFNAR2 mean fluorescence intensities (MFI) from patient SV40-F (B) and B-LCL (D) cells stained with an anti-IFNAR2 fluorescent antibody. Cells were from three healthy controls (C1, C2, and C3 or T1, T2, and T3), P1, P2, IRF7-deficient (IRF7 -/-), IFNGR2-deficient (IFNGR2 -/-), IFNGR1-deficient (IFNGR1 -/-), TYK2-deficient (TYK2 -/-), STAT1-deficient (STAT1 -/-), STAT2-deficient (STAT2 -/-), IRF9-deficient (IRF9 -/-), and IFNAR2-deficient (IFNAR2 -/-) patients and were assessed by flow cytometry. Mean (n=3) and SEM are shown. (C) Western blot of IFNAR1 in SV40-F cells from a healthy control, P1, P2, and an IFNAR2-deficient (IFNAR2 -/-) patient transduced with WT *IFNAR1*, WT *IFNAR2*, or an empty vector; GAPDH was used as a loading control. A representative blot from two experiments is shown. (E) Mean fluorescence intensities (MFI) of SV40-Fs from a healthy control, P1, P2, and an IFNAR2-deficient (IFNAR2 -/-) patient and transduced with WT *IFNAR1,* WT *IFNAR2,* or an empty vector (EV) and stained with an anti-IFNAR1 antibody. Mean (n=3) and SEM are shown. (F & H) Survival rates following VSV infection of primary fibroblasts either untreated (F) or pre-treated (H) with 1000 U/ml IFN-α2b for 24 hours prior to infection. Cells were from a healthy control, P1, and an IFNAR2-deficient patient that were either transduced with an empty vector (EV), WT *IFNAR1* (IFNAR1), or WT *IFNAR2* (IFNAR2). Mean (n=3) is shown. (G) IFN-β levels detected in the supernatant

of SV40-F cells either 0 or 24 h after infection with YFV-17D. Cells from two healthy controls (C1 and C2), P1, P2, an IRF7 deficient patient (IRF7 -/-), and a STAT1-deficient patient (STAT1 -/-) were included. The limit of quantitation (LOQ) is indicated by a dotted line. Mean (n=2) and range are shown.

Figure 3.S3

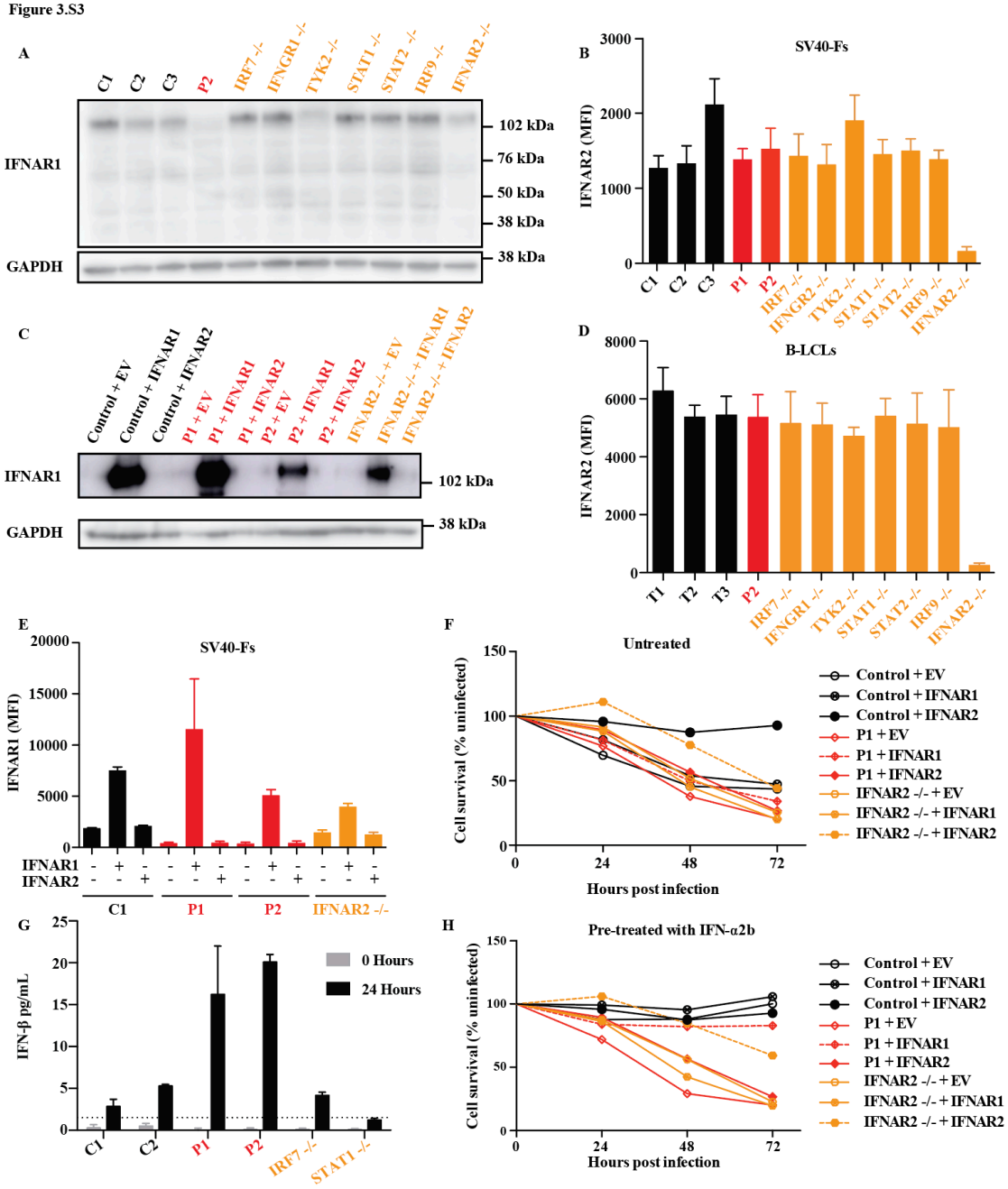
A
C1
C2
C3
P2
IRF7 -/-
IFNGR1 -/-
TYK2 -/-
STAT1 -/-
STAT2 -/-
IRF9 -/-
IFNAR2 -/-
IFNAR1
GAPDH
102 kDa
76 kDa
50 kDa
38 kDa
38 kDa
B
SV40-Fs
IFNAR2 (MFI)
C
Control + EV
Control + IFNAR1
Control + IFNAR2
P1 + EV
P1 + IFNAR1
P1 + IFNAR2
P2 + EV
P2 + IFNAR1
P2 + IFNAR2
IFNAR2 -/- + EV
IFNAR2 -/- + IFNAR1
IFNAR2 -/- + IFNAR2
IFNAR1
GAPDH
102 kDa
38 kDa
D
B-LCLs
IFNAR2 (MFI)
T1
T2
T3
P2
E
SV40-Fs
IFNAR1 (MFI)
IFNAR1
IFNAR2
C1
P1
P2
IFNAR2 -/-
F
Untreated
Cell survival (% uninfected)
Hours post infection
G
IFN-β pg/mL
0 Hours
24 Hours
H
Pre-treated with IFN-α2b
Cell survival (% uninfected)
Hours post infection

Figure 3.S4. IFNAR1 is essential for type I IFN-mediated intrinsic immunity to multiple viruses. (A & B) HSV-1-GFP replication levels, as assessed by GFP intensity, in SV40-F cells unstimulated (A) or pre-treated (B) with 1000 U/ml IFN-α2b followed by infection with HSV-1-GFP (MOI=0.01). Cells from three healthy controls were included (C1, C2, and C3), as well as those from P1, P2, IRF7-deficient (IRF7 -/-), STAT1-deficient (STAT1 -/-), STAT2-deficient (STAT2 -/-), IRF9-deficient (IRF9 -/-), and IFNAR2-deficient (IFNAR2 -/-) patients. Mean (n=2) and range are shown. (C & D) HSV-1 titers in SV40-F cells unstimulated (C) or pre-treated (D) with 1000 U/ml IFN-α2b for 16 hours, followed by infection with HSV-1 (MOI=0.01). Mean and range (n=2) are shown. Cells from three healthy controls were included (C1, C2, and C3), as well as those from P1, P2, IRF7-deficient (IRF7 -/-), STAT1-deficient (STAT1 -/-), STAT2-deficient (STAT2 -/-), IRF9-deficient (IRF9 -/-), and IFNAR2-deficient (IFNAR2 -/-) patients. (E & F) IAV titers in SV40-F cells unstimulated (E) or pre-treated (F) with 1000 U/ml IFN-α2b for 16 hours, followed by infection with (A/H1N1/CA/2009) IAV at MOI=1. Cells from three healthy controls were included (C1, C2, and C3), as well as those from P1, P2, IRF7-deficient (IRF7 -/-), STAT1-deficient (STAT1 -/-), STAT2-deficient (STAT2 -/-), IRF9-deficient (IRF9 -/-), and IFNAR2-deficient (IFNAR2 -/-) patients. Mean (n=2) and range are shown. (G & H) SV40-F cells stimulated for 16 hours with 1000 U/ml IFN-β prior to infection (H) or left untreated (G) were infected with 100 µl of YFV Asibi and viral titer was assessed by plaque assay on Huh7.5 cells at the given time points. Mean and range (n=2) are shown. Different time points represent independent infections. SV40-Fs from a healthy control, P1, P2, and an IFNAR2-deficient (IFNAR2 -/-) patient were included. (I & J) SV40-F cells stimulated for 16 hours with 1000 U/ml IFN-β prior to infection (J) or left untreated (I),

were infected with ZIKV (MOI = 0.05) and viral titer was assessed by plaque assay on Vero cells at the given time points. Mean and range (n=2) are shown. Different time points represent independent infections. SV40-Fs from a healthy control, P1, P2, and an IFNAR2-deficient (IFNAR2 -/-) patient were included.

Figure 3.S4

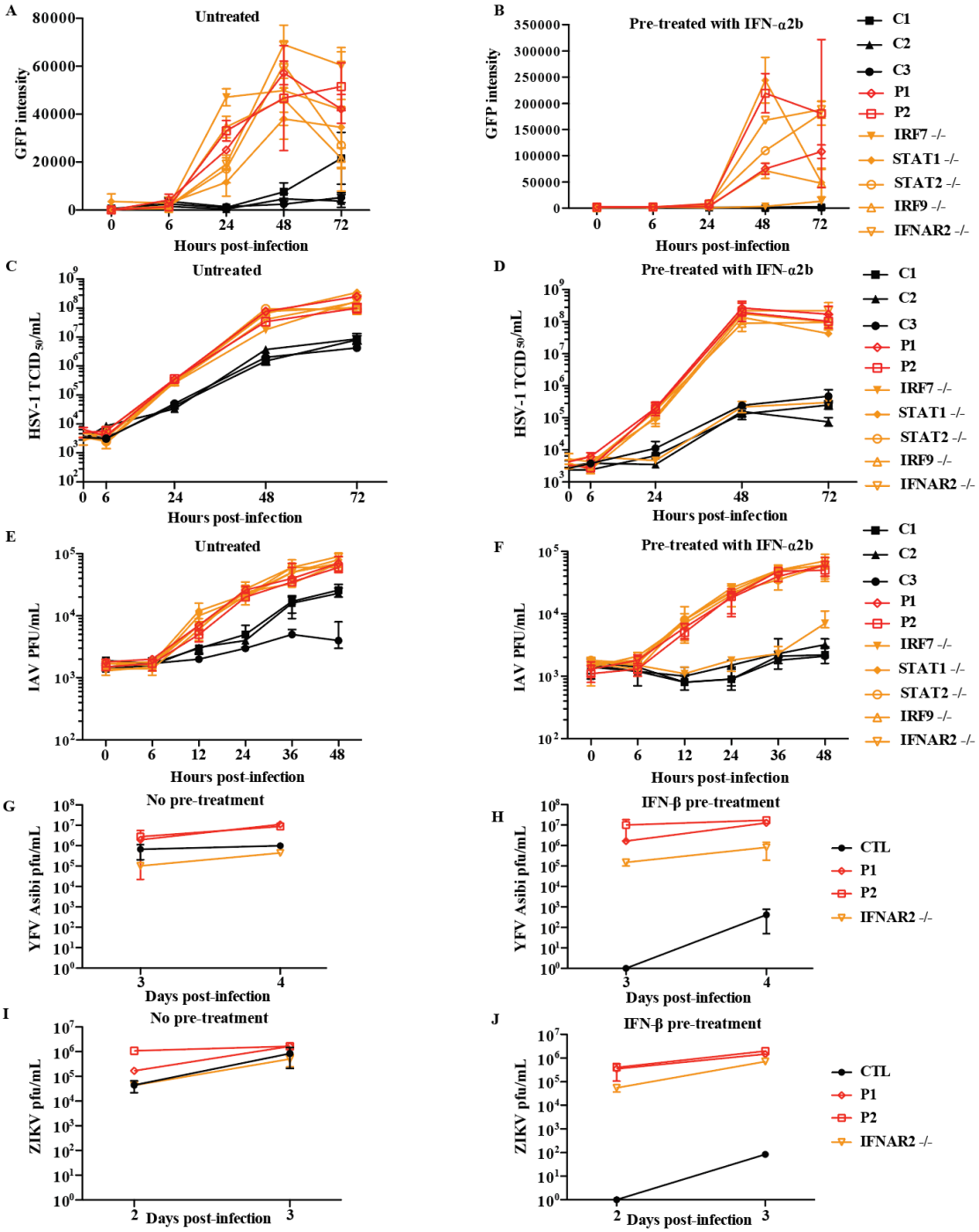
A
Untreated
GFP intensity
Hours post-infection
B
Pre-treated with IFN-α2b
GFP intensity
Hours post-infection
C1
C2
C3
P1
P2
IRF7 -/-
STAT1 -/-
STAT2 -/-
IRF9 -/-
IFNAR2 -/-
C
Untreated
HSV-1 TCID50/mL
Hours post-infection
D
Pre-treated with IFN-α2b
HSV-1 TCID50/mL
Hours post-infection
E
Untreated
IAV PFU/mL
Hours post-infection
F
Pre-treated with IFN-α2b
IAV PFU/mL
Hours post-infection
G
No pre-treatment
YFV Asibi pfu/mL
Days post-infection
H
IFN-β pre-treatment
YFV Asibi pfu/mL
Days post-infection
CTL
P1
P2
IFNAR2 -/-
I
No pre-treatment
ZIKV pfu/mL
Days post-infection
J
IFN-β pre-treatment
ZIKV pfu/mL
Days post-infection

Table 3.S1. Rare homozygous or possible compound heterozygous variants found by exome sequencing of P1 and P2. Genes listed in red are homozygous while those in black may be compound heterozygous or may occur on the same allele. † indicates a gene containing a stop-gain mutation, while ‡ indicates a gene that is predicted to be related to primary immunodeficiencies via a connectome analysis[100]. The consequences of the variations on coding sequences are given in parenthesis following each gene.

P1	P1 (cont.)	P2
URI1 (c.840_842delTGA)	KIRREL2 (c.32_34delTCC)	KCNN3 (c.G1092C)
CNTF (c.T101A, c.T494G)	CNTD2 (c.T524A)	KIAA1875-WDR97 (c.3123+1G>T, c.4750G>A)
SLC45A1 (c.130_131insCGGGAGATG)	ACSL3 (c.G1043A)	MADCAM1(c.736_737insAGGAG)
HTR2B (c.T848C)	MAFA (c.621_623delTGG)	IFNAR1†‡ (c.674-1G>A, c.G783A)
MTMR9 (c.T1153A)	TMPRSS13 (c.248_262delGGGCTGGAGATGCCT)	PIWIL3 (c.A2629C, c.A1996G)
PSG11 (c.G44C)	DYTN (c.C679T)	
MEOX2‡ (c.228_230delTGG)	THAP11 (c.367_369delCAG)	
CLN8 (c.A806T)	CXorf23 (c.1727_1728delTA)	
CNDP1 (c.43_44insTGC)	TMEM54 (c.G136A)	
MPRIP (c.534_539delCAGCAG)	NLRP10 (c.T752C)	
TMEM247 (c.382_383insAGCGGCAGCACGAGGTGGTGATGGAGCAGCTGCAGCGGG)	SESTD1 (c.A1310G)	
FADS6 (c.17_18insGATGGAACCTACGGAGCCCATGGAACCTACGGAGCCCATGGAACCTACGGAGCC)	APEX1‡ (c.953_954delTG)	
KIAA2018 (c.4410_4418delTGCTGCTGC)	DLC1‡ (c.G161T)	
ZNF407 (c.A515T, c.C4145T)	PLBD1 (c.74_76delGCA)	
SMPD1‡ (c.108_113delGTCGGC)	ANKRD62 (c.G1197C)	
TBL1Y (c.G274A)	MAML3‡ (c.1506delG)	
AOX1 (c.G173A)	RBM23 (c.1077_1078insGCC)	
BSN (c.G11015A)	HOXD9‡ (c.794_795insGCA)	
MAP3K4‡ (c.3566_3568delCTG)	DCP1B (c.782_783insGCA, c.C1532T)	
ATG3 (c.920dupT)	IFNAR1‡ (c.674-2A>G)	

Chapter 4:

Conclusions and future experiments

In my thesis research, I explored the human genetic basis of severe viral diseases in patients with inborn errors of the type I IFN signaling pathway. Unlike bacterial or fungal pathogens, viruses largely utilize the replication machinery of their hosts to multiply, exacerbating the challenge of the self/non-self conundrum at the heart of immunology. Similarly, this ability of viruses to repurpose host proteins and systems has made the development of therapeutics against viruses more difficult than has been the case for the development of antibacterials or antifungals, for example. In order to effectively treat viral diseases, it is therefore critical that we understand acutely the functions of viral effectors and how they interact with our own cells.

The experiments described herein provide striking evidence that both common and rare viral diseases may have unappreciated genetic etiologies. Notable in this regard is the discovery of AR IRF9 deficiency as a genetic basis for life-threatening influenza infections, adding to a still-growing list which includes AR IRF7, AD GATA2, and AD TLR3 deficiencies[41,64,68]. The clustering of these defects in genes related to both type I and type III IFN signaling, but not either individually, is also remarkable. Although initially thought to be largely redundant to type I IFNs, except with expression restricted to epithelial surfaces, type III IFNs have more recently been suggested to have unique functions, possibly as a consequence of altered transcriptional responses manifesting, at least partly, as a more evenly balanced pro- and anti-inflammatory responses[91,159–161]. The absence of severe influenza infections in patients lacking either type I or type III IFN receptors in isolation may indeed suggest that, *in natura*, both pathways are sufficient for control of viral replication. In mice, type III IFNs are thought to be the first IFNs produced following influenza challenge and they activate epithelial anti-viral immunity without the

inflammation associated with type I IFN activity[161]. Taken together, the available data in humans support a similar schema whereby type III IFNs are initially responsible for restricting IAV replication, with type I IFN becoming activated only when high viral burdens lead to escape from type III IFN control. Should this rule continue to hold in other cases of life-threatening influenza infections, treatment with type I and/or III IFNs may be of limited use. Instead, it may be more productive to identify the downstream restriction factors which are directly responsible for control of IAV replication and consider alternative mechanisms of inducing these factors, or otherwise mimicking their effects. Importantly, for patients with a known genetic etiology for severe influenza infections, prophylaxis via routine vaccination may likely be sufficient (as in the case of the IRF7 deficient child), although IVIgs may provide additional benefits. Further identification of genetic etiologies for severe influenza infection is certain to supplement our understanding of innate immunity while also focusing the development of anti-influenza or anti-viral therapeutics.

Conversely, the surprisingly narrow clinical phenotype of the two IFNAR1 deficient patients immediately confronts us with a profound medical mystery: how could patients with complete loss-of-function defects in such a critical pathway have survived until the ages of 9 and 14 while continuing to thrive? The most obvious hypothesis, although still exceptionally surprising, is that type I IFN related immunity is largely redundant for defense against environmental viruses in humans. Consistent with this hypothesis, the only currently described patient with AR IFNAR2 deficiency suffered a fatal encephalitis following routine inoculation with the MMR vaccine, but demonstrated no issue controlling respiratory viruses or CMV, with which they had also been infected.

This disconnect between cellular and clinical phenotypes is reminiscent of other PIDs, such as MyD88 or IRAK4 deficiencies, in which network redundancy or adaptive immunity combine to produce a relatively specific clinical phenotype[162,163]. Analogously, we might view the type I IFN response as a global anti-viral "fail-safe", with tissue-specific innate immunity coordinating with adaptive immunity to form the first line of defense. It is also possible that, rather than following from non-redundancy between type I and III IFNs, the patients' clinical specificity is due to non-redundancy with the type I IFN signaling pathway itself.

The type I IFNs are a family of pleiotropic cytokines encompassing 17 distinct proteins in humans that can further be divided into 13 IFN-αs, IFN-β, IFN-κ, IFN-ε, and IFN-ω. Intriguingly, the human type I IFNs all signal through the same heterodimeric receptor, all lack introns, and all are located on the short arm of chromosome 9. The abundance of distinct IFNs that seem functionally indistinguishable from one another has long been a mystery in the field of innate immunity. Recent work, especially that carried out by Paul Hertzog's group, has suggested there may be subtle functional differences between the type I IFNs. In mice, for example, IFN-ε is confined to the epithelium of the female reproductive tract where it is constitutively expressed and protects against viral and bacterial infections[164]. Unlike other IFNs, IFN-ε expression is hormonally regulated and was not induced by known pattern-recognition receptor (PRR) pathways[164]. Perhaps even more surprisingly, this group also demonstrated that a unique IFNAR1-IFN-β complex could assemble and productively signal in murine peritoneal exudate cells[164]. Given the evolving appreciation of non-redundancy among the various type I IFNs, another plausible explanation for the lack of overt disease in P1 and P2 is that one or more type I IFNs may

be able to coordinate with IFNAR2 in the absence of IFNAR1 and initiate an anti-viral program. The third hypothesis we advance to explain this mystery is that the patients' splice alleles are hypomorphic and that, among the hundreds of cell types within the body, some are able to generate correctly spliced *IFNAR1* transcripts, leading to expression of a functional protein and intact signaling in the type I IFN pathway. Even if the last hypothesis were found to be correct, the lack of IFN signaling we consistently observed in both lymphoid and myeloid compartments would still suggest further consideration of the first two hypotheses. In this way, our work highlights inter- and intra-network redundancies related to the type I and III IFN signaling pathways which lie at the heart of genetic susceptibility to severe viral infections.

In conclusion, the findings of my thesis could be extended in multiple ways. The identification of additional genetic etiologies for the conditions described herein will not only augment the growing body of literature demonstrating the human genetic basis of infectious diseases but will also clarify our mechanisms of anti-viral immunity. Innate immunity has armored us with a system of partially overlapping defenses whose subtlety and independence we are only beginning to grasp. The discovery of additional experiments of nature will allow us to untangle the unique aspects of the type I and III IFN signaling pathways, in addition to defining the aspects they share. With an improved understanding of innate immunity, we may expect to more ably treat the existing patients with severe viral diseases, as well as to develop additional methods of prophylaxis and prevent such diseases in the future.

EXPERIMENTAL PROCEDURES

Materials and Methods

Study Oversight

These studies were approved by the institutional review boards of The Rockefeller University, INSERM, University Hospitals Leuven, the National Institute of Infectious Diseases, Fundação Oswaldo Cruz, Rio de Janeiro, Brazil, or the National Institute of Allergy and Infectious Diseases, National Institutes of Health. Written informed consent was obtained from all patients or their guardians.

Case Reports

Chapter 2:

We report the case of a girl born in 2013 to consanguineous parents (first cousins, f=1/16) of Algerian descent, living in France, who was admitted to intensive care with acute respiratory distress secondary to infection with influenza A virus at the age of 23 months. According to her medical history, she was born after 39 weeks of gestation with a birth weight of 2910 g, height of 47 cm and Apgar score 10/10. Her family history was negative for previous severe infectious diseases.

Since the age of five months, the patient had a history of recurrent fevers (3-5 days per month) associated with digestive features including diarrhea, abdominal pain without any vomiting, transient cutaneous rash and intermittent urticaria, initially suggestive of an auto-inflammatory syndrome since no infectious agent was identified. Prior to any supportive treatment, interleukin 1 beta (IL-1β) and tumor necrosis factor alpha (TNFα) were positive, respectively at 17.9 pg/ml (0-15) and 25.1 pg/ml (0-20), whereas IL-6 and

IL-10 were normal and negative. MEFV, MVK, CIAS1, TRAPS were sequenced and found without any deleterious variation. Anti c1q antibodies were consistently positive, but sequencing of DNASE1L3 was normal.

She experienced five episodes of bronchiolitis revealing severe asthma (for which she was prescribed montelukast, albuterol, and ipratropium bromide), gingivostomatitis and adenitis, and four episodes of prolonged gastroenteritis. She was hospitalized in the pediatric intensive care unit (PICU) due to idiopathic biliary perforation 14 days after MMR vaccination at 16 months old; disseminated intravascular coagulation was suspected secondary to thrombopenia (27,000/mm3) and low prothrombin time (40%), associated with elevated liver enzymes (SGOT 274 UI/l and SGPT 128 UI/l). She was readmitted to PICU two months later with a suspicion of septic shock in the absence of a detectable pathogen, associated with elevated CRP (180 mg/l), lymphopenia (830/mm3), low platelet count (14 000/ mm3) and low PT (66%).

At 23 months of age, she was admitted to PICU with a severe influenza A infection resulting in acute respiratory distress syndrome requiring mechanical ventilation for six days. Since increased oxygen was required with cPAP (FiO2 100%), she was intubated. She developed severe acute respiratory distress syndrome, with bilateral infiltrates on chest radiography. She was placed under mechanical ventilation in a volume support mode, with a frequency of 35 per minute and 100% fiO2. All bacteriological and viral sputum culture were negative, except Influenza A virus. She was administered salbutamol, ipratropium bromide, ketamine, theophylline, magnesium sulfate, ceftriaxone and oseltamivir. The oseltamivir treatment was stopped after five days. On the third day, bilateral parotidis and cervical adenitis appeared and were treated by amoxicillin and clavulanic acid. She was

discharged from PICU after eight days, and her condition improved enough to be discharged after 22 days of hospitalization.

Standard immunological tests were performed. Serum levels of IgG, IgA, IgM were unremarkable. T and NK lymphocyte count were conserved, whereas a modest B lymphocytosis was measured. Lymphocyte proliferation was normal for PHA, tuberculin and candidin (N>50), but low in presence of tetanus, CMV and HSV antigens (N>10) (Table S1). T and B cell counts were within normal ranges. The patient was IgG seropositive for tetanus, diphtheria, haemophilus, measles, mumps, rubella and HBV (Ag HBs negative, anti HBs positive, anti HBc negative) following routine vaccination. She remained seronegative for HIV1/2, HAV, HCV, VZV, Parvovirus B19, EBV, CMV and pneumococcus despite proper vaccination for the latter.

IVIgs at 0.4g/kg/3 weeks were begun at two years and eight months of age because of recurrent viral infections, resulting in an improvement of her recurrent fever profile, digestive symptoms and susceptibility to viral infection.

Since IVIgs were started, the patient has been hospitalized on two occasions: once for acute respiratory distress secondary to metapneumovirus and once for febrile pseudo-occlusive syndrome with free fluid in Morrisson's pouch detected by sonogram secondary to symptoms of gastro-enteritis. At that time, RNA of parainfluenza 1,2,3,4 group was detected by PCR in the sputum but no pathogen was detected known to cause gastroenteritis (also negative were rhinovirus/enterovirus, metapneumovirus, influenza A and B, coronavirus, RSV A or B by PCR in the sputum, and adenovirus, norovirus, enterovirus and rotavirus by PCR in the stool). During neither episode was she admitted to PICU.

Chapter 3:

Patient 1 (P1) was born in Iran to consanguineous parents. He was evaluated at the age of one year for disseminated vaccine-strain measles. He had previously received Hepatitis B virus (HBV), BCG and influenza vaccinations without any adverse effect. Ten days after inoculation with the MMR vaccine, he presented with a generalized exanthem, fever and neurological symptoms consistent with encephalitis. Laboratory findings only showed moderate lymphocytosis with 7800 total leukocytes/uL, 29% neutrophils, 45% lymphocytes, 10% monocytes, 4% eosinophils, and mild hyponatremia. A computed tomography (CT) of the brain showed mild cerebral edema and analysis of CSF demonstrated leukocytosis (350 lymphocytes/uL, 2 neutrophils/uL). PCR for measles was positive both in blood and CSF, with negative bacterial cultures. Antibodies against measles and mumps were at the lower limit of the normal range, isohemagglutinin titers were normal and antibody responses to pneumococcal and HBV-antigens were also normal. Additionally, P1 was IgG^{+} and IgM^{-} for CMV, and CMV DNA was not detectable in his plasma. Lymphocyte subpopulations (T, B and NK cells) were in the normal range. His past medical history was characterized by frequent viral upper respiratory tract infections with a hospital admission for bronchiolitis, but was otherwise not significant. His growth and development were normal. His younger sister also developed meningoencephalitis one week after receiving MMR vaccination, and died of complications four weeks later. P1 is now 9 years old, in good health and has not manifested any other invasive infection (Figure 1A).

Patient 2 (P2) is a 14 year-old Brazilian girl born to non-consanguineous parents. Otherwise healthy until age 12, she presented with fever, hypotension, vomiting, and

lethargy 7 days following YF vaccination. Laboratory findings after admission demonstrated leukocytosis with total leukocytes at 28,200/uL, and thrombocytopenia with a platelet count of 21,000/uL. Consistent with renal and hepatic dysfunction, the patient was icteric on exam with an international normalized ratio (INR) of 2.0 and a partial thromboplastin time (PTT) of 66.4. She demonstrated ALT and AST levels of 187 IU/L and 623 IU/L, respectively, and had a creatinine of 2.71 mg/dL. Her condition rapidly deteriorated with bradycardia and diminished consciousness with a Glasgow Coma Score of 8, necessitating admission to the ICU, intubation, and mechanical ventilation. A CT of the chest demonstrated pleural effusions and atelectasis (Figure 1B). Neutralizing antibodies against YFV were detectable by plaque reduction neutralization test at a dilution titer of 1:640, as were antibodies against herpes 1 and 2 viruses, while antibodies against HAV, HBV, and HCV, as well as dengue virus and leptospirosis were negative. P2's serum was similarly IgG^+ and IgM^- against CMV antigens, with CMV DNA not detectable in her plasma by PCR. YFV was detected in the patient's blood by PCR analysis, and sequencing confirmed that this was the vaccine-strain virus, not wild-type YFV (Figure S1). A diagnosis of yellow fever vaccine-associated viscerotropic disease (YEL-AVD) was made. She was treated with an aggressive course of IV fluids, plasma and platelet transfusions, vasopressors, hydrocortisone, and was prophylactically given IV broad spectrum antibiotics. Her hypotension and thrombocytopenia resolved over the next week and, two weeks after her admission, she was discharged from the ICU and made a full recovery. One year after this episode, she remains healthy. Her circulating Ig levels and leukocyte subsets are normal. Notably, the patient received two MMR vaccines at 12 and 16 months of age,

and other live vaccines (oral poliovirus and bacillus Calmette-Guérin), without incident (Figure 1A).

Whole exome sequencing

Exome capture was performed with the SureSelect Human All Exon 50 Mb kit (Agilent Technologies). Paired-end sequencing was performed on a HiSeq 2000 (Illumina) generating 100-base reads. We aligned the sequences with the GRCh37 reference build of the human genome using the BWA aligner[165]. Downstream processing and variant calling were performed with the Genome Analysis Toolkit, SAMtools, and Picard[166,167]. Substitution and InDel calls were made with GATK Unified Genotyper. All variants were annotated using an annotation software system that was developed in-house[98,168,169].

Genetics

WES analysis of each patient revealed a total of 15,807 variants in P, 50,634 variants in P1, and 16,797 variants in P2. We filtered out all variations found in 1000 genomes database, the Genome Aggregation Database (GnomAD), our own database of 4,892 exomes for infectious diseases at a frequency of >1%, leaving 44, 48, and 11 non-synonymous coding variants in P, P1 and P2's exomes, respectively: 20, 30, and 6 were homozygous while 24, 18, and 5 were heterozygous. The heterozygous variants inherited from one parent were not considered in a model of complete penetrance. Excluding those in *IFNAR1*, none of the variants affected genes known to be related to immunity. The nonsense c.783G>A mutation had a CADD score of 37, and the two splicing mutations, c.674-1G>A and c.674-2A>G, had CADD scores of 23.6 and 24, respectively. In the IRF9 patient, excepting 4 heterozygous and 2 homozygous variants, none of the variants affected genes related to immunity. The IRF9 c.991G>A mutation had a CADD score of 32.21. A

genomic measure of individual homozygosity was plotted for the three patients, two European individuals from consanguineous families, and 37 individuals from non-consanguineous families from our in-house WES database. Homozygosity was computed as the proportion of the autosomal genome belonging to runs of homozygosity (ROHs). The ROHs were defined as ranging at least 1 Mb of length and containing at least 100 SNPs, and were estimated using the homozyg option of the PLINK software[170]. The centromeres were excluded because they are long genomic stretches devoid of SNPs and their inclusion might inflate estimates of homozygosity if both flanking SNPs are homozygous. The length of the autosomal genome was fixed at 2,673,768 kbs as previously described[171]. We estimated the selective pressure acting on IFNAR1 to be 2.762 (indicative of positive selection), by estimating the neutrality index (NI) at the population level: (PN/PS)/(DN/DS), where PN and PS are the number of non-synonymous and synonymous alleles, respectively, at population level (1000 Genomes Project) and DN and DS are the number of non-synonymous and synonymous fixed sites, respectively, for the coding sequence of *IFNAR1*[172]. We estimated the selective pressure acting on IRF9 to be 0.088 (indicative of purifying selection) with the same method.

Cells

Peripheral blood mononuclear cells (PBMCs) were isolated by Ficoll-Paque density gradient (Lymphoprep, Proteogenix) from the blood of patients and healthy donors. SV40-immortalized dermal fibroblasts, HEK293-T cells, and Vero cells were maintained in Dulbecco's modified Eagle medium (DMEM) supplemented with 10% fetal bovine serum. B-LCLs were grown in Roswell Park Memorial Institute (RPMI) 1640 medium supplemented with 10% fetal bovine serum. Primary fibroblasts were grown in DMEM/F-

12 (1:1) containing L-glutamine and Hepes supplemented with 10% fetal calf serum, amphotericin B (0.5 μg/ml), penicillin (100 U/ml) and streptomycin (100 μg/ml). For chapter 2, Stably-transfected dermal fibroblasts were obtained by transfecting pTRIPIRF9iresRFP using Lipofectamine 2000 (Invitrogen, Carlsbad, CA, USA) according to the manufacturer's protocol. Stable transfectants were selected by puromycin treatment (0.3ug/mL) and subsequent fluorescence activated cell sorting for RFP-expressing cells yielding >90% RFP^+ fibroblasts. Transfection of HEK293-T cells with IFNAR1 constructs in pCAGG-S was also accomplished using Lipofectamine 2000 (Invitrogen, Carlsbad, CA, USA) according to the manufacturer's protocol.

YFV Plaque Reduction Neutralization Test

Serum samples were used to quantify the levels of neutralizing antibodies specific to the 17DD-YF virus employing the micro plaque reduction neutralization test (micro-PRNT50). The assays were performed at Laboratório de Tecnologia Virológica, Bio-Manguinhos (LATEV, FIOCRUZ-RJ, Brazil). First, a viral suspension was prepared with YF 213/77 #002/16, diluted previously with the objective to obtain approximately 30 lysis plaques per well. Prior to neutralization, the serum sample was inactivated at 56°C for 30 min and submitted to serial 2-fold dilutions (1:5 – 1:640), and afterwards about thirty plaque-forming units (pfu) of yellow fever virus suspension was added to the samples in 96 well tissue culture plates. After addition of virus, the plates were incubated for 1 hour at 37°C in an incubator with 5% CO_2. A 50 ul cell suspension with 1,600,000 cells/ml were inoculated in all 96 wells of the plate and incubated at 37°C for 3 h under 5% CO_2 for adsorption/sedimentation. The media was then discarded and carboxymethylcellulose (2.5%) added and the cells were incubated for 6 days at 37°C with 5% CO_2. After

incubation, the plates were fixed in formaldehyde (5%) for at least 1 hour at room temperature and stained with 2% crystal violet for 30 minutes at room temperature. Both steps were followed by cleansing with running water.

The arithmetic mean of all viral plaques obtained without serum were estimated. From the mean, the 50% endpoint of the number of plaques was calculated. Afterwards, using the dilution with plaque numbers immediately above and below the endpoint, the serum dilution that would result in the 50% endpoint was estimated by linear regression. The result were expressed in reciprocals of dilution.

Measurement of antibodies against diphtheria, tetanus, rubella and measles

An enzyme-linked immunosorbent assay (ELISA) standardized at the Immunological Technology Laboratory of Bio-Manguinhos (LATIM, FIOCRUZ-RJ, Brazil) was used for antibody measurement. Standard diphtheria and tetanus curves were prepared using in house sera titrated against National Institute for Biological Standard Controls in England (NIBISC) International References. The diphtheria and tetanus antigen for coating ELISA plates were obtained from NIBISC. Anti-diphtheria and anti-tetanus ELISA titers were considered to be protective if they were equal to or higher than the cut-off of 0.1 IU/ml. Serum titers were calculated by four parameter logistic curve using SoftMax Pro, version 5.2 (Molecular Devices, USA)[173].

The ELISA tests for rubella and measles antibodies were performed at the Respiratory Virus Laboratory of Instituto Oswaldo Cruz (FIOCRUZ-RJ, Brazil) utilizing the kits Anti-Measles Vírus ELISA (IgG) and Anti-Rubella Virus ELISA (IgG) (EUROIMMUN, Germany) according to manufacturer instructions. Anti-Measles and

anti-Rubela ELISA titers were considered to be positive if they were equal to or higher than the cut-off of 275 IU/ml and 11 IU/ml respectively.

Plasmids

IFNAR1 or *IRF9* cDNA were cloned into the pGEM-T cloning vector (Promega, Madison, WI, USA). Site-directed mutagenesis was performed to obtain the indicated mutant constructs. All *IRF9* constructs were then subcloned into the pTRIP.CMV.IVSb.iresTagRFP_Dest vector using Gateway cloning technology (Life Technologies), while *IFNAR1* constructs were subcloned into pCAGGS for overexpression studies. For lentiviral vector production utilized in chapter 3, lentiviral vector transfer plasmids pCH_EF1a_IFNaR1_IRES_Bsd and pCH_EF1a_IFNaR2_IRES_Bsd were generated by cloning the codon optimized coding sequence for human *IFNAR1* isoform 1 (NM_000629 or NP_000620) and human *IFNAR2* into the multiple cloning site of the HIV-based lentiviral vector transfer plasmid pCH_EF1a_MCS_IRES_Bsd. Both cDNAs were ordered as a gBlock (IDT Haasrode, Belgium). Sequences were cloned in frame with the IRES-Bsd sequence. All constructs were resequenced to ensure no adventitious mutations were generated during the cloning.

Production of IFNAR1 and IFNAR2 lentiviral vectors

HIV-based viral vectors were produced by the Leuven Viral Vector Core as previously described (Ibrahimi et al. Hum Gene Therapy, 2009), by triple transient transfection of 293T cells with a Vesicular Stomatitis Virus Glycoprotein G envelope encoding plasmid, and a packaging plasmid together with the respective transfer plasmids using polyethylenimine (Polysciences, Amsterdam, The Netherlands), resulting in LV_IFNAR1, LV_IFNAR2 and LV_control (empty vector), respectively. After collecting

the supernatant, the medium was filtered using a 0.45-µm filter (Corning Inc, Seneffe, Belgium) and concentrated using a Vivaspin 50,000 MW column (Vivascience, Bornem, Belgium). The vector containing concentrate was aliquoted and stored at -80°C.

Generation of stably reconstituted cell lines

HIV-based vectors were used to transduce primary fibroblasts, in a serial dilution series. Cells were cultured and subjected to blasticidin selection (5 µg/ml). IFNAR1 expression was corroborated by qRT-PCR, WB, and cell surface staining.

Western blotting

Fibroblasts, with or without pretreatment with IFN-α2b (Schering, Kenilworth, NJ, USA) or IFN-γ (Imukin, Boehringer Ingelheim) for the specified times, were lysed in NP40 lysis buffer (280mM NaCl, 50mM Tris pH 8, 0.2mM EDTA, 2mM EGTA, 10% glycerol, 0.5% NP40) supplemented with 1mM DTT, PhosSTOP (Roche, Mannheim, Germany) and Complete protease inhibitor cocktail (Roche, Mannheim, Germany). 40 ug protein lysate per lane was resolved by SDS-PAGE and transferred to polyvinylidene fluoride (PVDF) membrane, which was probed with unconjugated primary antibodies and HRP-conjugated secondary antibodies. An anti-GAPDH (Santa Cruz) antibody was used as a loading control. IRF9 was probed with antibody recognizing the carboxy-terminus at a dilution of 1:1000 (ISGF-3γ p48 (H10), Santa Cruz Biotech). Endogenous IFNAR1 was probed with an antibody recognizing the amino-terminus at a dilution of 1:1000 (64G12, generously provided by Sandra Pellegrini), while a polyclonal anti-IFNAR1 was used to detect overexpressed protein (AP8550c, ABGENT, San Diego, CA, USA). SuperSignal West Femto Chemiluminescent substrate (Thermo Fisher Scientific) was used to visualize HRP activity, and this signal was detected by an Amersham Imager 600 (GE Life Sciences).

For knockdown studies of IRF9, knockdown efficiency was determined by immunoblotting. 30ug of total protein loaded per lane were separated on 4-12% NuPAGE Bis-Tris SDS-PAGE gels (Invitrogen), and then transferred onto nitrocellulose membranes using Trans-Blot Turbo Transfer System (Bio-Rad Laboratories). After blocking with 5% nonfat dry milk (Bio-Rad Laboratories) in PBS containing 0.1% Tween 20 (Sigma-Aldrich), membranes were blotted with the IRF9 antibody (ISGF-3γ p48 (H10), Santa Cruz Biotech), MAVS (clone #3993; Cell Signaling Technologies), or HSP90 (clone 68; BD), followed by incubation with appropriate HRP-conjugated secondary antibodies (Jackson ImmunoResearch Laboratories) and SuperSignal West Pico Chemiluminescent substrate or SuperSignal West Dura Extended Duration Substrate (Thermo Fisher Scientific). Signal was detected by ChemiDocTM Touch Imaging System (Bio-Rad Laboratories).

Flow Cytometry

For measuring surface expression on patients' cells, B-LCL and SV40-F cells (5 x 10^5 cells per well) were plated in 96-well plates and surface-stained with either purified mouse anti-IFNAR1 AA3 (provided by Sandra Pellegrini) or PE mouse anti-IFNAR2 (PBL Assay Science, Piscataway, NJ, USA) antibodies. Cells stained with AA3 were then washed once with PBS and incubated with a biotinylated rat anti-mouse secondary (Thermo Fisher Scientific) for 30 minutes before being washed once with PBS and incubated for 30 minutes with a PE-conjugated streptavidin (Thermo Fisher Scientific). The cells were then washed twice with PBS and analyzed by flow cytometry. Data were acquired on an LSRII flow cytometer (BD), and the results were analyzed with FlowJo (Tree Star).

For YFV infections, transduced fibroblasts were submitted to IFN-β pretreatment and YF17D infection as described below. Cells were detached after incubation for 10 minutes at room temperature in Accumax (STEMCELL, cat. 07921). Cells were then fixed in 4% paraformaldehyde for 20 minutes at room temperature prior to permeabilization with BD perm buffer (BD Biosciences, cat. 554723). BD perm buffer was used for antibody incubations and washes. Cells were incubated with primary antibodies for 1 hour on ice, washed, incubated with secondary antibodies for 30 minutes at room temperature, washed, and resuspended in PBS with 1% FBS prior to analysis using a BD LSRII flow cytometer. The primary antibody was a mouse anti-YFV (Santa Cruz Biotechnology cat. sc-58083, RRID:AB_630447) diluted 1:250, while the secondary antibody was a goat anti-mouse Alexa Fluor 647 (Invitrogen cat. A-21203) diluted 1:1000.

Electrophoretic mobility shift assays

EMSA was performed as previously described[174]. 25 minutes following stimulation, cell activation was blocked by incubation with cold 1X PBS, and the cells were gently lysed to remove cytoplasmic proteins while keeping the nucleus intact. Nuclear lysis buffer was then added and the recovered nuclear extracts were subjected to nondenaturing electrophoresis with alexa647 labeled GAS (from the FCγR1 promoter: 5′-ATGTATTTCCCAGAAA-3′) and ISRE (from the ISG15 promoter: 5′-GATCGGGAAAGGGAAACCGAAACTGAA-3′) probes. Gels were then imaged on an Amersham Imager 600 (GE Life Sciences) in the Cy5 channel.

Quantitative RT-PCR

For chapter 2, Total RNA from PBMCs was extracted using RNAqueous-Micro Kit (Ambio). Reverse transcription was performed using the High-Capacity cDNA Reverse

Transcription Kit (Applied Biosystems). Messenger RNAs were quantified with IRF9 probes Hs00960976-m1 (exon 1-2) and Hs00196051-m1 (exon 7-8) (Thermo Fischer Scientific) by qRT-PCR using Taqman Gene Expression Assay (Applied Biosystems) and normalized to the expression level of HPRT1.

RNA from B-LCLs and SV40-F cells stimulated with 1,000 IU/ml IFN-α2b, IFN-β, or IFN-γ for 2 or 8h, or primary fibroblasts treated for 6h, were lysed with RNA lysis buffer, treated with DNase, and RNA was purified according to the manufacturer's protocol (Zymo Research, Irvine, CA). Reverse transcriptase PCR was performed using random hexamers and the Superscript III reverse strand synthesis kit according to the manufacturer's recommendations (Thermo Fisher Scientific, Springfield Township, NJ). qRT-PCR was performed with Applied Biosystems Taqman assays using the β-glucuronidase (GUS) housekeeping gene for normalization for SV40-F cells, or B-actin for primary fibroblasts. Results are expressed using the ΔΔCt method, as described by the manufacturer.

Virus assays

VSV infections

SV40-F cells were infected with vesicular stomatitis virus (VSV) at a multiplicity of infection (MOI) of 3. The inoculum was absorbed onto the cells for 30 minutes at 25°C, washed twice with PBS and cultured in DMEM with 10% FBS at 37°C. Virus samples were collected at the indicated time points. Viral titers were determined by endpoint dilution on Vero cells using the Reed and Muench calculation[175]. Where indicated, cells were pretreated with IFN-α2b for 16h prior to virus infection. Primary fibroblasts were infected with Indiana stock VSV (MOI=9.3), with or without pretreatment with 10,000

U/ml IFN-α2b for 24 hours prior to infection. The inoculum was left on the cells, and cell survival was monitored with Resazurin assay kit (Abcam, catalog number ab112119) at 1, 2, and 3 days post-infection.

IAV and HSV-1 infections

SV40-fibroblasts were infected with influenza virus (A/California/4/2009) as previously described[125]. Briefly a viral inoculum was absorbed onto the cells (MOI=0.5) for 30 minutes at 25°C. Cells were then washed twice with Hank's balanced salt solution and cultured at 37°C in the presence of 0.1µg/ml TPCK-trypsin (Sigma-Aldrich, St. Louis, MO, USA). Virus samples were collected at the indicated times after infection and influenza titers were determined by plaque assay on MDCK cells. For HSV-1-GFP infection, SV40-transformed fibroblasts were plated in a 96-well dish and were infected with HSV-1-GFP (MOI=0.01) in DMEM supplemented with 2% FCS. GFP fluorescence was then assessed at 0, 8, 24, 48, and 72 hours post infection. HSV-1-GFP was a gift from Dr. Desai[176]. For HSV-1 (KOS strain, ATCC), SV40-Fs were seeded at a density of 10^5 cells per well in a 24 well plate and infected (MOI=0.01) in DMEM + 2% FCS. Supernatants were collected at the given time points post-infection and $TCID_{50}$ values were calculated following the method of Reed and Muench, after inoculation of Vero cells in 96-well plates[175].

RSV, PIV and HRV infections

Human rhinovirus HRV-A16 and recombinant respiratory syncytial virus (RSV) derived from the A2 strain and containing the enhanced GFP, were used as previously described (Lamborn et al., 2017). rgPIV3, a recombinant human parainfluenza virus type 3 derived from the JS strain and containing the enhanced GFP, was a gift from Dr. Peter

Collins, NIAID (Zhang et al., 2005). SV40-transformed fibroblasts were seeded at 100,000 cells per well in 12-well tissue culture plates in DMEM-Dulbecco's Modified Eagle Medium supplemented with 10% FBS, 2 mM L-glutamine, 100 U/mL penicillin, 100 µg/ml streptomycin (all from Invitrogen), and 55 µM 2-ME (Sigma-Aldrich) After overnight culture, cells were infected with RSV-GFP (MOI 0.5) or PIV3-GFP (MOI 0.1). At 24 and 48 hours after infection, cells were harvested and flow cytometric detection of GFP in RSV-infected viable cells was performed as previously described[45]. Flow cytometric detection of GFP in PIV3-infected viable cells was performed under similar conditions. For IRF9 siRNA knockdown experiments, human primary dermal fibroblasts were transfected with negative siRNA control, Stealth siRNA to IRF9 (Thermo Fisher Scientific; HSS173591), or siRNA to MAVS (Thermo Fisher Scientific; HSS148537), using the P3 Primary Cell 96-well Nucleofector kit (Lonza) as described[45]. 3 d after transfection, cells were infected with RSV (MOI 0.5), PIV (MOI 0.1), or HRV16 (MOI 10). RSV, PIV, and HRV virus replication were quantitated as described above.

YFV infections

Preparation of virus stocks.

YF17D viral stocks were derived from pACNR-2015FLYF-17Da plasmid, a derivative, to be fully described elsewhere, of the previously described pANCR-FLYF-Dx containing the full-length infectious YF17D genome under an SP6 promoter[177]. In pANCR-2015FLYF-17Da, the linearization site for preparation of RNA was changed to AfIII, an XhoI site within the YF coding region was restored, and adventitious mutations that had occurred during bacterial propogation of pANCR-FLYF-17Dx in the lab were corrected. Asibi viral stocks were derived from an analogous full length Asibi cDNA infectious clone

designated pACNR-2015FLYF-Asibi, to be fully described elsewhere. *In vitro*-generated RNA transcripts were electroporated in Huh7.5 cells[178]. Virus was harvested 24 h after transfection and titers of $6x10^5$ PFU/ml (17D) and $6x10^3$ FFU/ml (Asibi) were determined by plaque or focus forming assay on C3 fibroblasts. Single-use aliquots were stored frozen at –80°C until use.

Infection of cells.

Prior to infection, patient-derived fibroblasts were pretreated with or without 1000 U/ml IFN-β (PBL Assay Science) for 16 hours. 17D (or Asibi) was then inoculated to approximately 50,000 (or 20,000) fibroblasts in 24-well (or 48-well plates, respectively). For 17D infections, media was discarded and cells were incoluated with 250 µl of 17D diluted in Optimem (MOI=0.05) for 2 h at 37°C. Asibi infections were similar to 17D, except cells were incoluated with 100 µl of Asibi diluted in Optimem (MOI=0.03). Cells were then washed twice with culture media and incubated at 37°C with 0.5 ml of fresh culture media. At the indicated time points post-infection, media containing the virus produced by the fibroblasts were harvested and titered on Huh7.5 cells by plaque-forming assay.

Plaque assay.

Harvested media was serially diluted 1:10 in Optimem. Approximately 0.5 million Huh7.5 cells were inoculated with 400 µl of diluted virus in 6-well plates, for 2 hours at 37°C. After removal of the inoculum, a 3 ml of overlay of 1.2% Avicel in DMEM supplemented with 1x Pen/Strep and 2% FCS was added and cells were incubated for 3 days (17D) or 4 days (Asibi) at 37°C. After formaldehyde fixation, the cells were stained with crystal violet and the plaques were enumerated.

IFN-ß measurement

The concentration of IFN-β in the supernatant of infected cells was measured by ELISA using the VeriKine-HS™ Human IFN-β Serum ELISA Kit (PBL Assay Science), according to the manufacturer's instructions, using 50 µl of media.

ZIKV infections

Infection of cells.

Prior to the infection, the ZIKV stock titer of $1x10^6$ FFU/ml was determined by focus forming assay on C1 fibroblasts. IFN-β pre-treatment, virus infection (ZIKV MOI=0.05), and quantification of virus production were conducted on patient-derived fibroblasts as described above for Asibi, except Vero cells were inoculated with 300 µl of virus for the plaque-forming assays.

MeV infections

Approximately 50,000 patient-derived SV40-F cells were seeded in 48-well plates and pretreated or not with 1,000 U/ml IFN-α2b (PBL Assay Science) for 16 hours. Cells were incubated for one hour at 37°C with measles virus diluted in DMEM with 10% FCS (MOI=0.1). After virus inoculation, cells were washed twice with PBS and incubated at 37°C with 0.2 ml of fresh culture media. At the indicated timepoints post-infection, media containing the virus produced by the fibroblasts was harvested and $TCID_{50}$ values were calculated following the method of Reed and Muench after inoculation of Vero cells in 96-well plates.

VirScan analysis

Patient serum was analyzed by VirScan in two independent experiments as previously described[92]. Briefly, an oligonucleotide library encoding 56 amino acid peptides

tiling across the genomes of 206 viral species was synthesized on a releasable DNA microarray and cloned into T7 phage. Patient serum containing 2ug of IgG was added to the phage library and immunoprecipitation was performed with Protein A and G beads. Enriched peptides were identified by PCR and Illumina sequencing of the peptide cassette from the immunoprecipitated phage.

mRNA-seq analysis

Total RNA from IFN-a2b-stimulated B-LCL and primary fibroblast cells was isolated RNeasy kit; QIAGEN) and RNA integrity was assessed on an Agilent 2100 Bioanalyzer (Agilent Technologies). Poly (A)mRNA enrichment and cDNA library preparation was performed using a TruSeq Stranded mRNA Library Prep Kit (Illumina) in accordance with the manufacturer's recommendations. Paired-end sequencing was performed on HiSeq4000 (Illumina) with 150 cycles. Quality control of the raw fastq files was performed using FastQC[179]. The samples were then aligned to the reference genome (Ensembl GRCh37) using STAR aligner[180]. Aligned output was then converted to BAM files using SAMtools[166]. The resulting BAM files were used to quantify the read counts using the HTseq-count tool[181]. The output of technical repeats (patient samples that had been stimulated in duplicate) was found to have a high correlation coefficient (not shown). Subsequent downstream analysis was carried out in R statistical programming language[182]. Read counts of technical repeats were averaged and IFNa2b-responsive transcripts were identified by comparing stimulated against unstimulated conditions in the three healthy control subjects, using a minimal 1.5-fold change in expression (up-regulated or down-regulated) as cut-off. The response gene list include only those that had satisfied the filter criteria in all three controls. This resulted in a total of 1064 and 1576 genes that were

responsive in the IFN-a2b-stimulated B-LCL and primary fibroblasts, respectively. The gene lists were then used to identify, again using a 1.5-fold change as cut-off, IFN-a2b-responsive and unresponsive genes in the cells of IRF9-, STAT1- and STAT2-deficient patients. The overall residual responses in the patient's cells were computed by counting the responsive genes in each patient and cell type and by calculating the percentage out of the total number of response genes in each cell type. The response in the healthy control subject was set at 100%.

For B-LCL network analysis, a >5 fold cut-off was applied to the control groups to generate the target list of IFN-a2b induced genes. From the 749 up-regulated genes in the healthy controls, 84 were induced at >5 fold. This gene was then used to filter the IRF9-deficient patient, using the same >1.5 fold cut-off applied in mRNA-seq analysis. In the IRF9-deficient patient, a total of 37 genes were found to be induced at >1.5 fold and 47 were non-responsive. These two lists were then entered into Interferome v2.01 and queried for ISGs, using similar experimental criteria as the current study[183]. Of the 37 genes found to be responsive in the IRF9-deficient patient, 24 were identified as ISGs. Of the 47 non-responsive genes, 39 were identified as ISGs. The combined ISG gene lists for the IRF9-deficient patient was used to conduct network analysis in GeneMANIA, using biological process-based Gene Ontology weighting method and the maximum resultant genes set to 20[184]. The network was examined using both biological pathway (4.35%) and physical interactions (67.64%).

REFERENCES

1. Murphy, K., Travers, P., Walport, M. & Janeway, C. *Janeway's Immunobiology*. (W. W. Norton & Company, 2016).
2. Casanova, J.-L. Human genetic basis of interindividual variability in the course of infection. *PNAS* **112**, E7118–E7127 (2015).
3. Smith, K. A. Louis Pasteur, the Father of Immunology? *Front Immunol* **3**, (2012).
4. Berche, P. Louis Pasteur, from crystals of life to vaccination. *Clin. Microbiol. Infect.* **18 Suppl 5**, 1–6 (2012).
5. Blevins, S. M. & Bronze, M. S. Robert Koch and the 'golden age' of bacteriology. *International Journal of Infectious Diseases* **14**, e744–e751 (2010).
6. Kaufmann, S. H. E. & Schaible, U. E. 100th anniversary of Robert Koch's Nobel Prize for the discovery of the tubercle bacillus. *Trends in Microbiology* **13**, 469–475 (2005).
7. Koch, R. Ueber den augenblicklichen Stand der bakteriologischen Choleradiagnose. *Zeitschr. f. Hygiene.* **14**, 319–338 (1893).
8. Garnham, P. C. C. Charles Nicolle and Inapparent Infections. *The American Journal of Tropical Medicine and Hygiene* **26**, 1101–1104 (1977).
9. Daniel, T. M. The history of tuberculosis. *Respiratory Medicine* **100**, 1862–1870 (2006).
10. Flavia, S. M. A FAMILY PEDIGREE OF APPENDICITIS. *J Hered* **31**, 113–115 (1940).

11. Puffer, R. R. Familial Susceptibility to Tuberculosis. Its Importance as a Public Health Problem. *Familial Susceptibility to Tuberculosis. Its Importance as a Public Health Problem.* (1944).
12. Kallmann, F. J. & Reisner, D. Twin Studies on the Significance of Genetic Factors in Tuberculosis,. *am rev tuberc* **47**, 549–574 (1943).
13. Sørensen, T. I., Nielsen, G. G., Andersen, P. K. & Teasdale, T. W. Genetic and environmental influences on premature death in adult adoptees. *N. Engl. J. Med.* **318**, 727–732 (1988).
14. Bruton, O. C. Agammaglobulinemia. *Pediatrics* **9**, 722–728 (1952).
15. Newport, M. J. *et al.* A mutation in the interferon-gamma-receptor gene and susceptibility to mycobacterial infection. *N. Engl. J. Med.* **335**, 1941–1949 (1996).
16. Jouanguy, E. *et al.* Interferon-gamma-receptor deficiency in an infant with fatal bacille Calmette-Guérin infection. *N. Engl. J. Med.* **335**, 1956–1961 (1996).
17. Casanova, J.-L. Severe infectious diseases of childhood as monogenic inborn errors of immunity. *PNAS* **112**, E7128–E7137 (2015).
18. Dupuis, S. *et al.* Impairment of Mycobacterial But Not Viral Immunity by a Germline Human STAT1 Mutation. *Science* **293**, 300–303 (2001).
19. Altare, F. *et al.* Impairment of Mycobacterial Immunity in Human Interleukin-12 Receptor Deficiency. *Science* **280**, 1432–1435 (1998).
20. Bogunovic, D. *et al.* Mycobacterial Disease and Impaired IFN-γ Immunity in Humans with Inherited ISG15 Deficiency. *Science* **337**, 1684–1688 (2012).
21. Puel, A. *et al.* Chronic Mucocutaneous Candidiasis in Humans with Inborn Errors of Interleukin-17 Immunity. *Science* **332**, 65–68 (2011).

22. Ramoz, N. *et al.* Mutations in two adjacent novel genes are associated with epidermodysplasia verruciformis. *Nature Genetics* **32**, 579 (2002).

23. de Jong, S. J. *et al.* The human CIB1-EVER1-EVER2 complex governs keratinocyte-intrinsic immunity to β-papillomaviruses. *J. Exp. Med.* **215**, 2289–2310 (2018).

24. Kennedy, P. G. E. & Chaudhuri, A. Herpes simplex encephalitis. *Journal of Neurology, Neurosurgery & Psychiatry* **73**, 237–238 (2002).

25. Steiner, I. & Benninger, F. Update on herpes virus infections of the nervous system. *Curr Neurol Neurosci Rep* **13**, 414 (2013).

26. Abel, L. *et al.* Age-dependent Mendelian predisposition to herpes simplex virus type 1 encephalitis in childhood. *J. Pediatr.* **157**, 623–629, 629.e1 (2010).

27. Casrouge, A. *et al.* Herpes Simplex Virus Encephalitis in Human UNC-93B Deficiency. *Science* **314**, 308–312 (2006).

28. Zhang, S.-Y. *et al.* TLR3 Deficiency in Patients with Herpes Simplex Encephalitis. *Science* **317**, 1522–1527 (2007).

29. Dupuis, S. *et al.* Impaired response to interferon-alpha/beta and lethal viral disease in human STAT1 deficiency. *Nat. Genet.* **33**, 388–391 (2003).

30. Haller, O., Kochs, G. & Weber, F. The interferon response circuit: Induction and suppression by pathogenic viruses. *Virology* **344**, 119–130 (2006).

31. Puel, A. *et al.* The NEMO mutation creating the most-upstream premature stop codon is hypomorphic because of a reinitiation of translation. *Am. J. Hum. Genet.* **78**, 691–701 (2006).

32. Isaacs Alick, Lindenmann J. & Andrewes Christopher Howard. Virus interference. I. The interferon. *Proceedings of the Royal Society of London. Series B - Biological Sciences* **147**, 258–267 (1957).

33. Lazear, H. M., Schoggins, J. W. & Diamond, M. S. Shared and Distinct Functions of Type I and Type III Interferons. *Immunity* **50**, 907–923 (2019).

34. Herman, M. *et al.* Heterozygous TBK1 mutations impair TLR3 immunity and underlie herpes simplex encephalitis of childhood. *Journal of Experimental Medicine* **209**, 1567–1582 (2012).

35. Pérez de Diego, R. *et al.* Human TRAF3 adaptor molecule deficiency leads to impaired Toll-like receptor 3 response and susceptibility to herpes simplex encephalitis. *Immunity* **33**, 400–411 (2010).

36. Sancho-Shimizu, V. *et al.* Herpes simplex encephalitis in children with autosomal recessive and dominant TRIF deficiency. *J. Clin. Invest.* **121**, 4889–4902 (2011).

37. Andersen, L. L. *et al.* Functional IRF3 deficiency in a patient with herpes simplex encephalitis. *Journal of Experimental Medicine* **212**, 1371–1379 (2015).

38. Kenney, A. D. *et al.* Human Genetic Determinants of Viral Diseases. *Annual Review of Genetics* **51**, 241–263 (2017).

39. Byun, M. *et al.* Whole-exome sequencing-based discovery of STIM1 deficiency in a child with fatal classic Kaposi sarcoma. *Journal of Experimental Medicine* **207**, 2307–2312 (2010).

40. Byun, M. *et al.* Inherited human OX40 deficiency underlying classic Kaposi sarcoma of childhood. *Journal of Experimental Medicine* jem.20130592 (2013). doi:10.1084/jem.20130592

41. Ciancanelli, M. J. *et al.* Infectious disease. Life-threatening influenza and impaired interferon amplification in human IRF7 deficiency. *Science* **348**, 448–453 (2015).

42. Kerkmann, M. *et al.* Activation with CpG-A and CpG-B oligonucleotides reveals two distinct regulatory pathways of type I IFN synthesis in human plasmacytoid dendritic cells. *J. Immunol.* **170**, 4465–4474 (2003).

43. Izaguirre, A. *et al.* Comparative analysis of IRF and IFN-alpha expression in human plasmacytoid and monocyte-derived dendritic cells. *J. Leukoc. Biol.* **74**, 1125–1138 (2003).

44. Osterlund, P. I., Pietilä, T. E., Veckman, V., Kotenko, S. V. & Julkunen, I. IFN regulatory factor family members differentially regulate the expression of type III IFN (IFN-lambda) genes. *J. Immunol.* **179**, 3434–3442 (2007).

45. Lamborn, I. T. *et al.* Recurrent rhinovirus infections in a child with inherited MDA5 deficiency. *Journal of Experimental Medicine* **214**, 1949–1972 (2017).

46. Reikine, S., Nguyen, J. B. & Modis, Y. Pattern Recognition and Signaling Mechanisms of RIG-I and MDA5. *Front Immunol* **5**, (2014).

47. Kawasaki, T. & Kawai, T. Toll-Like Receptor Signaling Pathways. *Front Immunol* **5**, (2014).

48. Belkaya, S. *et al.* Inherited IL-18BP deficiency in human fulminant viral hepatitis. *Journal of Experimental Medicine* jem.20190669 (2019). doi:10.1084/jem.20190669

49. Duncan, C. J. A. *et al.* Human IFNAR2 deficiency: Lessons for antiviral immunity. *Sci Transl Med* **7**, 307ra154 (2015).

50. Moens, L. *et al.* A novel kindred with inherited STAT2 deficiency and severe viral illness. *J. Allergy Clin. Immunol.* **139**, 1995-1997.e9 (2017).

51. Hambleton, S. *et al.* STAT2 deficiency and susceptibility to viral illness in humans. *Proc. Natl. Acad. Sci. U.S.A.* **110**, 3053–3058 (2013).

52. Shahni, R. *et al.* Signal transducer and activator of transcription 2 deficiency is a novel disorder of mitochondrial fission. *Brain* **138**, 2834–2846 (2015).

53. Dussurget, O., Bierne, H. & Cossart, P. The bacterial pathogen Listeria monocytogenes and the interferon family: type I, type II and type III interferons. *Front. Cell. Infect. Microbiol.* **4**, (2014).

54. Short, K. R., Kroeze, E. J. B. V., Fouchier, R. A. M. & Kuiken, T. Pathogenesis of influenza-induced acute respiratory distress syndrome. *Lancet Infect Dis* **14**, 57–69 (2014).

55. Taubenberger, J. K. & Morens, D. M. 1918 Influenza: the mother of all pandemics. *Emerging Infect. Dis.* **12**, 15–22 (2006).

56. Taubenberger, J. K. & Morens, D. M. The pathology of influenza virus infections. *Annu Rev Pathol* **3**, 499–522 (2008).

57. Writing Committee of the WHO Consultation on Clinical Aspects of Pandemic (H1N1) 2009 Influenza *et al.* Clinical aspects of pandemic 2009 influenza A (H1N1) virus infection. *N. Engl. J. Med.* **362**, 1708–1719 (2010).

58. Dawood, F. S. *et al.* Children with asthma hospitalized with seasonal or pandemic influenza, 2003-2009. *Pediatrics* **128**, e27-32 (2011).

59. Knipe, D. M. & Howley, P. M. *Fields Virology*. (Lippincott Williams and Wilkins).

60. Shieh, W.-J. *et al.* 2009 pandemic influenza A (H1N1): pathology and pathogenesis of 100 fatal cases in the United States. *Am. J. Pathol.* **177**, 166–175 (2010).

61. Laboratory-Confirmed Influenza Hospitalizations. Available at: https://gis.cdc.gov/grasp/fluview/FluHospChars.html. (Accessed: 4th July 2019)

62. Pasquet, M. *et al.* High frequency of GATA2 mutations in patients with mild chronic neutropenia evolving to MonoMac syndrome, myelodysplasia, and acute myeloid leukemia. *Blood* **121**, 822–829 (2013).

63. Sole-Violan, J. *et al.* Lethal influenza virus A H1N1 infection in two relatives with autosomal dominant GATA-2 deficiency. *Crit Care* **17**, P15 (2013).

64. Sologuren, I. *et al.* Lethal Influenza in Two Related Adults with Inherited GATA2 Deficiency. *J. Clin. Immunol.* **38**, 513–526 (2018).

65. Ning, S., Pagano, J. S. & Barber, G. N. IRF7: activation, regulation, modification and function. *Genes Immun.* **12**, 399–414 (2011).

66. Asselin-Paturel, C. *et al.* Type I interferon dependence of plasmacytoid dendritic cell activation and migration. *J. Exp. Med.* **201**, 1157–1167 (2005).

67. Gitlin, L. *et al.* Essential role of mda-5 in type I IFN responses to polyriboinosinic:polyribocytidylic acid and encephalomyocarditis picornavirus. *Proc. Natl. Acad. Sci. U.S.A.* **103**, 8459–8464 (2006).

68. Lim, H. K. *et al.* Severe influenza pneumonitis in children with inherited TLR3 deficiency. *J. Exp. Med.* (2019). doi:10.1084/jem.20181621

69. Asgari, S. *et al.* Severe viral respiratory infections in children with *IFIH1* loss-of-function mutations. *Proceedings of the National Academy of Sciences* **114**, 8342–8347 (2017).

70. Zaki, M. *et al.* Recurrent and Prolonged Infections in a Child with a Homozygous IFIH1 Nonsense Mutation. *Front. Genet.* **8**, (2017).

71. Glocker, E.-O. *et al.* Inflammatory bowel disease and mutations affecting the interleukin-10 receptor. *N. Engl. J. Med.* **361**, 2033–2045 (2009).

72. Begue, B. *et al.* Defective IL10 signaling defining a subgroup of patients with inflammatory bowel disease. *Am. J. Gastroenterol.* **106**, 1544–1555 (2011).

73. Kreins, A. Y. *et al.* Human TYK2 deficiency: Mycobacterial and viral infections without hyper-IgE syndrome. *J. Exp. Med.* **212**, 1641–1662 (2015).

74. Boisson-Dupuis, S. *et al.* Inborn errors of human STAT1: allelic heterogeneity governs the diversity of immunological and infectious phenotypes. *Curr. Opin. Immunol.* **24**, 364–378 (2012).

75. Eletto, D. *et al.* Biallelic JAK1 mutations in immunodeficient patient with mycobacterial infection. *Nature Communications* **7**, 13992 (2016).

76. Bousfiha, A. *et al.* The 2017 IUIS Phenotypic Classification for Primary Immunodeficiencies. *J. Clin. Immunol.* **38**, 129–143 (2018).

77. Picard, C. *et al.* International Union of Immunological Societies: 2017 Primary Immunodeficiency Diseases Committee Report on Inborn Errors of Immunity. *J. Clin. Immunol.* **38**, 96–128 (2018).

78. Collin, M., Dickinson, R. & Bigley, V. Haematopoietic and immune defects associated with GATA2 mutation. *Br. J. Haematol.* **169**, 173–187 (2015).

79. Onodera, K. *et al.* GATA2 regulates dendritic cell differentiation. *Blood* **128**, 508–518 (2016).

80. Johnson, K. D. *et al.* Cis-element mutated in GATA2-dependent immunodeficiency governs hematopoiesis and vascular integrity. *J. Clin. Invest.* **122**, 3692–3704 (2012).

81. Honda, K. *et al.* IRF-7 is the master regulator of type-I interferon-dependent immune responses. *Nature* **434**, 772 (2005).

82. Sato, M. *et al.* Positive feedback regulation of type I IFN genes by the IFN-inducible transcription factor IRF-7. *FEBS Lett.* **441**, 106–110 (1998).

83. Wilk, E. *et al.* RNAseq expression analysis of resistant and susceptible mice after influenza A virus infection identifies novel genes associated with virus replication and important for host resistance to infection. *BMC Genomics* **16**, 655 (2015).

84. Hatesuer, B. *et al.* Deletion of Irf3 and Irf7 Genes in Mice Results in Altered Interferon Pathway Activation and Granulocyte-Dominated Inflammatory Responses to Influenza A Infection. *JIN* **9**, 145–161 (2017).

85. Staeheli, P., Grob, R., Meier, E., Sutcliffe, J. G. & Haller, O. Influenza virus-susceptible mice carry Mx genes with a large deletion or a nonsense mutation. *Mol. Cell. Biol.* **8**, 4518–4523 (1988).

86. Ciancanelli, M. J., Abel, L., Zhang, S.-Y. & Casanova, J.-L. Host genetics of severe influenza: from mouse Mx1 to human IRF7. *Curr. Opin. Immunol.* **38**, 109–120 (2016).

87. Iwasaki, A. & Pillai, P. S. Innate immunity to influenza virus infection. *Nat. Rev. Immunol.* **14**, 315–328 (2014).

88. Koerner, I., Kochs, G., Kalinke, U., Weiss, S. & Staeheli, P. Protective Role of Beta Interferon in Host Defense against Influenza A Virus. *Journal of Virology* **81**, 2025–2030 (2007).

89. Kaminski, M. M., Ohnemus, A., Cornitescu, M. & Staeheli, P. Plasmacytoid dendritic cells and Toll-like receptor 7-dependent signalling promote efficient

protection of mice against highly virulent influenza A virus. *J. Gen. Virol.* **93**, 555–559 (2012).

90. Mordstein, M. *et al.* Interferon-lambda contributes to innate immunity of mice against influenza A virus but not against hepatotropic viruses. *PLoS Pathog.* **4**, e1000151 (2008).
91. Klinkhammer, J. *et al.* IFN-λ prevents influenza virus spread from the upper airways to the lungs and limits virus transmission. *Elife* **7**, (2018).
92. Xu, G. J. *et al.* Viral immunology. Comprehensive serological profiling of human populations using a synthetic human virome. *Science* **348**, aaa0698 (2015).
93. Fu, X. Y., Kessler, D. S., Veals, S. A., Levy, D. E. & Darnell, J. E. ISGF3, the transcriptional activator induced by interferon alpha, consists of multiple interacting polypeptide chains. *Proc. Natl. Acad. Sci. U.S.A.* **87**, 8555–8559 (1990).
94. Veals, S. A., Santa Maria, T. & Levy, D. E. Two domains of ISGF3 gamma that mediate protein-DNA and protein-protein interactions during transcription factor assembly contribute to DNA-binding specificity. *Mol. Cell. Biol.* **13**, 196–206 (1993).
95. Kimura, T. *et al.* Essential and non-redundant roles of p48 (ISGF3 gamma) and IRF-1 in both type I and type II interferon responses, as revealed by gene targeting studies. *Genes Cells* **1**, 115–124 (1996).
96. Belkadi, A. *et al.* Whole-exome sequencing to analyze population structure, parental inbreeding, and familial linkage. *Proc. Natl. Acad. Sci. U.S.A.* **113**, 6713–6718 (2016).

97. Casanova, J.-L., Conley, M. E., Seligman, S. J., Abel, L. & Notarangelo, L. D. Guidelines for genetic studies in single patients: lessons from primary immunodeficiencies. *J. Exp. Med.* **211**, 2137–2149 (2014).

98. Kircher, M. *et al.* A general framework for estimating the relative pathogenicity of human genetic variants. *Nat. Genet.* **46**, 310–315 (2014).

99. Itan, Y. *et al.* The mutation significance cutoff: gene-level thresholds for variant predictions. *Nat. Methods* **13**, 109–110 (2016).

100. Itan, Y. *et al.* The human gene connectome as a map of short cuts for morbid allele discovery. *PNAS* **110**, 5558–5563 (2013).

101. Itan, Y. *et al.* The human gene damage index as a gene-level approach to prioritizing exome variants. *Proc. Natl. Acad. Sci. U.S.A.* **112**, 13615–13620 (2015).

102. Boisson, B. *et al.* Immunodeficiency, autoinflammation and amylopectinosis in humans with inherited HOIL-1 and LUBAC deficiency. *Nat. Immunol.* **13**, 1178–1186 (2012).

103. John, J. *et al.* Isolation and characterization of a new mutant human cell line unresponsive to alpha and beta interferons. *Mol. Cell. Biol.* **11**, 4189–4195 (1991).

104. Rengachari, S. *et al.* Structural basis of STAT2 recognition by IRF9 reveals molecular insights into ISGF3 function. *Proc. Natl. Acad. Sci. U.S.A.* **115**, E601–E609 (2018).

105. Tang, X. *et al.* Acetylation-dependent signal transduction for type I interferon receptor. *Cell* **131**, 93–105 (2007).

106. Jaworska, J., Gravel, A. & Flamand, L. Divergent susceptibilities of human herpesvirus 6 variants to type I interferons. *Proc Natl Acad Sci U S A* **107**, 8369–8374 (2010).

107. Arimoto, K. *et al.* STAT2 is an essential adaptor in USP18-mediated suppression of type I interferon signaling. *Nat Struct Mol Biol* **24**, 279–289 (2017).

108. Darnell, J. E., Kerr, I. M. & Stark, G. R. Jak-STAT pathways and transcriptional activation in response to IFNs and other extracellular signaling proteins. *Science* **264**, 1415–1421 (1994).

109. Stark, G. R. & Darnell, J. E. The JAK-STAT pathway at twenty. *Immunity* **36**, 503–514 (2012).

110. Taniguchi, T., Ogasawara, K., Takaoka, A. & Tanaka, N. IRF family of transcription factors as regulators of host defense. *Annu. Rev. Immunol.* **19**, 623–655 (2001).

111. Mostafavi, S. *et al.* Parsing the Interferon Transcriptional Network and Its Disease Associations. *Cell* **164**, 564–578 (2016).

112. Chapgier, A. *et al.* Human complete Stat-1 deficiency is associated with defective type I and II IFN responses in vitro but immunity to some low virulence viruses in vivo. *J. Immunol.* **176**, 5078–5083 (2006).

113. de Weerd, N. A. *et al.* Structural basis of a unique interferon-β signaling axis mediated via the receptor IFNAR1. *Nat. Immunol.* **14**, 901–907 (2013).

114. Bravo García-Morato, M. *et al.* Impaired control of multiple viral infections in a family with complete IRF9 deficiency. *J. Allergy Clin. Immunol.* (2019). doi:10.1016/j.jaci.2019.02.019

115. Wlodarski, M. W. *et al.* Prevalence, clinical characteristics, and prognosis of GATA2-related myelodysplastic syndromes in children and adolescents. *Blood* **127**, 1387–1397 (2016).

116. Burns, C. *et al.* A novel presentation of homozygous loss-of-function STAT-1 mutation in an infant with hyperinflammation-A case report and review of the literature. *J Allergy Clin Immunol Pract* **4**, 777–779 (2016).

117. Hahm, B., Trifilo, M. J., Zuniga, E. I. & Oldstone, M. B. A. Viruses evade the immune system through type I interferon-mediated STAT2-dependent, but STAT1-independent, signaling. *Immunity* **22**, 247–257 (2005).

118. O'Donnell, L. A. *et al.* STAT1-independent control of a neurotropic measles virus challenge in primary neurons and infected mice. *J. Immunol.* **188**, 1915–1923 (2012).

119. Lou, Y.-J. *et al.* IRF-9/STAT2 [corrected] functional interaction drives retinoic acid-induced gene G expression independently of STAT1. *Cancer Res.* **69**, 3673–3680 (2009).

120. Abdul-Sater, A. A. *et al.* Different STAT Transcription Complexes Drive Early and Delayed Responses to Type I IFNs. *J. Immunol.* **195**, 210–216 (2015).

121. Li, W. *et al.* Type I interferon-regulated gene expression and signaling in murine mixed glial cells lacking signal transducers and activators of transcription 1 or 2 or interferon regulatory factor 9. *J. Biol. Chem.* **292**, 5845–5859 (2017).

122. Shaghaghi, M. *et al.* Combined immunodeficiency presenting with vaccine-associated paralytic poliomyelitis: a case report and narrative review of literature. *Immunol. Invest.* **43**, 292–298 (2014).

123. Pöyhönen, L., Bustamante, J., Casanova, J.-L., Jouanguy, E. & Zhang, Q. Life-threatening infections due to live attenuated vaccines: early manifestations of inborn errors of immunity. *Journal of Allergy and Clinical Immunology* (2019).

124. Morfopoulou, S. *et al.* Deep sequencing reveals persistence of cell-associated mumps vaccine virus in chronic encephalitis. *Acta Neuropathol* **133**, 139–147 (2017).

125. Hernandez, N. *et al.* Life-threatening influenza pneumonitis in a child with inherited IRF9 deficiency. *J. Exp. Med.* (2018). doi:10.1084/jem.20180628

126. Nascimento Silva, J. R. *et al.* Mutual interference on the immune response to yellow fever vaccine and a combined vaccine against measles, mumps and rubella. *Vaccine* **29**, 6327–6334 (2011).

127. Seligman, S. J., Cohen, J. E., Itan, Y., Casanova, J.-L. & Pezzullo, J. C. Defining risk groups to yellow fever vaccine-associated viscerotropic disease in the absence of denominator data. *Am. J. Trop. Med. Hyg.* **90**, 267–271 (2014).

128. Piehler, J., Thomas, C., Garcia, K. C. & Schreiber, G. Structural and dynamic determinants of type I interferon receptor assembly and their functional interpretation. *Immunol. Rev.* **250**, 317–334 (2012).

129. Uzé, G., Lutfalla, G. & Gresser, I. Genetic transfer of a functional human interferon alpha receptor into mouse cells: cloning and expression of its cDNA. *Cell* **60**, 225–234 (1990).

130. Ragimbeau, J. *et al.* The tyrosine kinase Tyk2 controls IFNAR1 cell surface expression. *The EMBO Journal* **22**, 537–547 (2003).

131. Takaoka, A. *et al.* Cross talk between interferon-gamma and -alpha/beta signaling components in caveolar membrane domains. *Science* **288**, 2357–2360 (2000).

132. Belkowski, L. S. & Sen, G. C. Inhibition of vesicular stomatitis viral mRNA synthesis by interferons. *J. Virol.* **61**, 653–660 (1987).

133. Honda, K., Takaoka, A. & Taniguchi, T. Type I Inteferon Gene Induction by the Interferon Regulatory Factor Family of Transcription Factors. *Immunity* **25**, 349–360 (2006).

134. Minegishi, Y. *et al.* Human tyrosine kinase 2 deficiency reveals its requisite roles in multiple cytokine signals involved in innate and acquired immunity. *Immunity* **25**, 745–755 (2006).

135. Neven, B. *et al.* A Mendelian predisposition to B-cell lymphoma caused by IL-10R deficiency. *Blood* **122**, 3713–3722 (2013).

136. Karaca, N. E. *et al.* Early Diagnosis and Hematopoietic Stem Cell Transplantation for IL10R Deficiency Leading to Very Early-Onset Inflammatory Bowel Disease Are Essential in Familial Cases. *Case Reports Immunol* **2016**, 5459029 (2016).

137. Gao, X. *et al.* Mutation of IFNLR1, an interferon lambda receptor 1, is associated with autosomal-dominant non-syndromic hearing loss. *J. Med. Genet.* **55**, 298–306 (2018).

138. Gardner, C. L. & Ryman, K. D. Yellow Fever: A Reemerging Threat. *Clin Lab Med* **30**, 237–260 (2010).

139. Monath, T. P. *et al.* An Inactivated Cell-Culture Vaccine against Yellow Fever. *New England Journal of Medicine* **364**, 1326–1333 (2011).

140. Pereira, R. C. *et al.* An inactivated yellow fever 17DD vaccine cultivated in Vero cell cultures. *Vaccine* **33**, 4261–4268 (2015).

141. Monath, T. P. & Vasconcelos, P. F. C. Yellow fever. *Journal of Clinical Virology* **64**, 160–173 (2015).

142. Monath, T. P. *et al.* Live virus vaccines based on a yellow fever vaccine backbone: standardized template with key considerations for a risk/benefit assessment. *Vaccine* **33**, 62–72 (2015).

143. Dengue vaccine: WHO position paper, September 2018 - Recommendations. *Vaccine* (2018). doi:10.1016/j.vaccine.2018.09.063

144. Halstead, S. B. Safety issues from a Phase 3 clinical trial of a live-attenuated chimeric yellow fever tetravalent dengue vaccine. *Hum Vaccin Immunother* **14**, 2158–2162 (2018).

145. Pulendran, B. *et al.* Case of Yellow Fever Vaccine–Associated Viscerotropic Disease with Prolonged Viremia, Robust Adaptive Immune Responses, and Polymorphisms in CCR5 and RANTES Genes. *J Infect Dis* **198**, 500–507 (2008).

146. Reinhardt, B., Jaspert, R., Niedrig, M., Kostner, C. & L'age-Stehr, J. Development of viremia and humoral and cellular parameters of immune activation after vaccination with yellow fever virus strain 17D: a model of human flavivirus infection. *J. Med. Virol.* **56**, 159–167 (1998).

147. Silva, M. L. *et al.* Clinical and Immunological Insights on Severe, Adverse Neurotropic and Viscerotropic Disease following 17D Yellow Fever Vaccination. *Clin Vaccine Immunol* **17**, 118–126 (2010).

148. Querec, T. D. *et al.* Systems biology approach predicts immunogenicity of the yellow fever vaccine in humans. *Nature Immunology* **10**, 116–125 (2009).

149. Gaucher, D. *et al.* Yellow fever vaccine induces integrated multilineage and polyfunctional immune responses. *J. Exp. Med.* **205**, 3119–3131 (2008).

150. Fernandez-Garcia, M. D. *et al.* Vaccine and Wild-Type Strains of Yellow Fever Virus Engage Distinct Entry Mechanisms and Differentially Stimulate Antiviral Immune Responses. *MBio* **7**, e01956-01915 (2016).

151. Erickson, A. K. & Pfeiffer, J. K. Dynamic Viral Dissemination in Mice Infected with Yellow Fever Virus Strain 17D. *J. Virol.* **87**, 12392 (2013).

152. Hoyos-Bachiloglu, R. *et al.* A digenic human immunodeficiency characterized by IFNAR1 and IFNGR2 mutations. *J. Clin. Invest.* **127**, 4415–4420 (2017).

153. Holland, S. M. *et al.* Abnormal regulation of interferon-gamma, interleukin-12, and tumor necrosis factor-alpha in human interferon-gamma receptor 1 deficiency. *J. Infect. Dis.* **178**, 1095–1104 (1998).

154. Dorman, S. E. *et al.* Viral infections in interferon-gamma receptor deficiency. *J. Pediatr.* **135**, 640–643 (1999).

155. Cunningham, J. A. *et al.* Disseminated bacille Calmette-Guérin infection in an infant with a novel deletion in the interferon-gamma receptor gene. *Int. J. Tuberc. Lung Dis.* **4**, 791–794 (2000).

156. Rosenzweig, S. D. *et al.* A Novel Mutation in IFN-γ Receptor 2 with Dominant Negative Activity: Biological Consequences of Homozygous and Heterozygous States. *The Journal of Immunology* **173**, 4000–4008 (2004).

157. de Weerd, N. A. *et al.* Structural basis of a unique interferon-β signaling axis mediated via the receptor IFNAR1. *Nat. Immunol.* **14**, 901–907 (2013).

158. Vairo, D. *et al.* Severe impairment of IFN-γ and IFN-α responses in cells of a patient with a novel STAT1 splicing mutation. *Blood* **118**, 1806–1817 (2011).

159. Ye, L., Schnepf, D. & Staeheli, P. Interferon-λ orchestrates innate and adaptive mucosal immune responses. *Nat. Rev. Immunol.* (2019). doi:10.1038/s41577-019-0182-z

160. Davidson, S. *et al.* IFNλ is a potent anti-influenza therapeutic without the inflammatory side effects of IFNα treatment. *EMBO Mol Med* **8**, 1099–1112 (2016).

161. Galani, I. E. *et al.* Interferon-λ Mediates Non-redundant Front-Line Antiviral Protection against Influenza Virus Infection without Compromising Host Fitness. *Immunity* **46**, 875-890.e6 (2017).

162. von Bernuth, H. *et al.* Pyogenic bacterial infections in humans with MyD88 deficiency. *Science* **321**, 691–696 (2008).

163. Picard, C. *et al.* Pyogenic bacterial infections in humans with IRAK-4 deficiency. *Science* **299**, 2076–2079 (2003).

164. Fung, K. Y. *et al.* Interferon-ε protects the female reproductive tract from viral and bacterial infection. *Science* **339**, 1088–1092 (2013).

165. Li, H. & Durbin, R. Fast and accurate short read alignment with Burrows-Wheeler transform. *Bioinformatics* **25**, 1754–1760 (2009).

166. Li, H. *et al.* The Sequence Alignment/Map format and SAMtools. *Bioinformatics* **25**, 2078–2079 (2009).

167. McKenna, A. *et al.* The Genome Analysis Toolkit: a MapReduce framework for analyzing next-generation DNA sequencing data. *Genome Res.* **20**, 1297–1303 (2010).

168. Adzhubei, I. A. *et al.* A method and server for predicting damaging missense mutations. *Nat. Methods* **7**, 248–249 (2010).

169. Ng, P. C. & Henikoff, S. Predicting deleterious amino acid substitutions. *Genome Res.* **11**, 863–874 (2001).

170. Purcell, S. *et al.* PLINK: a tool set for whole-genome association and population-based linkage analyses. *Am. J. Hum. Genet.* **81**, 559–575 (2007).

171. McQuillan, R. *et al.* Runs of homozygosity in European populations. *Am. J. Hum. Genet.* **83**, 359–372 (2008).

172. Stoletzki, N. & Eyre-Walker, A. Estimation of the neutrality index. *Mol. Biol. Evol.* **28**, 63–70 (2011).

173. Martins, R. de M. *et al.* Immunogenicity, reactogenicity and consistency of production of a Brazilian combined vaccine against diphtheria, tetanus, pertussis and Haemophilus influenzae type b. *Mem. Inst. Oswaldo Cruz* **103**, 711–718 (2008).

174. Chapgier, A. *et al.* Novel STAT1 alleles in otherwise healthy patients with mycobacterial disease. *PLoS Genet.* **2**, e131 (2006).

175. Reed, L. J. & Muench, H. A SIMPLE METHOD OF ESTIMATING FIFTY PER CENT ENDPOINTS. *Am J Epidemiol* **27**, 493–497 (1938).

176. Desai, P. & Person, S. Incorporation of the Green Fluorescent Protein into the Herpes Simplex Virus Type 1 Capsid. *Journal of Virology* **72**, 7563–7568 (1998).

177. Bredenbeek, P. J. *et al.* A stable full-length yellow fever virus cDNA clone and the role of conserved RNA elements in flavivirus replication. *J. Gen. Virol.* **84**, 1261–1268 (2003).

178. Blight, K. J., McKeating, J. A. & Rice, C. M. Highly permissive cell lines for subgenomic and genomic hepatitis C virus RNA replication. *J. Virol.* **76**, 13001–13014 (2002).

179. Andrews, S. FastQC A Quality Control tool for High Throughput Sequence Data. *http://www.bioinformatics.babraham.ac.uk/projects/fastqc/* Available at: http://www.bioinformatics.babraham.ac.uk/projects/fastqc/. (Accessed: 11th September 2018)

180. Dobin, A. *et al.* STAR: ultrafast universal RNA-seq aligner. *Bioinformatics* **29**, 15–21 (2013).

181. Anders, S., Pyl, P. T. & Huber, W. HTSeq--a Python framework to work with high-throughput sequencing data. *Bioinformatics* **31**, 166–169 (2015).

182. R Core Team. R: a language and environment for statistical computing. Available at: https://www.gbif.org/tool/81287/r-a-language-and-environment-for-statistical-computing. (Accessed: 11th September 2018)

183. Rusinova, I. *et al.* Interferome v2.0: an updated database of annotated interferon-regulated genes. *Nucleic Acids Res.* **41**, D1040-1046 (2013).

184. Warde-Farley, D. *et al.* The GeneMANIA prediction server: biological network integration for gene prioritization and predicting gene function. *Nucleic Acids Res.* **38**, W214-220 (2010).